Adhesion and Interphase Properties of Reinforced Polymeric Composites

Kyle Bernd Caldwell

A dissertation

submitted in partial fulfillment of the

requirements for the degree of

Doctor of Philosophy

University of Washington

2017

Reading Committee:

John Berg, Chair

Brian Hayes

Felix Nguyen

Program Authorized to Offer Degree:

Chemical Engineering

© Copyright 2017

Kyle Bernd Caldwell

University of Washington

Abstract

Adhesion and Interphase Properties of Reinforced Polymeric Composites

Kyle Bernd Caldwell

Chair of the Supervisory Committee:
Rehnberg Professor of Chemical Engineering: John C. Berg
Chemical Engineering

Reinforced polymeric composites are an increasingly utilized material with a wide range of applications. Fiber reinforced polymeric composites, in particular, possess impressive mechanical properties at a fraction of the weight of many other building materials. There will always, however, be a demand for producing lighter, stiffer, and stronger materials. Understanding the mechanism of adhesion and ways to engineer the reinforcement-matrix interphase can lead to the development of new materials with improved mechanical properties, and even impart additional functionality such as electrical conductivity. The performance of reinforced polymeric composites is critically dependent upon the adhesion between the reinforcement and the surrounding polymer. The relative adhesion between a filler and a thermoplastic matrix can be predicted using calculable thermodynamic quantities such as the Gibbs free energy of mixing. A recent model, COSMO-

SAC, is capable of predicting the adhesion between organo-silane treated glass surfaces and several thermoplastic materials. COSMO-SAC uses information based on the charge distribution of a molecule's surface to calculate many thermodynamic properties. Density functional theory calculations, which are relative inexpensive computations, generate the information necessary to perform the COSMO-SAC analysis and can be performed on any given molecule. The flexibility of the COSMO-SAC model is one of the main advantages it possesses over other methods for calculating thermodynamic quantities.

In many cases the adhesion between a reinforcing fiber and the surrounding matrix may be improved by incorporating interphase modifiers in the vicinity of the fiber surface. The modifiers can improve the fracture toughness and modulus of the interphase, which may improve the stress transfer from the matrix to the fiber. In addition, the interphase modifiers may improve the mechanical interlock between the fiber surface and the bulk polymer, leading to improved adhesion. In recent years, the use of so called "migrating agents" have been used to self-assemble nanoparticle reinforced fiber-matrix interphases in thermosetting resin systems. The inclusion of a modest amount of thermoplastic migrating agent can lead to the formation of a self-assembled interphase, without causing aggregation of nanoparticles in the bulk phase. Formulations containing excess migrating agent, however, can induce aggregation in the bulk of increasing severity with increasing migrating agent concentration. Several techniques were used to study the mechanism by which the migrating agents operate including, scanning electron microscopy, and in situ fluorescence microscopy. The self-assembly mechanism by which migrating agents operate is described well by depletion forces, which are depend on the geometry of the approaching objects, as well as the migrating agent molecular weight and concentration.

TABLE OF CONTENTS

LIST OF FIGURES

LIST OF TABLES

ACKNOWLEDGEMENTS

I would like to thank everyone who supported me during the course of my Ph.D. First and foremost, to my wife, brother, and father who encouraged me to pursue academic goals during a period of many personal trials. To Dr. Matthew Crane, Elena Pandres, Brian Gerwe, Dr. Susan Liu, William Voje, and Dr. Elisa Harrison – Thank you for the caffeination and lunchtime discussions, I'll never have another lunch crew quite as awesome as you all.

I would also like to thank Dr. Benjamin Rutz, Dr. Matthew Gacek, Dr. Edward Michor and Benjamin Ponto for their collaboration and recommendations. I would like to acknowledge Dr. Felix Nguyen, of Toray CMA, for many helpful discussions. I'd especially like to thank Dr. Brian Hayes for his invaluable knowledge of composite materials and for all of his mentorship over the years.

Lastly, I would like to thank my adviser, John C. Berg, for the mentorship, support, and advice he has given me over the years.

DEDICATION

This work is dedicated to the memory of my mother, Roseanna Morales Caldwell (1952-2017)

Chapter 1. OVERVIEW OF ADHESION AND ENGINEERED INTERPHASES IN REINFORCED COMPOSITES

c.f. K.B. Caldwell, and J.C. Berg, *Reviews of Adhesion and Adhesives,* **5**, 1-54 (2017)

1.1 REINFORCED POLYMERIC COMPOSITES

Reinforced polymeric composites have found increasing use in recent years. They can possess excellent mechanical properties at a fraction of the weight compared to many other building materials. In addition, they are often resistant to corrosion, depending on the reinforcement, may possess additional functionality. In high end applications, such as the aerospace and defense markets, there will always be justification for creating materials with improved material properties at reduced weight.

There are many types of reinforcements that can be used, each with their own unique set of applications. Nanoparticles, carbon nanotubes, and clays are common reinforcements, and their proper dispersion into the matrix is critical to achieve the desired properties. Many strategies have been employed to precisely control the spatial arrangement and dispersion state of particulate fillers embedded in polymeric media [1–6]. Silane coupling agents are commonly used, for example, to improve particle dispersion by improving the chemical compatibility between the particles and the polymeric matrix [7–9]. Other surface treatments, such as adsorbing surfactants or grafting polymers to filler surfaces can be useful in keeping 2D materials, such as clays or graphene, intercalated and well dispersed [10,11]. In other scenarios, such as with electrically conductive composites, percolated networks of conducting nanofillers, such as silver nanoparticles or carbon nanotubes, are desired and particle-particle contacts are required to achieve the desired

properties. Many techniques exist for controlling the spatial distribution of nanoparticles in bulk polymers or in thin films of polymeric material and many morphologies can be achieved [12–16].

Chopped or continuous fibers are another common reinforcement in polymeric composites. Often times the fibers are oriented randomly, leading to a composite with nearly isotropic properties. Continuous fiber reinforced polymers can also be prepared, and are intrinsically anisotropic, with fiber dominated properties in the transverse direction of the fibers. Layers of these composites, called plies, can be laminated together to form composites with the desired mechanical properties in all directions. Figure 1.1demonstrates a continuous fiber reinforced composite and particulate filled composite material with good dispersion.

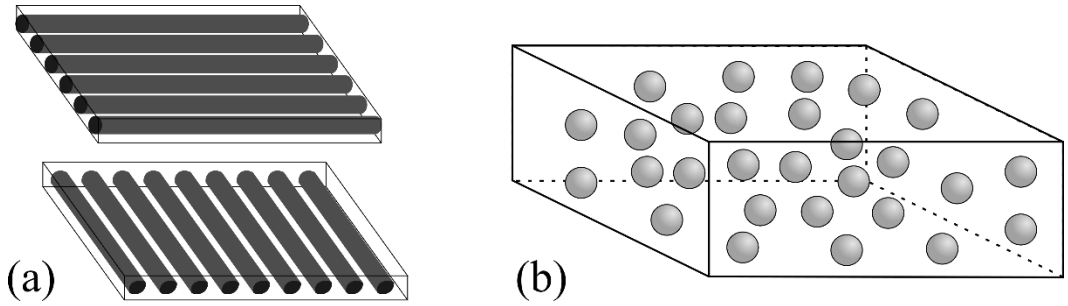

Figure 1.1 – Schematic of (a) fiber and (b) particulate reinforced polymeric composites

The polymer matrix may consist of either a thermoplastic, or a thermosetting polymer (as shown in Figure 1.2. Thermoplastics consist of individual polymer chains that are entangled within each other. Heating a thermoplastic above its melting point allows for flow and processing of the material, upon which subsequent cooling can solidify the material. Thermosetting polymers, on the other hand are composed of reactive monomers that upon the addition of heat or light undergo an irreversible crosslinking chemical reaction, leading to an effectively infinite molecular weight polymer. Thermosets may be composed of a single monomer that is reactive towards itself, or may

be composed of several components that are only reactive towards other monomers, such as an epoxy-amine based system.

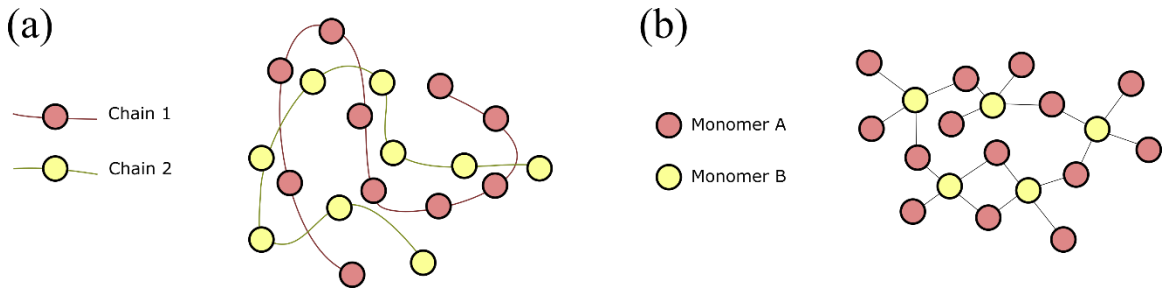

Figure 1.2 – Representation of (a) thermoplastic and (b) thermosetting polymers

The mechanical properties of a reinforced polymeric composite depend on the properties of the reinforcement and the polymer matrix as well as the properties of filler-matrix interface and interphase. The interphase is a thin (0.1 – 1.0 μm) region between the filler surface and the bulk matrix with different mechanical properties than the bulk polymer, shown schematically in Figure 1.3. Many factors influence the interphase properties including the filler morphology and chemistry, as well as the presence of any adsorbed material [17]. It is generally recognized that bond between the filler and matrix be both strong and tough in order to achieve good mechanical properties [18]. Prediction of the adhesion between the filler and the matrix is a useful in the development of new materials. Another strategy for improving mechanical properties is to modify the interphase with adhesion promoters such as silane-coupling agents or nanoscopic material to improve the mechanical interlock between the filler and the matrix.

There are broadly speaking, three main mechanisms of adhesion, one of which is contact adhesion (Figure 1.4-A). Two surfaces in contact with one another can interact by a variety of mechanisms, including dispersion forces, dipole forces, acid-base interactions, or covalent mean to name the most common types. This type of adhesion is relevant to solid-solid interfaces, solid-

liquid interfaces and even liquid-liquid interfaces. Increasing the surface roughness can effectively improve the adhesion between two phases due to the increased contact area [19].

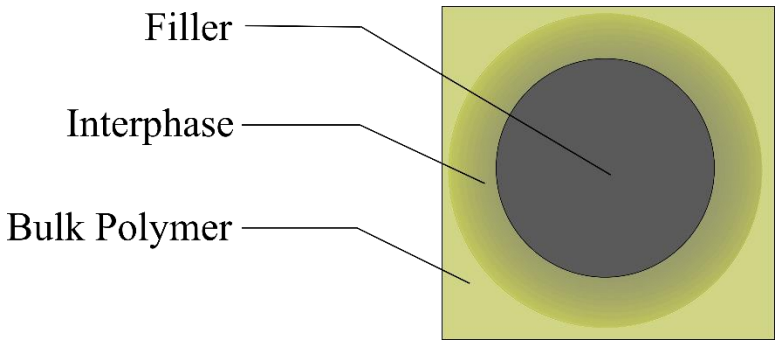

Figure 1.3 – Depiction of the filler-matrix interphase

Adhesion can also arise from the mechanical interlock of the adhesive wetting a porous adherend, as shown in Figure 1.4-B. This type of adhesion is, as the name implies, mechanical in nature. The structure of the porous network of the adherend leads to the structural reinforcement of the interface. This type of mechanism is exclusive for liquid adhesives, or adhesives that can be made to flow and wick into the porous surface of the adherend. In the context of composites, liquid thermosetting resins and thermoplastic polymer can fill the pores of many different substrates, given the proper wetting conditions. The structure of the adherend surface largely determines the improvements in interfacial strength for these types of systems [20,21].

In the case of polymer-polymer adhesion, a third mechanism wherein the polymer chains of each phase interdigitate, or interdiffuse, with each other, shown in Figure 1.4-C. The formation of such an interphase is reliant upon the mutual solubility of the polymers and typically that both polymers are above their glass transition temperatures [22]. Below the glass transition temperature, the polymer chains may not have enough flexibility to interdigitate and from an interdigitated or interpenetrating network. This mechanism is important for surfaces functionalized with silane coupling agents embedded in a polymer matrix [7,9].

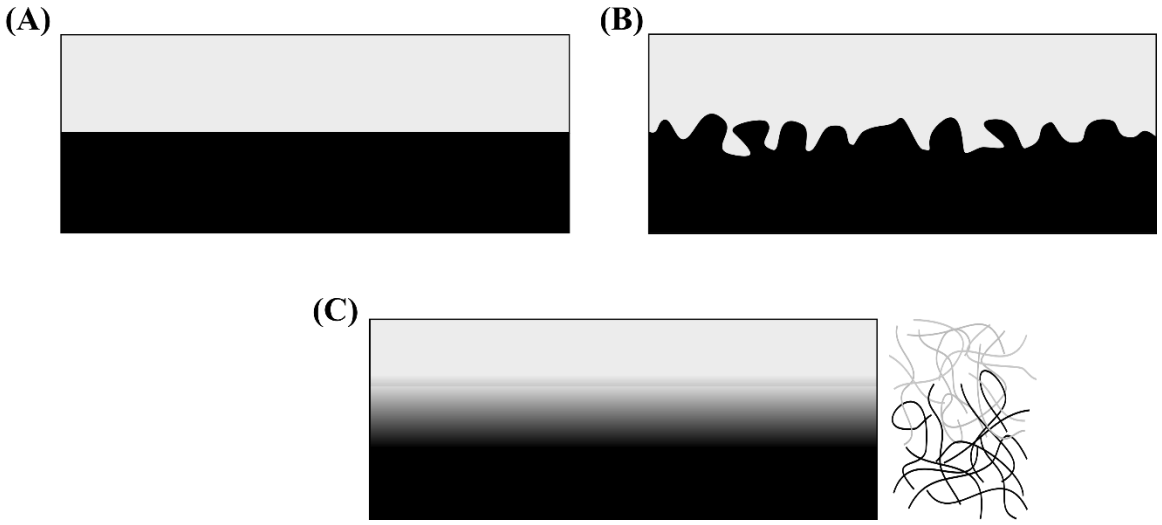

Figure 1.4 – Mechanisms of adhesion. (A) Contact adhesion, (B) Mechanical interlock, (C) polymer interdiffusion.

1.2 Engineered Interphases in Fiber Reinforced Composites

1.2.1 *Introduction*

In fiber reinforced polymeric composites (FRPCs) the fiber-matrix interphase can determine many of the mechanical properties of the composite [17,23]. The carbon-fiber epoxy interface, in particular is plagued by relatively weak adhesion often limiting the mechanical properties of their structural composites [24,25]. Many methods have been employed to alter the interphase properties including chemical modification of the fiber surface [26–30], utilizing advanced fiber sizing packages [25,31–35], and more recently by including nanoparticles into the interphase by various methods.

Nanoparticles have been shown to improve the interfacial properties through a number of mechanisms. Firstly, nanoparticles can improve the mechanical interlock between the fibers and the matrix by adding additional surface roughness [19]. In addition, nanoparticle reinforced interphases can improve the stress transfer by grading the modulus from the stiff fiber reinforcement to the softer polymer matrix [36,37]. Many types of nanoparticles have successfully

been used as interphase modifiers including metal oxide particles [38–48], polymeric particles [49–51], carbon nanotubes [52–59], as well as graphitic structures and their oxides [37,60–62].

Aside from improving mechanical properties such as the modulus, interfacial shear strength and toughness of the resulting FRPC, the incorporation of nanoparticles can impart additional functionality to the composite. Carbon fibers decorated with an electrically percolated network of carbon nanotubes have been used as strain gauges for microcrack detection [56,63], and electromagnetic shielding [64]. ZnO nanowire arrays grown from fiber surfaces have demonstrated piezoelectric properties resulting in composites with energy harvesting or dampening properties [44,65,66]. Depending on the type of reinforcing material and the morphology of the resulting interphase layer many other unique properties can be imparted to the final composite material.

The distribution and dispersion of the reinforcements in the interphase and in the bulk polymer are important parameters to consider when preparing engineered interphases. Figure 1.5 depicts the various scenarios that may be formed when preparing FRPC with engineered interphases. The nanoscopic reinforcements may be evenly dispersed in the bulk phase and the interphase, with no accumulation at the fiber-matrix interphase. Alternatively, the reinforcements may form a dense layer around the fiber's surface, while remaining well dispersed in the bulk phase. In the case of deposited or grown interphases, there may be a reinforced interphase with no reinforcements present in the bulk phase. Finally, a reinforced interphase may be formed, but aggregates of the reinforcements may exist in the bulk phase. The optimal distribution and dispersion state of the nanoscopic reinforcements depends on the end use of the composite. For example, a dense layer of conductive nanoparticles within the interphase may be required to achieve electrical conductivity in composites with otherwise unconducive fibers.

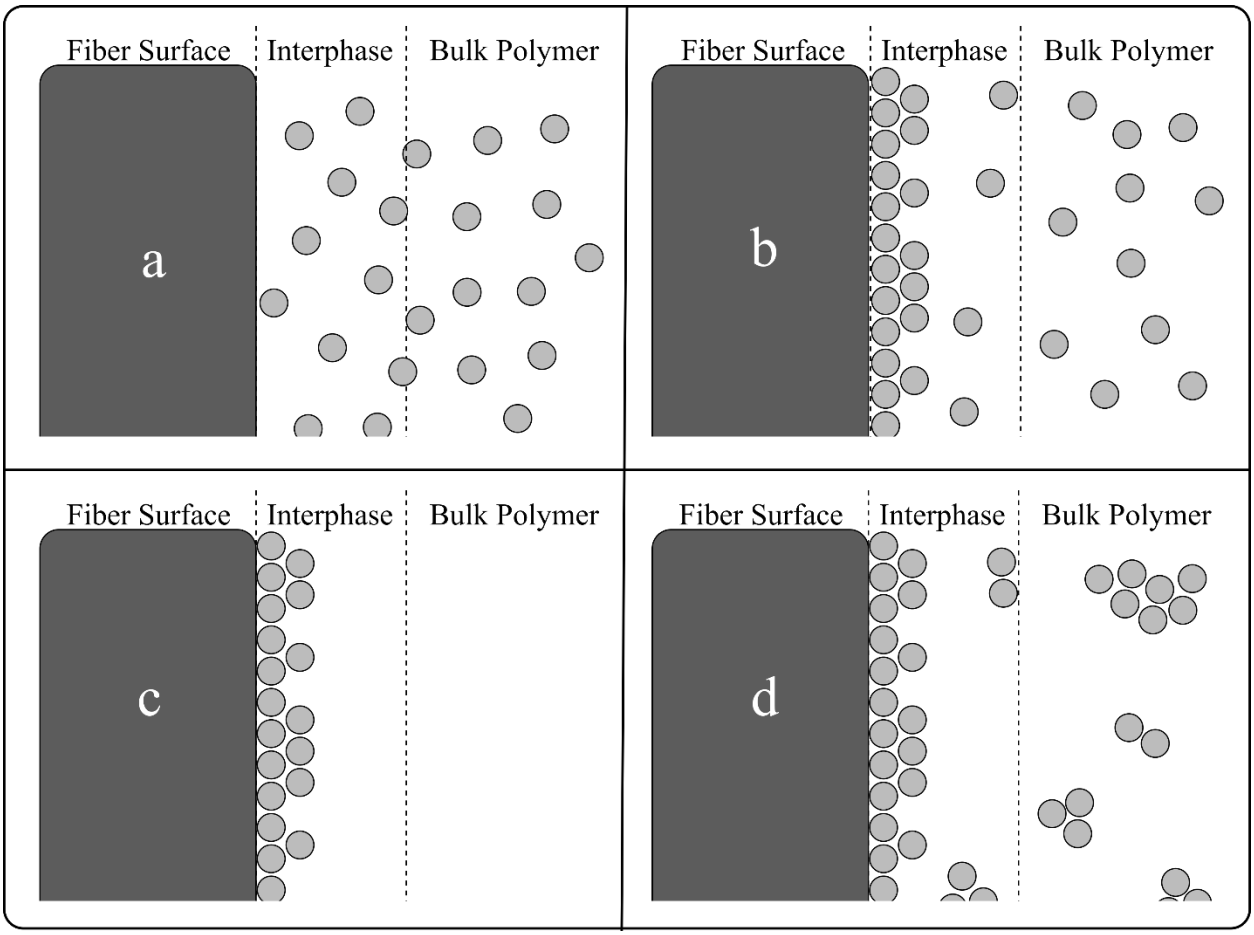

Figure 1.5 – Various scenarios for nanoparticle reinforced fibrous composite materials.

In this chapter, three strategies for preparing FRPCs with reinforced interphases are discussed. The first strategy is to grow structured interphases directly from the fiber surface using seeded growth techniques, graft polymerization, chemical vapor deposition (CVD), or electroless plating methods. The adhesion between the fiber surface and the grown interphase is often poor, and can lead to reduced mechanical properties unless the fiber surface is pretreated to improve the compatibility with the grown material. The properties of the resulting composites also depend on the morphology and density of the grown interphase, which is largely controllable by tuning the reaction conditions. Another strategy for modifying FRPC interphases is to deposit nanomaterials onto a fiber surface, which can be accomplished through electro-deposition, the use of advanced

sizing packages, or covalent particle attachment. Lastly, the self-assembly of nanoparticle-rich interphases from an initially homogeneous thermosetting resin mixture using so-called "migrating agents" is discussed, and other possible methods to prepare self-assembled interphases such as phase-separation and polymer mediated depletion interaction are proposed.

1.2.2 *Grown Interphases*

Seeded growth techniques and other aqueous solution processing techniques can be used to grow nanoscale features from fiber surfaces such as nanowhiskers or other high aspect ratio materials. CVD is the most commonly used technique to grow single-walled carbon nanotubes (SWCNTs) on a variety of fiber surfaces including carbon [64,67–70], glass [71], and ceramic [72] fibers. Multi-walled carbon nanotubes (MWCNTs) have also successfully been grown from fiber surfaces via a similar seeded growth technique [64], at much milder growth conditions than are required for SWCNTs. Aqueous solution processing is commonly employed to grow metal oxide NWs such as ZnO [40,65,66,73–76], α-FeOOH [77], MnO_2 [78] from a variety of fiber surfaces. Grown interphases are often used to improve the adhesion between the reinforcing fiber and the bulk matrix and the quality of the interphase is critically important in determining the ultimate mechanical properties of the resulting composite. Fibers with grown interphases have also been successfully used to prepare composites with applications in chemical sensing [77], electromagnetic interference (EMI) shielding [64], and energy harvesting [65,66].

Growing interphases from fiber surfaces typically requires several processing steps, including removal of adsorbed processing aids or sizings from the fibers, deposition and annealing of nanoparticle seeds or precursors onto fibers, and finally the subsequent growth of the interphase. For example, SWCNTs are typically grown from catalytic Ni seeds via CVD at temperatures ranging from 700-1200 °C, while MWCNTs can be grown at more moderate temperatures around

550 °C [64]. carbon fibers exposed to these relatively harsh reaction conditions can thermally degrade, leading to a reduction in the modulus and tensile strength of the bare fibers. Any grown interfacial layer must, therefore, overcome any decreases associated with fiber degradation in the resulting multiscale composite to be practical. In the case of ZnO nanowhiskers, however, the fiber processing conditions are relatively benign, requiring only solution based chemistry with moderate adjustments in pH and relatively low processing temperatures (≤ 150 °C) [40,65,73–75,79].

Growing structured interphases results in the elimination of the original fiber-matrix interface and the creation of two new interfaces, one between the fiber surface and the grown interphase, and the other between the grown interphase material and the bulk polymer, as shown in Figure 1.6. If the adhesion of either of the created interfaces is weaker than the original fiber-matrix interface the resulting mechanical properties of the composite could be compromised [79]. The surface chemistry of the fibers with grown ZnO nanowhisker interphases was shown to affect the interfacial shear strength (IFSS), which is a measure of the interphase strength and adhesion, of the resulting composites [76], indicating the necessity of a strongly adhered precursor layer. In addition, the grown interphase material should be fully wet by the bulk resin for optimal adhesion, as any trapped voids would result in reduced stress transfer and strength of the interphase region.

Composites with grown interphases are easily processed because they do not alter any of the bulk resin properties. Nanomaterials dispersed in the bulk resin, however, often lead to processing problems because the dispersed nanofillers increase the viscosity of the resin, and the particles can be physically filtered by the reinforcing fibers leading to aggregate formation and unevenly distributed particles [80]. Dispersed high aspect ratio nanofillers such as nanowhiskers and CNTs are especially difficult to process by vacuum assisted resin transfer molding (VARTM), while woven fiber mats with ZnO nanowhisker arrays are readily processed using VARTM [66].

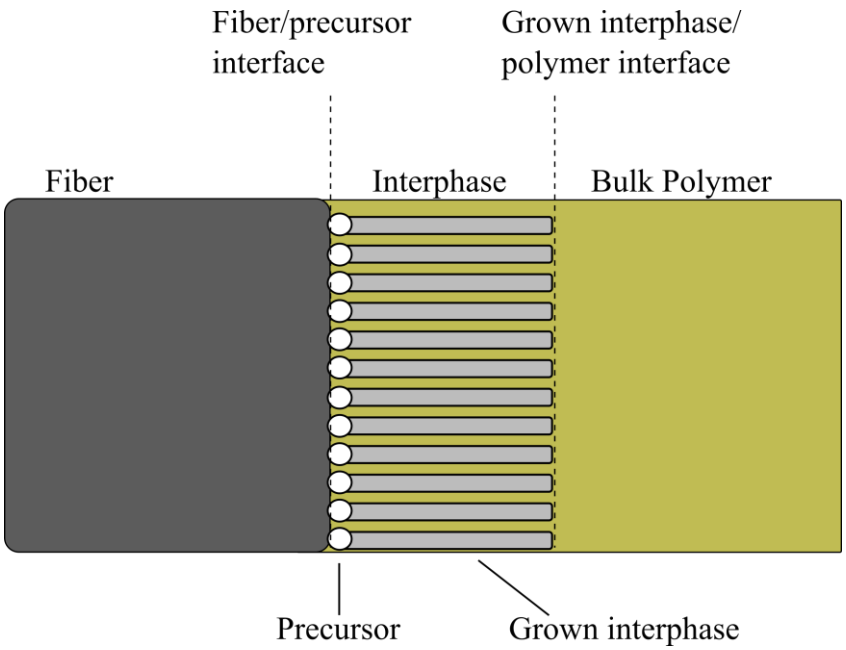

Figure 1.6 - Image of a fiber with a grown interphase, using a seeded growth type procedure. The precursor is initially deposited on the fiber surface, and the interphase is subsequently grown from the precursor. The fibers are subsequently impregnated with a polymeric matrix material.

Growing interphases from fiber surfaces is a widely-used method to control the fiber-matrix interphase properties. The increased surface area, improved mechanical interlock, and the presence of a graded modulus contribute toward the improved adhesion between the fiber and the matrix. However, incomplete wetting of the interphase layer by the matrix material can lead to voids in the interphase and reduced interphase properties, as depicted in Figure 1.7. In addition, the adhesion between the fiber surface and the precursor layer is often poor, leading to interfacial failure at the fiber surface sometimes resulting in an observed decrease in interphase properties like the IFSS. Surface pretreatment of the fibers can increase the chemical compatibility with the precursor, and is often needed to prevent failure at the fiber-precursor interface [79].

A benefit of seeded growth techniques is that the morphology of the grown interphase is largely controllable by varying the seeding, growth or annealing conditions. The orientation, alignment, uniformity, and aspect ratio of the grown interphase are all important parameters to

consider, and should be optimized for each application. Typically, more uniformly aligned interphases lead to greater improvements in the IFSS compared to randomly oriented interphases. Grown NW arrays showed that NW length and diameter are important factors for improving the IFSS, although the results are convoluted with the total increase in total interphase material content associated with larger NWs. Studies that investigate the effects of the interphase morphology at a fixed interphase content would more fairly assess the effects of the interphase morphology on the composite properties.

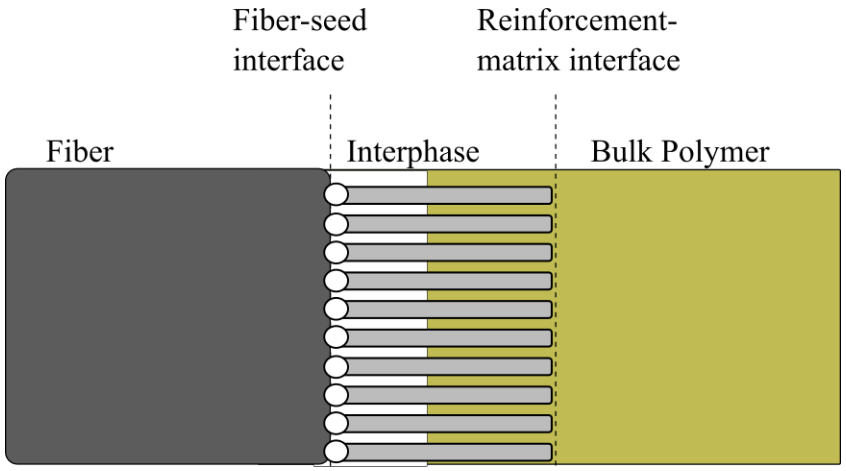

Figure 1.7 – Incomplete wetting of a grown interphase by the bulk polymer

Many different materials can be grown from fiber surfaces enabling the production of multifunctional multiscale composites with a wide variety of applications in energy harvesting, damage detection, EMI shielding, and microwave absorption. Additionally, grown interphases can tailor the electrical, thermal and mechanical properties of the resulting composites. Depending upon the growth conditions and type of reinforcing fiber, however, the mechanical properties of the reinforcing fiber can be severely decreased, reducing the overall properties of the composite. New nanowire synthesis and growth techniques that are benign to the fiber may lead to additional multifunctional composites that do not have to sacrifice any mechanical properties of the fiber.

Another potential drawback of using grown interphases in FRPCs to improve the interphase mechanical properties is that often micrometer sized coatings are required to achieve meaningful improvements, significantly increasing the effective diameter of the fiber. Ultimately the increased fiber diameter would decrease the quantity of reinforcing fibers for a given resin volume fraction, leading to a decrease in mechanical properties or weight savings in the final composite. The application of grown interphases in unidirectional high-volume fraction composites seems limited unless the required thickness of the interphase can be decreased to achieve similar improvements.

1.2.3 *Deposited Interphases*

Unlike grown interphases, where the interphase material is grown directly from the fiber surface, composites with nanoparticle reinforced interphases may be prepared by depositing some previously prepared interphase material at fiber surfaces using a variety of techniques. The use of electrostatic attraction [39], electrophoretic deposition [57,58,81], advanced fiber sizings [82–85], and chemical reactions [46–48] are the most common methods to deposit interphases at fiber surfaces. Often, combinations of these techniques can be used to achieve a more robust interphase; for example, electrostatic attraction can be used in combination with chemical reaction to direct reactive nanoparticles to fiber surfaces and subsequently bond them to the fiber surface [50].

The inclusion of nanomaterials in advanced fiber sizing packages has recently been used to successfully reinforce the fiber-matrix interphase. Traditional sizing packages may contain many components including film-formers, surfactants, silane coupling agents, lubricants as well as other processing aids dispersed in a low viscosity, volatile solution. Sizings are applied to fibers through a generic dip coating process and the quality of the resulting film, called the size, depends on the fiber withdrawal rate, the sizing formulation, and the drying conditions. The inclusion of well dispersed nanoparticles into the sizing formulation presents an easy method for incorporating

nanoparticles into the interphase that is readily scalable at an industrial level, and is shown schematically in Figure 1.8. Similar to grown interphases, these advanced sizing packages can improve the mechanical properties of composites by improving the mechanical interlock and interphase toughness. The deposition of a uniform, aggregate free, nanoparticle interphase is essential to obtain the best results. Ultrasonication and shear mixing can been used to help keep the particles well dispersed during the deposition [84].

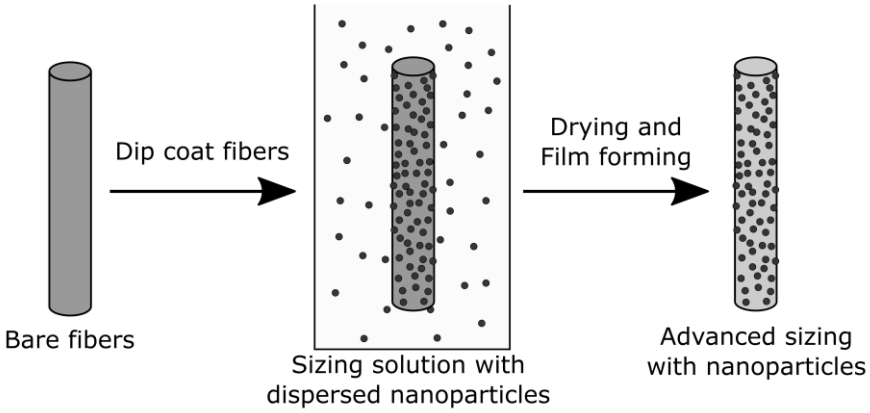

Figure 1.8 –Process for applying advanced fibers sizings with nanoparticles.

Electrostatic and electrophoretic deposition (EPD) of nanoparticles at fiber surfaces is almost always conducted in an aqueous solution due to the low viscosity, high dielectric constant and facile control of pH and ionic strength. The deposition of nanoparticles to fiber surfaces is achieved through coulombic attraction between oppositely charged fibers and nanoparticles. Since most metal oxides and carbon fibers typically charge negatively in water over a wide range of pH values, some surface functionalization or external bias is often required to set up the attractive potential between the particles and fibers. Silane coupling agents [7–9] are commonly used to alter the surface chemistry of nanoparticles or fibers, although many other alternative functionalization strategies exist. In the case of a conductive fiber reinforcement, such as a metal or carbon fiber, an

external voltage source can be used to directly impart the desired charge onto the fiber surface, with some control over the magnitude, as shown in Figure 1.9.

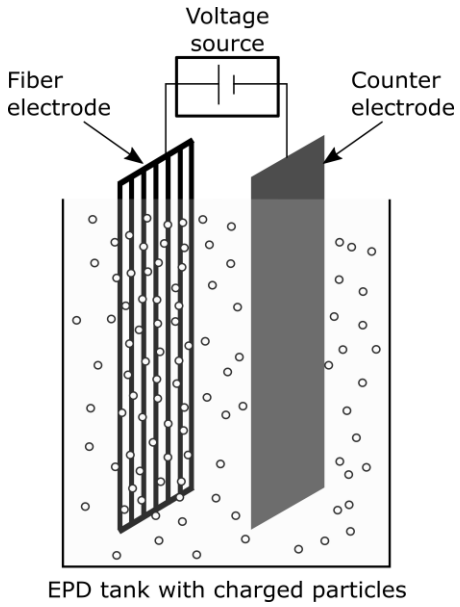

Figure 1.9 – Electrophoretic deposition of charged nanoparticles to oppositely charged fiber surfaces.

EPD, while a simple and versatile method, can damage the mechanical properties of the fibers, especially if they are coated with a sizing. Schaefer et al. [57] demonstrated that carbon fibers exposed to a 5 V/cm electric field for 1 minute decreased the Weibull modulus and average tensile strength for both sized and unsized fibers. The decreased Weibull modulus indicates that additional surface flaws may be introduced, while the decreased tensile strength indicates that the bulk fiber may also be damaged. Sized fibers were found to experience greater decreases in the tensile properties, likely due to the degradation or dissolution of the sizing. Their results showed that the fiber tensile properties decreases were proportional to the EPD processing time as well. The determined IFSS of the EPD damaged carbon fibers, however, showed a significant 70% increase in the IFSS, compared to the sized fibers. When functionalized carbon nanotubes were deposited

with the same EPD conditions, a 207% increase in the IFSS was obtained, compared to the sized fibers. While these improvements in the IFSS are impressive, the decrease in fiber tensile properties may ultimately limit the use of EPD for preparing structural composites.

The imposition of an external electric field to draw nanoparticles towards fiber surfaces, as is used in EPD, is not necessary if the two surfaces have opposite charges in a given solution. Most fibers and interphase modifiers, however, possess a negative surface charge in aqueous solutions over a wide range of pH values, often requiring surface functionalization of the fiber, the nanomaterial, or both to achieve the desired electrostatic attraction. Silane coupling agents and other surface modifications are commonly employed to impart positive or negative surface charge to fibers or the nanomaterials with good success. The resulting coverage of nanoparticles depends on the ionic strength of the electrolyte solution. In low ionic strength solutions, the particle-particle repulsive forces can limit surface coverage. As the ionic strength increases this repulsive range, measured by the Debye length, decreases allowing for a more densely packed surface. If the ionic strength is increased further the electrostatic forces may be screened out completely, and the particles may deposit as aggregates or not deposit at all. Thus, in order to achieve a uniformly modified interphase the surface chemistry of the fibers and particles should be optimized, as well as the pH and ionic strength of the electrolyte solution. Figure 1.10 shows the coverage of the 26 nm particles in solutions of varying KNO_3 concentrations.

Rutz and Berg [39] studied the effects of four different sizes of polyethylenimine functionalized silica nanoparticles deposited onto glycidyloxypropyltrimethoxysilane treated glass fibers using electrostatics. The surface coverage was shown to depend on the ionic strength, which was altered by increasing the background salt content. The optimization of the salt content was performed for 16 nm, 26 nm, 71 nm, and 100 nm particles. The measured improvements of the

IFSS were size dependent, with a maximum increase of 35% for the 26 nm particles compared to the bare fibers and approximately 8% over the GPS coated fibers. Smaller particles than this were hypothesized to not significantly improve the surface roughness of the fiber, and larger particles were not well adhered to the fiber surface.

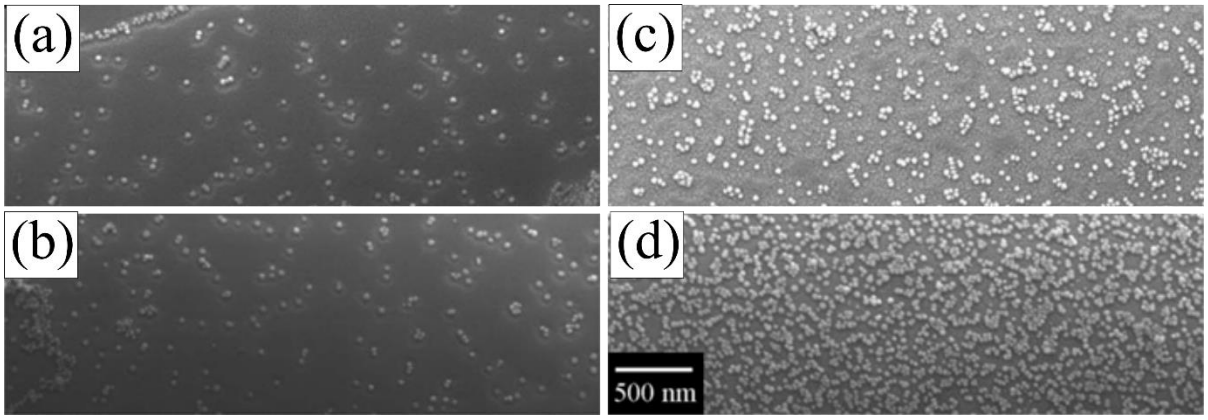

Figure 1.10 - 26 nm PEI-functionalized silica particles deposited onto GPS-functionalized E-glass fiber surfaces at varying KNO_3 concentrations. (a) 0 μM, (b) 50 μM, (c) 250 μM, and (d) 750 μM. Image adapted from [35].

Multilayers of nanoparticles can be deposited in the fiber-matrix interphase through the use of alternating electrostatic interactions in a layer-by-layer (LBL) process [86,87], in which the fiber coating is composed of alternating layers of oppositely charged material. In the LBL method, the first deposited layer has a charge opposite that of the fiber, leading to electrostatic attraction. If the coating is dense enough the surface charge can be reversed and a second layer, with the same charge as the original fiber, can be deposited. The LBL coating process can be repeated nearly indefinitely, up to several hundreds of layers [88] with alternating layers of positive and negative charge, until the desired thickness of the interphase is reached. Layers can consist of cationic or anionic polymers, or charged nanoparticles affording some flexibility in designing the interphase. A depiction of the LBL process is shown in Figure 1.11.

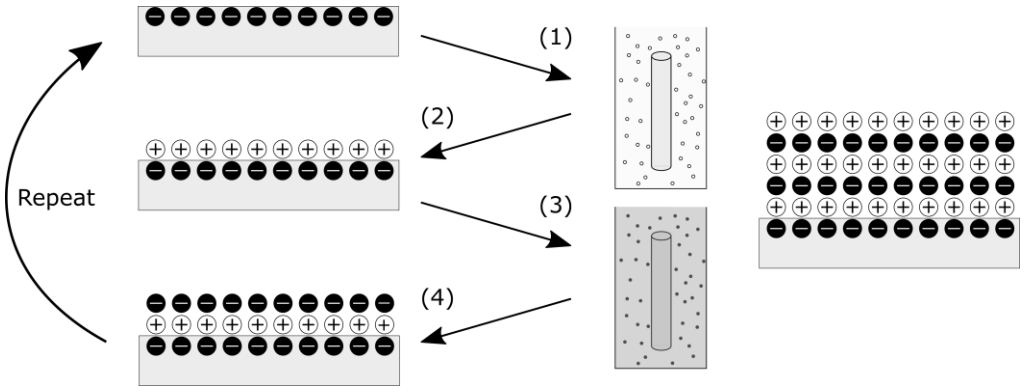

Figure 1.11 – Representation of the LBL process for an initially negatively charged substrate. (1) Immersion of a negative surface in a solution containing positive material. (2) Rinsing and drying. (3) Immersion in solution of negative material. (4) Rinsing and drying. Steps (1-4) may be repeated many times to achieve a desired coating thickness.

LBL deposition in FRPCs dates back to the 70's where it was utilized to create thick interphases around glass fiber surfaces [87]. Peiffer [89] found that the coating thickness and the glass transition temperature of the deposited interphase had significant impacts on the notched Izod impact strength. The positive layers consisted of ~35 nm alumina particles, while the negative layers consisted of a variety of different latex particles all approximately 1 μm in diameter. The latex particles were melted and lightly crosslinked to create the final film before the fibers were embedded in an epoxy matrix. They found that films approximately 2 μm thick tended to have the best impact strength regardless of the latex type, and that interphases with glass transition temperatures below room temperature significantly improved the impact strength. Their results highlighted that significantly flexible interphases can provide additional energy absorption compared to more brittle interphases.

LBL deposition of gold nanoparticles coated with a semifluorinated silane were used to achieve super-hydrophobicity on electrospun poly(methyl methacrylate) fiber surfaces [90]. Altering the surface roughness can significantly alter the wetting characteristics to either promote or hinder wetting if the intrinsic contact angle on a flat surface is less than or greater than 90°,

respectively [91–93]. A similar strategy could be used to improve the wetting of reinforcing fibers in FRPCs, provided that the intrinsic contact angle is less than 90°.

The dispersion state of the nanofillers, as well as their adhesion to both the fiber and matrix are extremely important parameters for composites with deposited interphases. If the particles are not well dispersed during the deposition process, aggregates can be deposited on the fiber surface, which act as local stress concentrators. The uses of shear mixing, electrostatic repulsion, and ultrasonication [81] have all been successful in reducing the number of deposited aggregates and exfoliating 2D materials such as clays or graphene. As with fibers with grown interphases, the adhesion strengths at the fiber-nanoparticle interface and the nanoparticle-matrix interface, are critically important parameters. If the adhesion is weak at either interface the mechanical properties of the interphase and thus of the overall composite may be reduced. Surface functionalization of the fibers, the nanoparticles, or both, can help to alleviate problems associated with poor nanoparticle adhesion, especially if nanoparticles are made reactive towards the fiber and the matrix material.

Care should be taken to ensure that the deposition method does not significantly damage the fiber tensile properties, especially with electrophoretic deposition onto conductive fiber surfaces. Sizings present on fibers used as electrodes are especially susceptible to degradation, leading to decreases in the tensile strength of the fibers. Electrostatic attraction and reaction deposited interphases are considerably less damaging to the reinforcing fibers, but typically require unsized fibers in order to deposit the interphase. Advanced fiber sizing packages formulated with nanoparticles provide an especially appealing method to improve interphase properties without damaging the fibers, since the technology based around sizing packages is extremely well-developed industrially.

1.2.4 *Self-Assembled Interphases*

The self-assembly of nanoparticles into well-defined structures in thermoplastics or thermosets is an extremely active area of research [12,15,16,94–96] with many applications. The use of self-assembly methods to direct nanoparticles to the fiber-matrix interphase, however, has received much less attention, and only a few examples exist in the literature. Recently, so-called "migrating agents", which are typically thermoplastic additives, have been used to spontaneously direct nanoparticles, which were previously in the bulk resin, to carbon surfaces in a thermosetting epoxy resin during the course of the cure (see Figure 1.12) [41–43,49,97]. Migrating agents have successfully been used to direct various types of nanoparticles to carbon fiber and glass fiber surfaces with a variety of surface finishes, indicating that the self-assembly process is fairly robust.

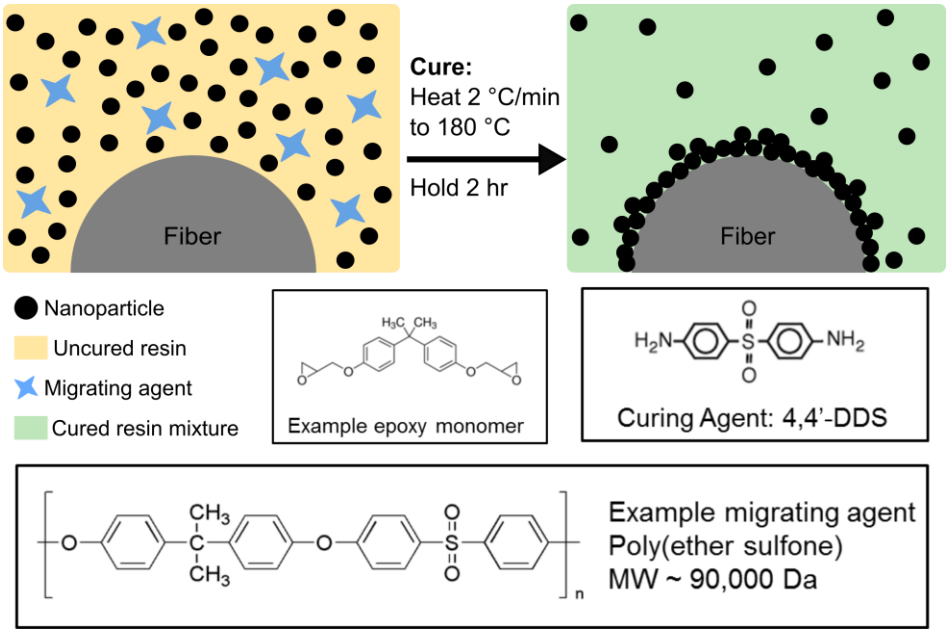

Figure 1.12 - Components used to form self-assembled nanoparticle reinforced interphases using migrating agents

Self-assembled dendritic nanoparticle reinforced interphases improved several composite mechanical properties [49]. The 0° flexural, tensional and compressive strengths, and ILLS all showed modest improvements (over 10%) compared to the resin without the interphase, while the

mode I fracture toughness showed an increase of approximately 200% over that of the resin without nanoparticles and migrating agent. Because no data were presented with nanoparticles in the absence of migrating agent, it is unclear exactly how much the localization of nanoparticles in the interphase improved the composite mechanical properties over what the particles alone would have accomplished, although inclusion of the nanoparticles to the interphase seemed to promote cohesive failure in the bulk resin instead of interfacial failure at the fiber surfaces, indicating improved interphase strength. Functionalizing the particles to have strong interactions with, or to be reactive towards, the fiber surface may further improve the mechanical properties of the resulting composites.

Polyether sulfone (PES) migrating agents that are incorporated into an epoxy resin, composed of tetraglycidyl diaminodiphenylmethane (TGDDM) and 4,4'-diamino diphenyl sulfone (4,4'-DDS), can concentrate ~100 nm epoxy functionalized silica nanoparticles at sized carbon fiber surfaces. SEM micrographs of mode I fracture surfaces of FRPC, as seen in Figure 25, demonstrate that the inclusion of the PES migrating agent at 4 wt% to an epoxy resin containing 6 wt% epoxy functionalized nanoparticles is able to preferentially accumulate nanoparticles in the vicinity of a sized carbon fiber without disturbing the dispersion state of the particles in the bulk phase. When PES in not included in the formulation, no particle accumulation is observed in the vicinity of the fiber surfaces, and interfacial failure is observed at the fiber surface.

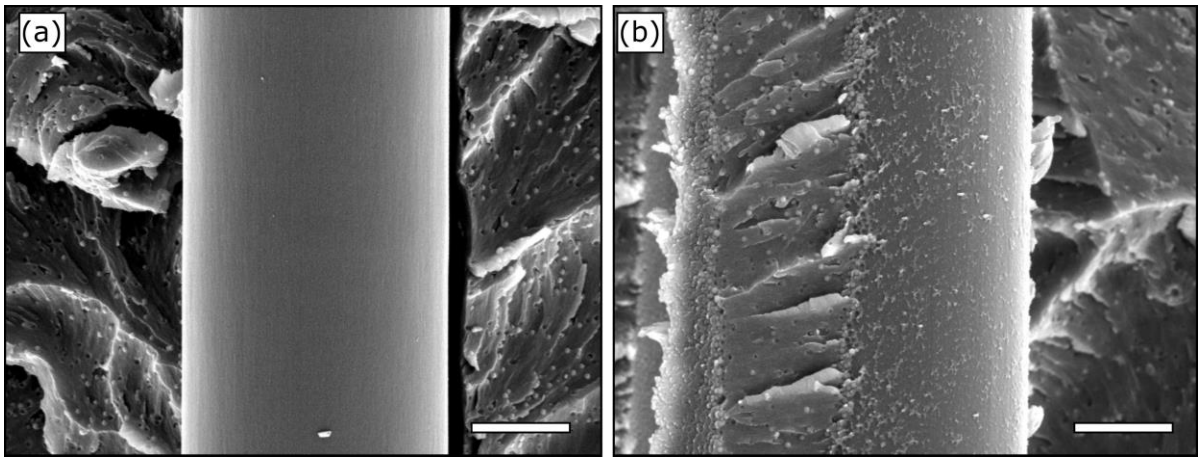

Figure 1.13 - SEM micrographs of sized carbon fibers embedded in an epoxy matrix (a) 6 wt% 100 nm particles without migrating agent and (b) 6 wt % 100 nm particles with 4 wt% PES migrating agent. Scale bars represent 2 μm.

While the use of migrating agents to prepare self-assembled nanoparticle-reinforced interphases is a relatively recent topic of research, migrating agents present several advantages over methods to incorporate nanoparticles near fiber surfaces. First, they avoid the necessity for aqueous solution processing, which can generate large amounts of waste and sometimes damage fiber sizings. Secondly, the use of migrating agents does not require any alteration of the fiber surface chemistry or sizing materials. And thirdly, it is easily scalable since the only additional step required is to blend in the thermoplastic migrating agent to the resin mixture before the cure begins.

Nanoparticle-reinforced fiber-matrix interphases may also be prepared by a phase separation process. Arguably, from a thermodynamic perspective, the most important parameter for determining into which phase a given nanoparticle will reside is the relative wettability of the particle in each phase. However, the kinetics of the phase separation can arrest nanoparticles before they reach their desired thermodynamic location. Thus, the particle mobility, which is related to the melt viscosity and the particle size, as well as the kinetics of phase separation are important to

consider. In thermosetting systems that undergo reactive phase separation, the heating schedule can significantly alter the rates of reaction and phase separation leading to differences in the final resin morphology. By carefully tuning the wettability of the particle surface, often by surface functionalization, and controlling the phase separation kinetics, particles can be preferentially sequestered into one of the phases, or concentrated at the interface between the two phases [16,98–101].

The relative wettability of a nanoparticle between two phases is described by the wetting parameter, *w*, as described by Young's Equation (1.1)

$$w = \frac{\sigma_{2P} - \sigma_{1P}}{\sigma_{12}} \tag{1.1}$$

where σ_{1P} is the interfacial tension between the particle and phase 1, σ_{2P} is the interfacial tension between the particle and phase 2, while σ_{12} is the interfacial tension between phase 1 and 2. Assuming equilibrium conditions are met, if *w* is greater than 1, the particles will be found only in phase 1. While if *w* is less than -1, the particles will reside only in phase 2. For values of *w* between -1 and 1 the particles are thermodynamically preferred to reside at the interface between the phases. Interfacial tensions can be estimated from knowledge of the polar and dispersion components of the surface tensions using various techniques that are beyond the scope of this review. The reader is referred to Taguet et al. [13] for a list of surface tensions of some common polymers and particulate fillers. The temperature dependence of the surface and interfacial tensions must also be taken into account when trying to estimate the wetting parameter.

There are two potential cases by which phase separation could lead to the formation of self-assembled, nanoparticle-rich, fiber-matrix interphases, as shown in Figure 1.14. The first scenario requires that the fiber surface and the particle are both preferentially wet by the same phase, i.e. the wetting parameter is of the same sign and greater than 1 in absolute magnitude for the fiber

and particle. In this scenario, a phase separation event would lead to a fiber wet by a single polymer phase that also contains nanoparticles, as shown in Figure 1.14 (b). In the second scenario, the fiber is wet completely by a single phase, while the particle is intermediately wet between both phases ($-1 < w < 1$). Here the nanoparticles should preferentially concentrate at the polymer-polymer interface near the fiber surface, and at the other polymer-polymer interfaces in the bulk, as seen in Figure 1.14 (c). Nanoparticle aggregation within the phases or at the interface between two phases should be avoided to prevent local stress concentrations, and may be achieved by adequate surface functionalization of the nanoparticles to provide steric repulsion between particles.

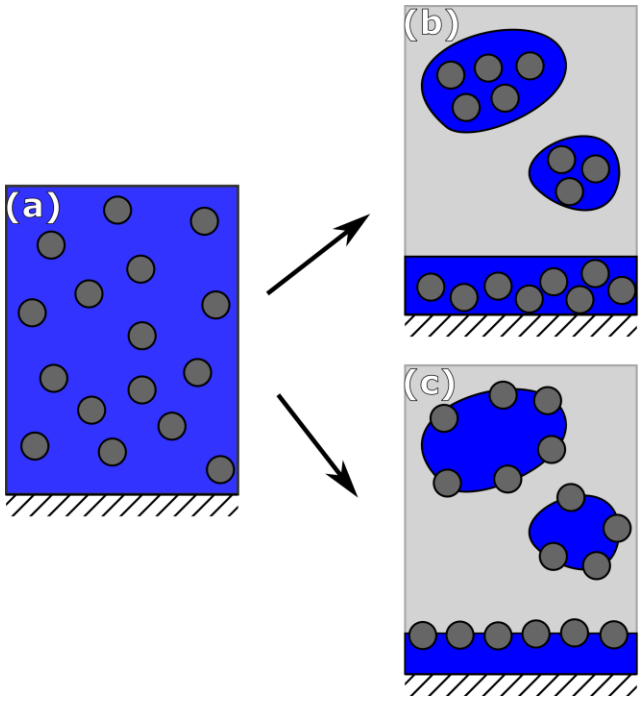

Figure 1.14 - Possible mechanism by which phase separation may assemble an interphase at fiber surfaces. (a) A well-dispersed nanoparticle filled homogeneous polymer blend before phase separation. (b) Morphology predicted if the particles are completely wet by a single phase (represented as the dark blue region). If the fiber surface is also wet by the same phase, an interphase may develop as proposed. (c) Morphology for particles that are wet by both phases and the resultant interphase structure.

Lastly, the use of polymer-mediated depletion forces to form self-assembled interphases shows much promise. Depletion forces, first described by Asakura and Oosawa [102], arise from the presence of a dissolved thermoplastic polymer, or other entity, which is excluded from the region of volume, known as the overlap volume, between two objects as they begin to approach one another. Figure 1.15 illustrates the depletion interaction for two scenarios. First for two smooth, similarly sized spheres approaching one another, and secondly for a smooth sphere approaching a flat surface in a macromolecule solution. The shape of the overlap volume between the objects depends directly on the geometry of the two approaching objects and can be calculated by computing the integral of the intersection of the two objects. For simple geometric shapes closed-form solutions for the overlap volume exist, while for more complicated geometries, such as a sphere approaching a cylinder with surface features, numerical methods can be used to compute the overlap volume [103].

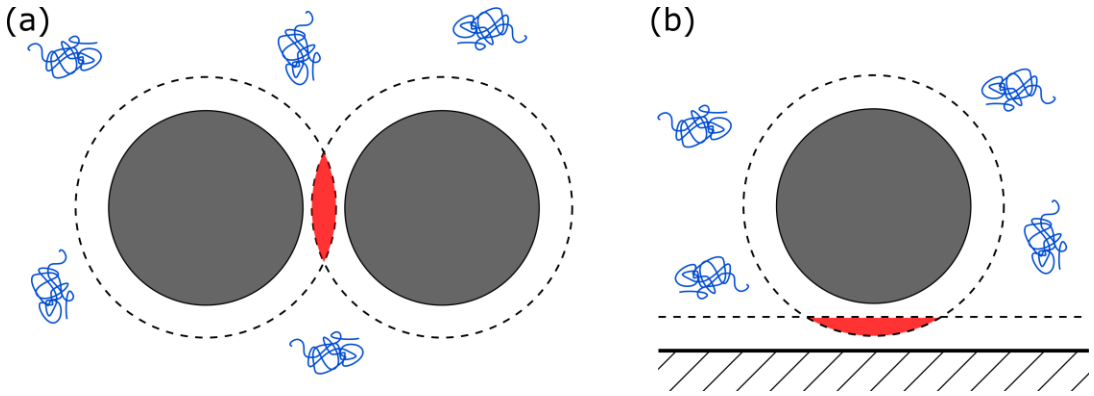

Figure 1.15 - Depiction of depletion interaction (a) between two colloidal spheres in a polymeric solution, and (b) between a sphere and a flat surface. Dashed lines represent the excluded volume, and the overlap volumes are shown in red.

The strength of the depletion force is directly proportional to the overlap volume, which indicates that certain geometries should be favored heavily. Exploiting geometric features and surface roughness has led to the self-assembly of many different structures in low viscosity media. In the context of self-assembled interphases in FRPCs, the geometric dependence of the depletion

force could be exploited to produce self-assembled interphases without inducing the formation of aggregate structures in the surrounding matrix.

The Gibbs free energy associated with depletion interaction depends on the osmotic pressure difference and the overlap volume, and is given simply by Equation (1.2).

$$\Delta G_{dep} = -\Pi_b V_o \tag{1.2}$$

where Π_b is the bulk osmotic pressure, and V_o is the overlap volume, which is dependent upon the geometry and surface roughness of larger entities, and the size of the depletant. The bulk osmotic pressure for macromolecule solutions is well approximated by Equation (1.3).

$$\Pi_b = c_b RT\left(\frac{1}{MW} + c_b B_2\right) \tag{1.3}$$

where c_b is the bulk macromolecule mass concentration, R is the universal gas constant, T is the absolute temperature, MW is the molecular weight of the macromolecule, and B_2 is the second osmotic virial coefficient.

The overlap volume for a sphere approaching a second similarly sized sphere, $V_{s\text{-}s}$, is given by Equation (1.4),

$$V_{s-s} = \frac{\pi}{6}(D_d - S_o)^2\left(3R_p + D_d + \frac{S_o}{2}\right), \text{ for } S_o \leq D_d \tag{1.4}$$

where D_d is the diameter of the depletant, S_o is the distance of closet approach between the bare particle surfaces, and R_p is the radius of the spheres. For macromolecule depletants, the value of D_d is approximately twice that of the radius of gyration, R_g, of the polymer if the solution is dilute enough. In more concentrated polymer solutions, specifically above the overlap concentration of the polymer, D_d is more closely approximated by the correlation length, i.e., the average distance between entanglement points in the entangled polymers. In the so-called “colloidal limit” of

depletion interaction, where the approaching objects are much larger than the depletants, i.e., $R_p >> D_d$, the equation for the overlap volume between two spheres simplifies to Equation (1.5).

$$V_{s-s} = \frac{\pi}{2} R_p (D_d - S_o)^2, \text{ for } R_p \gg D_d \,\&\, S_o \leq D_d \tag{1.5}$$

The overlap volume between a sphere and a cylinder is more complicated, and a simple closed-form solution does not exist, but can be readily computed using numerical methods. The sphere-cylinder geometry, however, can be well approximated by a sphere approaching a flat plate if the cylinders are significantly larger than the spheres, which is the case for small nanoparticles (< 0.1 μm) approaching reinforcing fibers (~10 μm). The overlap volume between a smooth sphere approaching a flat plate, $V_{s\text{-}p}$, is expressed by Equation (1.6).

$$V_{s-p} = \frac{\pi}{3} (D_d - S_o)^2 \left(3R_p + \frac{D_d}{2} + S_o\right), \text{ for } S_o \leq D_d \tag{1.6}$$

In the colloid limit, where the depletants are significantly smaller than the particles, the sphere-plate overlap volume simplifiers further to Equation (1.7), which is twice that of equal sized spheres.

$$V_{s-p} = \pi R_p (D_d - S_o)^2, \text{ for } R_p \gg D_d \,\&\, S_o \leq D_d \tag{1.7}$$

The forces associated with the depletion interaction are typically quite small, of the order of a few kT, but are responsible for a variety of self-assembly phenomena in low viscosity media, for example, the formation of micelle-like structures consisting of Janus particles containing smooth and rough surface patches [94]. Yarlagadda [103] demonstrated the importance of the shape of the overlap volume in promoting or preventing depletion forces from acting on two surfaces, showing that different types of aggregates were formed at varying polymer (depletant) concentrations. Figure 1.16 shows examples of the types of structures formed in the study. At low polymer concentrations, and therefore relatively weak depletion forces, nanoparticles only deposited themselves at edge sites, which had the largest overlap volume for a given separation distance.

Increasing the polymer concentration led to surface aggregation, with dispersed nanoparticles in the bulk. Higher concentrations of polymer caused surface aggregation as well as aggregation in the bulk phase, while still higher concentrations of polymer caused rapid aggregation in the bulk phase.

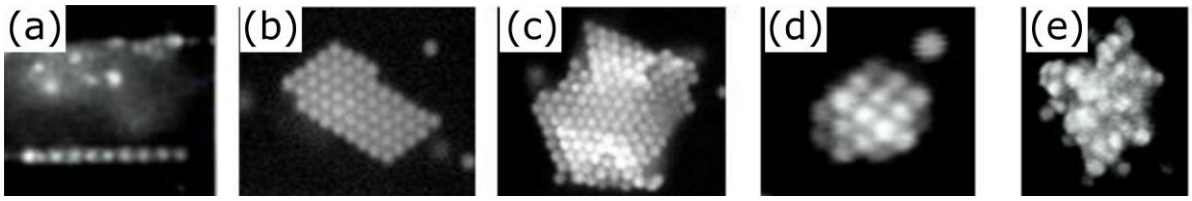

Figure 1.16 - Micrographs of 1 μm particles in increasing order depletion strength. (a) Edge nucleation, (b) surface nucleation, (c) surface nucleation and growth into the bulk, (d) bulk nucleation and growth, and (e) rapid bulk aggregation. Adapted from [120], with permission from the author.

The use of depletion interactions to form self-assembled interphases in fiber reinforced thermoplastic composites remains unstudied, but has potential in thermosetting resins. The inclusion of macromolecules into a resin solution containing both nanoparticles and fibers could, under the appropriate conditions, deposit nanoparticles at the surface without causing significant nanoparticle aggregation in the bulk phase, again due to the increased overlap volume between a nanoparticle and fiber. The overlap volume, and thereby the depletion force, between a sphere and a flat plate, which closely resembles the particle-fiber geometry, is exactly double the overlap volume between two equally sized spheres for a given separation distance [104]. Depletion interactions thus correctly describe the qualitative behavior seen with the self-assembled interphase of nanoparticles at carbon fiber surfaces using migrating agents, as shown below in Figure 30. The migrating agent is a thermoplastic polymer that upon inclusion in moderate amounts forms a dense self-assembled interphase around fiber surfaces during the course of the cure, with well dispersed nanoparticles in the bulk phase. The inclusion of larger amounts of the

migrating agent resulted in a similar interphase, but also caused aggregation of the nanoparticles in the bulk, consistent with an increase in the depletion force.

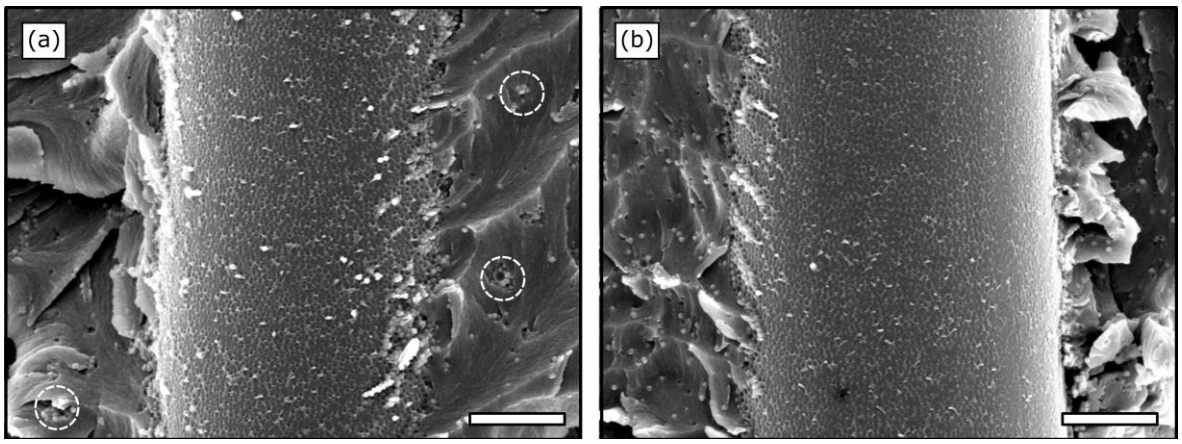

Figure 1.17 - SEM images of carbon fiber embedded in an epoxy matrix containing (a) 6.7 wt% PES migrating agent and 5.6 wt% 100 nm silica particles. (b) 3.5 w% PES migrating agent and 5.8 wt% 100 nm silica particles. Some nanoparticle aggregates in the bulk resin are circled in white. Scale bars represent 2 μm.

Depletion interactions are relatively unstudied outside of aqueous polymeric solutions, and many additional complications arise when used in thermosetting solutions, such as their increased and increasing viscosity, as well as the limited reaction time that may prevent the system from reaching the thermodynamically stable configuration. The processing conditions, especially the cure cycle, must be carefully controlled in order to optimize the interphase self-assembly conditions. Similar to many other techniques used to prepare nanoparticle reinforced interphases, the adhesion of the particles to the fibers may depend on the surface chemistry of the particles and the fibers, and surface functionalization may be needed to improve the particle adhesion to fibers. Nevertheless, the inclusion of nanoparticles into the interphase may result in a graded modulus which can improve the stress transfer to the reinforcing fibers, even in the absence of particle attachment. Additionally, the particles may act as crack arresters, deflectors, or both, to increase the toughness of the interphase.

The adhesion of the particles in self-assembled interphases may be poor unless adequate fiber treatment, or nanoparticle functionalization are performed. The incorporation of thermally or optically activated reactions of particles with the fibers, the matrix, or both, may also improve the adhesion of the particles without significantly altering the self-assembly process. Even if the particles are poorly adhered to fibers or the matrix, multifunctional properties such as improved conductivity, or electromagnetic shielding may still be imparted to composites using self-assembled interphases.

Self-assembled interphases have the potential to be easily scaled since only additional mixing steps would be required. The self-assembly process, however, would need to be specific enough to cause localization of nanoparticles in the fiber-matrix interphase without causing significant aggregation in the bulk resin, which can lead to reduced mechanical properties. In addition, the kinetics of the self-assembly process is extremely important, and depending on the processing conditions particles may become kinetically trapped before the interphase is formed.

1.2.5 *Summary*

There are many methods for modifying the fiber-matrix interphase in FRPCs with nanoparticles, each with its own set of applications, advantages and disadvantages. Interphases can be grown from fiber surfaces using seeded growth techniques or electrochemical methods. Nanomaterials can also be deposited onto fibers through the use of many different techniques including electrophoretic deposition, electrostatic attraction, chemical reaction or physical adsorption in a coating process. Recently self-assembled interphases have been prepared that develop during the course of a thermoset cure through the use of migrating agents. These techniques or combinations of them can be used to prepare fiber-matrix interphases with improved mechanical properties often accompanied by additional functionality in the resulting composite.

FRPCs for strain sensing applications, improved EMI shielding, increased electrical conductivity, and piezoelectric responses, to name a few, have all been successfully demonstrated.

The morphology of the nanomaterial present in the interphase can significantly alter the final composite properties. The presence of aggregates in the interphase generally leads to reductions in the mechanical properties of the interphase, and should be avoided. For deposited particles, appropriate surface functionalization combined with sonication is often sufficient to produce interphases with well-dispersed particles. The alignment of grown interphases can be improved by altering the seeding or growth conditions, often leading to greater improvements in mechanical properties. The dispersion state of nanoparticles in the bulk phase, if present, is equally important, and processes that rely on the self-assembly of the fiber-matrix interphase should be optimized to avoid aggregation in the bulk phase as well as in the interphase.

The inclusion of interphase modifiers can improve the mechanical properties through a variety of mechanisms. First, the additional surface roughness imparted to the fiber surface by the nanoparticles can improve the mechanical interlock between the fiber and the matrix. Secondly, nanoparticles located in the interphase may act as crack arresters or deflectors, resulting in interphases with significantly improved fracture energies. Thirdly, the presence of a graded modulus in the interphase can help to improve the stress transfer between the matrix and the reinforcing fiber. In addition, nanoparticle reinforced interphases may improve the wettability of the resin, which can also increase the stress transfer to the reinforcing fibers. These factors are all reliant on sufficient adhesion of the particles with the matrix and the fiber surface, and poor adhesion can result in premature failure of the composite. Nanoparticle modified interphases typically fail at either the fiber-nanoparticle interface, or the nanoparticle-matrix interface, and If the adhesion in either of these locations is weaker than adhesion between the fiber and the bulk

resin failure may occur at lower applied stresses than the unmodified composites. Fiber surfaces can be modified to improve the strength of the interactions with the interphase modifiers. Additionally, nanoparticle surface functionalization can result in improved adhesion with the fibers, the matrix or both. Chemically bonding nanoparticles to the fiber surface is a particularly effective method at improving particle adhesion, but is size dependent. For example, larger spherical particles benefit proportionately less from covalent attachment because of the reduced relative contact area they have with fiber surfaces.

Another important consideration is that the preparation methods used to prepare modified interphases can lead to undesired reductions in the modulus and tensile strength of the reinforcing fiber itself. For example, traditional CVD conditions to grow carbon nanotubes from fiber surfaces, certain fiber pretreatments, and the electrophoretic deposition process can all lead to significant reductions in the fiber tensile strength. The inclusion of nanoparticles in a sizing package, low temperature processing of unsized fibers, or forming self-assembled interphases tend to be the gentlest treatments resulting in little or no reductions in the tensile properties of the fibers.

Nanoparticles included in the fiber-matrix interphase can drastically alter the mechanical properties of the resulting FRPC, and impart a wide variety of additional functionalities. The dispersion quality, interphase morphology, and adhesion of the nanomaterials to the fibers and the reinforcing matrix are all critically important in producing the highest quality composites. New synthetic routes and deposition methods can lead to composites with an even wider range of properties and applications.

1.3 REFERENCES

1. Mackay ME, Tuteja A, Duxbury PM, Hawker CJ, Horn BV, Guan Z, Chen G, Krishnan RS. General Strategies for Nanoparticle Dispersion. Science. 2006 Mar 24;311(5768):1740–3.

2. Kumar MS, Raju NMS, Sampath PS, Jayakumari LS. Effects Of Nanomaterials On Polymer Composites - An Expatiate View. Reviews on Advanced Materials Science. 2014;38(1):40–54.

3. Chen C, Justice RS, Schaefer DW, Baur JW. Highly dispersed nanosilica–epoxy resins with enhanced mechanical properties. Polymer. 2008 Aug 11;49(17):3805–15.

4. Alzina C, Sbirrazzuoli N, Mija A. Epoxy–Amine Based Nanocomposites Reinforced by Silica Nanoparticles. Relationships between Morphologic Aspects, Cure Kinetics, and Thermal Properties. J Phys Chem C. 2011 Nov 24;115(46):22789–95.

5. Sprenger S. Epoxy resins modified with elastomers and surface-modified silica nanoparticles. Polymer. 2013 Aug 16;54(18):4790–7.

6. Johnsen BB, Kinloch AJ, Mohammed RD, Taylor AC, Sprenger S. Toughening mechanisms of nanoparticle-modified epoxy polymers. Polymer. 2007 Jan 12;48(2):530–41.

7. Arkles B. Gelest - Silane coupling agents [Internet]. 2006 [cited 2016 Aug 19]. Available from: http://ijsae.in/ijsaeems/index.php/ijsae/article/view/869

8. Plueddemann, E. P. Silane Coupling Agents. 2nd ed. New York: Springer US; 1991. 253 p.

9. Materne T, Buyl F, Witucki GL. Organosilane Technology in Coating Applications: Review and Perspectives [Internet]. Dow Corning; 2004 [cited 2016 Aug 19]. Available from: http://www.dowcorning.com/content/publishedlit/26-1402-01.pdf

10. Ock HG, Ahn KH, Lee SJ. Effect of electric field on polymer/clay nanocomposites depending on the affinities between the polymer and clay. J Appl Polym Sci. 2016 Jul 5;133(25):1–6.

11. Survant L, Andrejevic M, Picker J, Van Den Hoek J, Fossum E, Lagadic I. Surface-initiated polymerization of styrene from one-step prepared thiol-functionalized organoclays. Polyhedron. 2016 Aug 16;114:37–41.

12. Yan L-T, Xie X-M. Computational modeling and simulation of nanoparticle self-assembly in polymeric systems: Structures, properties and external field effects. Progress in Polymer Science. 2013 Feb;38(2):369–405.

13. Taguet A, Cassagnau P, Lopez-Cuesta J-M. Structuration, selective dispersion and compatibilizing effect of (nano)fillers in polymer blends. Progress in Polymer Science. 2014 Aug;39(8):1526–63.

14. Renna LA, Boyle CJ, Gehan TS, Venkataraman D. Polymer Nanoparticle Assemblies: A Versatile Route to Functional Mesostructures. Macromolecules. 2015 Sep 22;48(18):6353–68.

15. Costanzo PJ, Beyer FL. Thermally Driven Assembly of Nanoparticles in Polymer Matrices. Macromolecules. 2007 May 1;40(11):3996–4001.

16. Williams RJJ, Hoppe CE, Zucchi IA, Romeo HE, dell'Erba IE, Gómez ML, Puig J, Leonardi AB. Self-assembly of nanoparticles employing polymerization-induced phase separation. Journal of Colloid and Interface Science. 2014 Oct 1;431:223–32.

17. Herrera-Franco PJ, Drzal LT. Comparison of methods for the measurement of fibre/matrix adhesion in composites. Composites. 1992;23(1):2–27.

18. Ho H, Drzal LT. Non-linear numerical study of the single-fiber fragmentation test. Part I: Test mechanics. Composites Engineering. 1995 Jan 1;5(10):1231–44.

19. Packham DE. Surface energy, surface topography and adhesion. International Journal of Adhesion and Adhesives. 2003;23(6):437–48.

20. Gao X, Jensen RE, Li W, Deitzel J, McKnight SH, Gillespie JW. Effect of Fiber Surface Texture Created from Silane Blends on the Strength and Energy Absorption of the Glass Fiber/Epoxy Interphase. Journal of Composite Materials. 2008 Mar 1;42(5):513–34.

21. Mishnaevsky Jr. L. Nanostructured interfaces for enhancing mechanical properties of composites: Computational micromechanical studies. Composites Part B: Engineering. 2015 Jan;68:75–84.

22. Brockmann W, Geiß PL, Klingen J, Schröder B. Adhesion. In: Adhesive Bonding: Materials, Applications and Technology [Internet]. Wiley-VCH Verlag GmbH & Co. KGaA; 2008. p. 11–28. Available from: http://onlinelibrary.wiley.com/doi/10.1002/9783527623921.ch3/summary

23. Netravali AN, Mittal KL. Interface / Interphase in Polymer Nanocomposites. Beverly, MA: Wiley-Scrivener; 2017.

24. Kim J-K, Mai Y-W. Engineered Interfaces in Fiber Reinforced Composites. Elsevier; 1998. 417 p.

25. Drzal LT. The role of the fiber-matrix interphase on composite properties. Vacuum. 1990 Jan 1;41(7):1615–8.

26. Ramanathan T, Bismarck A, Schulz E, Subramanian K. The use of a single-fibre pull-out test to investigate the influence of acidic and basic surface groups on carbon fibres on the adhesion to poly (phenylene sulfide) and matrix-morphology-dependent fracture behaviour. Composites science and technology. 2001;61(12):1703–1710.

27. Ferreira L, Evangelista MB, Martins MCL, Granja PL, Esteves JL, Barbosa MA. Improving the adhesion of poly(ethylene terephthalate) fibers to poly(hydroxyethyl methacrylate) hydrogels by ozone treatment: Surface characterization and pull-out tests. Polymer. 2005 Nov 14;46(23):9840–50.

28. Hoecker F, Karger-Kocsis J. Surface energetics of carbon fibers and its effects on the mechanical performance of CF/EP composites. Journal of applied polymer science. 1996;59(1):139–153.

29. Vautard F, Ozcan S, Meyer H. Properties of thermo-chemically surface treated carbon fibers and of their epoxy and vinyl ester composites. Composites Part A: Applied Science and Manufacturing. 2012 Jul;43(7):1120–33.

30. Sharma M, Gao S, Mäder E, Sharma H, Wei LY, Bijwe J. Carbon fiber surfaces and composite interphases. Composites Science and Technology. 2014 Oct 6;102:35–50.

31. Dey M, Deitzel JM, Gillespie Jr. JW, Schweiger S. Influence of sizing formulations on glass/epoxy interphase properties. Composites Part A: Applied Science and Manufacturing. 2014 Aug;63:59–67.

32. Jensen RE, McKnight SH. Inorganic–organic fiber sizings for enhanced energy absorption in glass fiber-reinforced composites intended for structural applications. Composites Science and Technology. 2006 Mar;66(3–4):509–21.

33. Rausch J, Zhuang RC, Mäder E. Application of nanomaterials in sizings for glass fibre/polypropylene hybrid yarn spinning. Materials Technology. 2009 Mar 1;24(1):29–35.

34. Yang Y, Lu C-X, Su X-L, Wu G-P, Wang X-K. Effect of nano-SiO2 modified emulsion sizing on the interfacial adhesion of carbon fibers reinforced composites. Materials Letters. 2007 Jul;61(17):3601–4.

35. Drzal LT, Rich MJ, Koenig MF, Lloyd PF. Adhesion of Graphite Fibers to Epoxy Matrices: II. The Effect of Fiber Finish. The Journal of Adhesion. 1983 Nov 1;16(2):133–52.

36. Chen L, Jin H, Xu Z, Li J, Guo Q, Shan M, Yang C, Wang Z, Mai W, Cheng B. Role of a gradient interface layer in interfacial enhancement of carbon fiber/epoxy hierarchical composites. J Mater Sci. 2014 Sep 23;50(1):112–21.

37. Chen L, Jin H, Xu Z, Shan M, Tian X, Yang C, Wang Z, Cheng B. A design of gradient interphase reinforced by silanized graphene oxide and its effect on carbon fiber/epoxy interface. Materials Chemistry and Physics. 2014 May 15;145(1–2):186–96.

38. Wang C, Li J, Sun S, Li X, Wu G, Wang Y, Xie F, Huang Y. Controlled growth of silver nanoparticles on carbon fibers for reinforcement of both tensile and interfacial strength. RSC Advances. 2016;6(17):14016–26.

39. Rutz BH, Berg JC. Electrostatic deposition of silica nanoparticles between E-glass fibers and an epoxy resin. J Appl Polym Sci. 2015 Feb 20;132(8):1–9.

40. Lin Y, Ehlert G, Sodano HA. Increased Interface Strength in Carbon Fiber Composites through a ZnO Nanowire Interphase. Advanced Functional Materials. 2009 Aug 24;19(16):2654–60.

41. Nguyen FN, Yoshioka K, Haro AP. Reinforced interphase and bonded structures thereof. WO2012116261 A1, 2012.

42. Nguyen FN, Haro AP, Kobayashi D, Nakayama Y, Ichikawa T, Endo M, Yoshioka K, Aston E, Khoo J. Carbon fiber's surface chemistry and self-assembled interphase formation in fiber reinforced polymer composites. In: Proceedings of the International conference on composite materials. Montreal, Canada; 2013.

43. Nguyen FN, Nakayama Y, Kobayashi D, Kamae T, Kenichi Y. Carbon fiber's surface and its effects on an interphase formation for ultimate adhesion-related performances. In: Proceedings of the Society for the Advancement of Materials and Process Engineering. Baltimore, MD; 2012.

44. Malakooti MH, Hwang H-S, Sodano HA. Power generation from base excitation of a Kevlar composite beam with ZnO nanowires. In: Proc of SPIE - Behavior and Mechanics of Multifuncitional Materials and Composites [Internet]. 2015 [cited 2016 Nov 15]. p. 1–6. Available from: http://dx.doi.org/10.1117/12.2084391

45. Kim CH, Kim B-H, Yang KS. TiO2 nanoparticles loaded on graphene/carbon composite nanofibers by electrospinning for increased photocatalysis. Carbon. 2012 Jun;50(7):2472–81.

46. Jiang D, Liu L, Long J, Xing L, Huang Y, Wu Z, Yan X, Guo Z. Reinforced unsaturated polyester composites by chemically grafting amino-POSS onto carbon fibers with active double spiral structural spiralphosphodicholor. Composites Science and Technology. 2014 Aug 21;100:158–65.

47. Song B, Meng LH, Huang YD. Improvement of interfacial property between PBO fibers and epoxy resin by surface grafting of polyhedral oligomeric silsesquioxanes (POSS). Applied Surface Science. 2012 Oct;258(24):10154–9.

48. Zhao F, Huang Y. Grafting of polyhedral oligomeric silsesquioxanes on a carbon fiber surface: novel coupling agents for fiber/polymer matrix composites. J Mater Chem. 2011 Mar 1;21(11):3695–703.

49. Nguyen FN, Haro AP, Yoshioka K. Effects of a Nanomaterial-Toughened Interphase in Carbon Fiber Reinforced Polymer Composite. In: Proceedings of the Society for the Advancement of Materials and Process Engineering. Wichita, KS; 2013.

50. Leonard GC, Hosseinpour D, Berg JC. Modulus-Graded Interphase Modifiers in E-Glass Fiber/Thermoplastic Composites. Journal of Adhesion Science & Technology. 2009 Nov;23(16):2031–46.

51. Merlini C, Rosa BS, Müller D, Ecco LG, Ramôa SDAS, Barra GMO. Polypyrrole nanoparticles coated amorphous short silica fibers: Synthesis and characterization. Polymer Testing. 2012 Dec;31(8):971–7.

52. Loyola BR, Zhao Y, Loh KJ, Saponara VL. The electrical response of carbon nanotube-based thin film sensors subjected to mechanical and environmental effects. Smart Mater Struct. 2013;22(2):025010.

53. Thostenson ET, Li WZ, Wang DZ, Ren ZF, Chou TW. Carbon nanotube/carbon fiber hybrid multiscale composites. Journal of Applied Physics. 2002 May 1;91(9):6034–7.

54. Bekyarova E, Thostenson ET, Yu A, Kim H, Gao J, Tang J, Hahn HT, Chou T-W, Itkis ME, Haddon RC. Multiscale Carbon Nanotube−Carbon Fiber Reinforcement for Advanced Epoxy Composites. Langmuir. 2007 Mar 1;23(7):3970–4.

55. Zhang J, Liu J, Zhuang R, Mäder E, Heinrich G, Gao S. Single MWNT-Glass Fiber as Strain Sensor and Switch. Adv Mater. 2011 Aug 9;23(30):3392–7.

56. Gao S, Zhuang R-C, Zhang J, Liu J-W, Mäder E. Glass Fibers with Carbon Nanotube Networks as Multifunctional Sensors. Adv Funct Mater. 2010 Jun 23;20(12):1885–93.

57. Schaefer JD, Rodriguez AJ, Guzman ME, Lim C-S, Minaie B. Effects of electrophoretically deposited carbon nanofibers on the interface of single carbon fibers embedded in epoxy matrix. Carbon. 2011 Jul;49(8):2750–9.

58. An Q, Rider AN, Thostenson ET. Electrophoretic deposition of carbon nanotubes onto carbon-fiber fabric for production of carbon/epoxy composites with improved mechanical properties. Carbon. 2012 Sep;50(11):4130–43.

59. Zhang J, Zhuang R, Liu J, Mäder E, Heinrich G, Gao S. Functional interphases with multi-walled carbon nanotubes in glass fibre/epoxy composites. Carbon. 2010 Jul;48(8):2273–81.

60. Zhang X, Fan X, Yan C, Li H, Zhu Y, Li X, Yu L. Interfacial Microstructure and Properties of Carbon Fiber Composites Modified with Graphene Oxide. ACS Appl Mater Interfaces. 2012 Mar 28;4(3):1543–52.

61. Qin W, Vautard F, Drzal LT, Yu J. Mechanical and electrical properties of carbon fiber composites with incorporation of graphene nanoplatelets at the fiber–matrix interphase. Composites Part B: Engineering. 2015 Feb;69:335–41.

62. Park JK, Do I-H, Askeland P, Drzal LT. Electrodeposition of exfoliated graphite nanoplatelets onto carbon fibers and properties of their epoxy composites. Composites Science and Technology. 2008 Jun;68(7–8):1734–41.

63. Wiegand N, Mäder E. Multifunctional Interphases: Percolation Behavior, Interphase Modification, and Electro-Mechanical Response of Carbon Nanotubes in Glass Fiber Polypropylene Composites. Adv Eng Mater. 2016 Mar 1;18(3):376–84.

64. Boroujeni AY, Tehrani M, Manteghi M, Zhou Z, Al-Haik M. Electromagnetic Shielding Effectiveness of a Hybrid Carbon Nanotube/Glass Fiber Reinforced Polymer Composite. J Eng Mater Technol. 2016 Jun 13;138(4):041001–041001.

65. H. Malakooti M, A. Patterson B, Hwang H-S, A. Sodano H. ZnO nanowire interfaces for high strength multifunctional composites with embedded energy harvesting. Energy & Environmental Science. 2016;9(2):634–43.

66. Malakooti MH, Hwang H-S, Sodano HA. Morphology-Controlled ZnO Nanowire Arrays for Tailored Hybrid Composites with High Damping. ACS Applied Materials & Interfaces. 2015 Jan 14;7(1):332–9.

67. Lv P, Feng Y, Zhang P, Chen H, Zhao N, Feng W. Increasing the interfacial strength in carbon fiber/epoxy composites by controlling the orientation and length of carbon nanotubes grown on the fibers. Carbon. 2011 Nov;49(14):4665–73.

68. Zhang Q, Liu J, Sager R, Dai L, Baur J. Hierarchical composites of carbon nanotubes on carbon fiber: Influence of growth condition on fiber tensile properties. Composites Science and Technology. 2009 Apr;69(5):594–601.

69. Sharma SP, Lakkad SC. Compressive strength of carbon nanotubes grown on carbon fiber reinforced epoxy matrix multi-scale hybrid composites. Surface and Coatings Technology. 2010 Oct 15;205(2):350–5.

70. Agnihotri P, Basu S, Kar KK. Effect of carbon nanotube length and density on the properties of carbon nanotube-coated carbon fiber/polyester composites. Carbon. 2011 Aug;49(9):3098–106.

71. Shah TK, Gardner SH, Alberding MR, Malecki HC. Cnt-infused glass fiber materials and process therefor [Internet]. US20100192851 A1, 2010 [cited 2016 Nov 14]. Available from: http://www.google.com/patents/US20100192851

72. Shah TK, Gardner SH, Alberding MR, Malecki HC. Cnt-infused ceramic fiber materials and process therefor [Internet]. US20120189846 A1, 2012 [cited 2016 Nov 14]. Available from: http://www.google.ch/patents/US20120189846

73. Deka BK, Kong K, Park Y-B, Park HW. Large pulsed electron beam (LPEB)-processed woven carbon fiber/ZnO nanorod/polyester resin composites. Composites Science and Technology. 2014 Oct 6;102:106–12.

74. Galan U, Lin Y, Ehlert GJ, Sodano HA. Effect of ZnO nanowire morphology on the interfacial strength of nanowire coated carbon fibers. Composites Science and Technology. 2011 May;71(7):946–54.

75. Kong K, Deka BK, Kwak SK, Oh A, Kim H, Park Y-B, Park HW. Processing and mechanical characterization of ZnO/polyester woven carbon–fiber composites with different ZnO concentrations. Composites Part A: Applied Science and Manufacturing. 2013 Dec;55:152–60.

76. Ehlert GJ, Galan U, Sodano HA. Role of Surface Chemistry in Adhesion between ZnO Nanowires and Carbon Fibers in Hybrid Composites. ACS Appl Mater Interfaces. 2013 Feb 13;5(3):635–45.

77. Du S, Ren Z, Wu J, Xi W, Fu H. Vertical α-FeOOH nanowires grown on the carbon fiber paper as a free-standing electrode for sensitive H2O2 detection. Nano Res. 2016 Aug 1;9(8):2260–9.

78. Luo Y, Jiang J, Zhou W, Yang H, Luo J, Qi X, Zhang H, Yu DYW, Li CM, Yu T. Self-assembly of well-ordered whisker-like manganese oxide arrays on carbon fiber paper and its application as electrode material for supercapacitors. Journal of Materials Chemistry. 2012;22(17):8634–40.

79. Ehlert GJ, Sodano HA. Zinc Oxide Nanowire Interphase for Enhanced Interfacial Strength in Lightweight Polymer Fiber Composites. ACS Appl Mater Interfaces. 2009 Aug 26;1(8):1827–33.

80. Sadeghian R, Gangireddy S, Minaie B, Hsiao K-T. Manufacturing carbon nanofibers toughened polyester/glass fiber composites using vacuum assisted resin transfer molding for enhancing the mode-I delamination resistance. Composites Part A: Applied Science and Manufacturing. 2006 Oct;37(10):1787–95.

81. Guo J, Lu C, An F, He S. Preparation and characterization of carbon nanotubes/carbon fiber hybrid material by ultrasonically assisted electrophoretic deposition. Materials Letters. 2012 Jan 1;66(1):382–4.

82. Gao X, Gillespie Jr. JW, Jensen RE, Li W, (Gama) Haque BZ, McKnight SH. Effect of fiber surface texture on the mechanical properties of glass fiber reinforced epoxy composite. Composites Part A: Applied Science and Manufacturing. 2015 Jul;74:10–7.

83. Gao X, Jensen RE, McKnight SH, Gillespie Jr. JW. Effect of colloidal silica on the strength and energy absorption of glass fiber/epoxy interphases. Composites Part A: Applied Science and Manufacturing. 2011 Nov;42(11):1738–47.

84. Qin W, Vautard F, Askeland P, Yu J, Drzal L. Modifying the carbon fiber–epoxy matrix interphase with silicon dioxide nanoparticles. RSC Adv. 2015;5(4):2457–65.

85. Qin W, Vautard F, Askeland P, Yu J, Drzal LT. Incorporation of silicon dioxide nanoparticles at the carbon fiber-epoxy matrix interphase and its effect on composite mechanical properties. Polym Compos. 2015 Jul 1;1–9.

86. Pardieu E, Pronkin S, Dolci M, Dintzer T, Pichon BP, Begin D, Pham-Huu C, Schaaf P, Begin-Colin S, Boulmedais F. Hybrid layer-by-layer composites based on a conducting polyelectrolyte and Fe3O4 nanostructures grafted onto graphene for supercapacitor application. J Mater Chem A. 2015 Nov 10;3(45):22877–85.

87. Peiffer DG, Nielsen LE. Preparation and mechanical properties of thick interlayer composites. J Appl Polym Sci. 1979 Apr 15;23(8):2253–64.

88. Podsiadlo P, Kaushik AK, Arruda EM, Waas AM, Shim BS, Xu J, Nandivada H, Pumplin BG, Lahann J, Ramamoorthy A, Kotov NA. Ultrastrong and Stiff Layered Polymer Nanocomposites. Science. 2007 Oct 5;318(5847):80–3.

89. Peiffer DG. Impact strength of thick-interlayer composites. J Appl Polym Sci. 1979 Sep 15;24(6):1451–5.

90. Ma M, Gupta M, Li Z, Zhai L, Gleason KK, Cohen RE, Rubner MF, Rutledge GC. Decorated Electrospun Fibers Exhibiting Superhydrophobicity. Adv Mater. 2007 Jan 20;19(2):255–9.

91. Wenzel RN. Surface Roughness and Contact Angle. J Phys Chem. 1949 Sep 1;53(9):1466–7.

92. Yuan Y, Lee TR. Contact Angle and Wetting Properties. In: Bracco G, Holst B, editors. Surface Science Techniques [Internet]. Springer Berlin Heidelberg; 2013 [cited 2016 Dec 15]. p. 3–34. (Springer Series in Surface Sciences). Available from: http://link.springer.com/chapter/10.1007/978-3-642-34243-1_1

93. Shirtcliffe NJ, McHale G, Newton MI, Chabrol G, Perry CC. Dual-Scale Roughness Produces Unusually Water-Repellent Surfaces. Adv Mater. 2004 Nov 4;16(21):1929–32.

94. Kraft DJ, Ni R, Smallenburg F, Hermes M, Yoon K, Weitz DA, van Blaaderen A, Groenewold J, Dijkstra M, Kegel WK. Surface roughness directed self-assembly of patchy particles into colloidal micelles. Proceedings of the National Academy of Sciences. 2012;109(27):10787–10792.

95. Boal AK, Ilhan F, DeRouchey JE, Thurn-Albrecht T, Russell TP, Rotello VM. Self-assembly of nanoparticles into structured spherical and network aggregates. Nature. 2000 Apr 13;404(6779):746–8.

96. Chervanyov AI. Polymer-mediated interactions and their effect on the coagulation–fragmentation of nano-colloids: a self-consistent field theory approach. Soft Matter. 2015 Jan 28;11(6):1038–53.

97. Nguyen FN, Haro AP, Tun S, Yoshioka K. Hard nanomaterial-toughened carbon fiber reinforced polymer composite. In: Proceedings of the Society for the Advancement of Materials and Process Engineering. Wichita, KS; 2013.

98. Araki T, Tanaka H. Wetting-induced depletion interaction between particles in a phase-separating liquid mixture. Phys Rev E. 2006 Jun 19;73(6):061506.

99. Girard-Reydet E, Sautereau H, Pascault JP, Keates P, Navard P, Thollet G, Vigier G. Reaction-induced phase separation mechanisms in modified thermosets. Polymer. 1998;39(11):2269–79.

100. Elias L, Fenouillot F, Majeste JC, Cassagnau P. Morphology and rheology of immiscible polymer blends filled with silica nanoparticles. Polymer. 2007 Sep 21;48(20):6029–40.

101. Chiu JJ, Kim BJ, Yi G-R, Bang J, Kramer EJ, Pine DJ. Distribution of Nanoparticles in Lamellar Domains of Block Copolymers. Macromolecules. 2007 May;40(9):3361–5.

102. Asakura S, Oosawa F. On Interaction between Two Bodies Immersed in a Solution of Macromolecules. The Journal of Chemical Physics. 1954 Jul 1;22(7):1255–6.

103. Yarlagadda SC. Dynamics of hard and soft colloids in confined geometries and on structured surfaces [PhD thesis]. [Atlanta, USA]: Georgia Tech; 2015.

104. Mravlak M. Depletion force [Internet]. University of Ljubljana; 2008 [cited 2015 Apr 1]. Available from: http://mafija.fmf.uni-lj.si/seminar/files/2007_2008/depletion.pdf

Chapter 2. PREDICTING ADHESION IN PARTICLE FILLED THERMOPLASTICS USING COSMO-SAC

c.f. K. Caldwell and J.C. Berg, *Journal of Adhesion Science and Technology* **28**, 1312–1322 (2014).

2.1 ABSTRACT

Successful efforts have been made at predicting the adhesion between several polymer matrices and the surface of a glass filler, treated with various coupling agents using thermodynamic descriptors. A good thermodynamic criterion has been shown to be the (negative) Gibbs free energy of mixing $(-\Delta G_{mix})_{0.5}$, for a solution containing molecules representative of the repeat units of the polymer and the exposed functional groups of the silane coupling agents. Group contribution methods, such as UNIFAC allow for straightforward calculations of $(-\Delta G_{mix})_{0.5}$; however, the UNIFAC database remains incomplete, and furthermore requires a subscription to access the most current database. Recently new predictive models based on the surface charge distribution of molecules and statistical thermodynamics have been developed to predict properties of solutions. In this work one such method, COSMO-SAC, is used to calculate $(-\Delta G_{mix})_{0.5}$ and compare the results to a previously determined database of relative practical adhesion strengths between various polymer matrices and the organo-functional groups of silane coupling agents. The results obtained from COSMO-SAC show good agreement with the experimental database, except for the cases of significant steric effects and systems containing amines. Overall, the adhesion predictions obtained from COSMO-SAC calculations are comparable to the UNIFAC predictions, although UNIFAC was more successful in predicting adhesion for the amine containing compounds. Steric effects are not considered formally by either model, and significant reformulations would be required to account for them.

2.2 INTRODUCTION

The adhesion between an entity embedded in a polymeric matrix is critically important in many fields. In many cases a maximum value of adhesion is desired, as is the case for a repaired structural component. Moderate levels of adhesion may be desired in other cases, such as bulletproof glass where debonding is required to dissipate the impact energy of a bullet. Estimation of the adhesion is difficult because there are many mechanisms of adhesion including, mechanical interlock, polymer diffusion, physical and chemical interactions [1]. Mechanical interlock is achieved by the wetting of a porous or jagged material by an adherent that leads to a purely mechanical reinforcement of the interphase. Smooth materials, therefore, cannot engage in the mechanical interlocking mechanism. When two flexible, polymeric interfaces are joined the polymer chains from each surface may diffuse within each other leading to the formation of an interpenetrating network. The polymers must be mutually soluble to an extent and possess significant chain mobility to diffuse into this interphase region. Often times, heating above the glass transition temperatures is necessary to achieve the formation such a network. Lastly the London dispersion forces, acid-base interactions, dipole interactions and chemical bonding all contribute to the adhesion between two surfaces regardless of the surface types.

There are many experimental ways to measure the adhesion strength of an adhesive bond between two materials, including single particle composite debonding experiments [2]. In such experiments a single smooth spherical particle is embedded in the center of a polymer matrix and strained until the matrix debonds from a spherical particle. The measured stress at debonding is proportional to the adhesion strength. Because smooth particles are used the contributions from mechanical interlock can be eliminated when performing comparative studies using the SPC

technique. Probing the effects of the chemical adhesion can be achieved using this method by surface functionalizing the particles. The chemical adhesion should be proportional to the thermodynamic compatibility between the surface of the particles and the bulk polymer matrix. Indeed, the relative practical adhesion between silane coated glass beads and thermoplastic polymer matrices can be successfully predicted by the (negative) Gibbs free energy of mixing, $(-\Delta G_{mix})_{0.5}$, at equimolar amounts of the polymer repeat unit and the functional group of the silane coupling agent [2–4]. The choice of equimolar amounts is presumed to represent the interdigitation between the two compounds within the interphase region surrounding the silica surface. The Gibbs free energy of mixing was previously calculated using the group contribution method UNIFAC [5], and good correlation with the experimental data was found. UNIFAC, however, possesses some fundamental limitations. Firstly, the group interaction database remains, to date, incomplete, thereby limiting its accuracy for compounds containing functional groups not documented in the database. In addition, due to the nature of the algorithm, isomer effects remain uncaptured, e.g., UNIFAC cannot distinguish the differences between 2-Decane and 5-Decane.

More recently, methods based on the surface charge density of molecules have been developed to describe solution thermodynamics. Most notably the "Conductor Like Screening Model for Real Solvent" model [6], (COSMO-RS) and the "Conductor Like Screening Model – Segment Activity Coefficient" [7], (COSMO-SAC) have been successful in predicting many solution properties including vapor-liquid equilibrium data. These COSMO-based calculations require a minimal number of parameters (which have already been optimized), and the so called "sigma profile" for each molecule in solution. The sigma profile is readily computed from the surface charge distribution of the molecule, which can be calculated using a density functional theory (DFT) calculation, and describes the proportions of the molecule containing a given surface

polarization. Due to the success of the models, large, open-access databases of sigma profiles have been prepared and maintained [8], and are often included in computational chemistry packages.

In this section the COSMO-SAC program, as developed in [7], and the sigma profile database developed at Virginia Tech [8], were used to determine the negative molar Gibbs free energy of mixing and use it to predict the adhesion between four different thermoplastic matrices and various silane functionalized silica surfaces. Sigma profiles not found in the database were computed from DFT calculations using the Gaussian 09 [9] software package. The successful implementation of the COSMO-SAC method provides a flexible methodology for predicting the adhesion of silanized surfaces embedded in thermoplastic polymer matrices via the thermodynamic criterion, $(-\Delta G_{mix})_{0.5}$.

2.3 MATERIALS AND METHODS

2.3.1 *Lists of Compounds Investigated*

Previous works have compiled a database of relative practical adhesion for particle filled composites with various polymer matrices containing silane treated silica spheres [2–4]. The relative adhesion was measured using the single particle composite technique. The polymers used as the composite matrix are listed in Table 2.1. Of the polymers investigated Poly(vinyl butryal) (PVB), Poly(methyl methacrylate) (PMMA), and Poly(ethyl methacrylate) (PEMA) are all amorphous polymers, while Poly(ethylene terephthalate) (PET) is a semi-crystalline polymer. The particular blend of PVB used in the previous work contained approximately 12% unreacted vinyl alcohol groups. The silane coupling agents used in the previous works are listed in Table 2.2, and represent a wide range of chemistries. Table 2.2 also denotes which organo-functional silanes were tested for each polymer matrix.

Table 2.1 – Names and structures of polymer matrices investigated

Matrix polymer	Representative repeat unit
Poly(vinyl butyral)	-[2-propyl-1,3-dioxane-4,6-diyl)methylene]$_{0.88}$ -[Vinyl]$_{0.12}$-
Poly(Methyl Methacrylate)	-[methyl methacrylate]-
Poly(Ethyl Methacrylate)	-[ethyl methacrylate]-
Poly(ethylene terephthalate)	-[ethylene terephthalate]-

Table 2.2 - Names and structures of organo-functional silanes investigated

Organo-functional silane	Organo-functional group	Polymer Matrix			
		PVB	PMMA	PEMA	PET
n-Octadecyl (o)	-$(CH_2)_{17}CH_3$				x
n-Octyl (o)	-$(CH_2)_7CH_3$	x	x	x	x
7-Oct-1-enyl (7o)	-$(CH_2)_6CH{=}CH_2$		x	x	
Chloromethyl (cm)	-CH_2Cl	x	x	x	
Chloroproyl (cp)	-$(CH_2)_3Cl$	x	x	x	x
3-Iodopropyl (i)	-$(CH_2)_3I$	x		x	
3-Bromopropyl (b)	-$(CH_2)_3Br$			x	
Vinyl (v)	-$CH{=}CH_2$		x	x	x
Phenyl (p)	-Ph		x	x	
Mono-amino (ma)	-$(CH_2)_3NH_2$	x			
Di-amino (da)	-$(CH_2)_3NH(CH_2)_2NH_2$	x			
Tri-amino (ta)	-$(CH_2)_3NH(CH_2)_2NH(CH_2)_2NH_2$	x			
3-Methacylo (3m)	-$(CH_2)_3COO(CH_3)CH_2{=}C$	x	x	x	x
Phenylamino (pa)	-$(CH_2)_3NHPh$	x			
Dihydroimidazole (di)	-$(CH_2)_3$Imidazole	x			

2.3.2 *Sigma Profile Generation via DFT*

While the sigma profile database contains over 1,000 common compounds, not all of the groups of interest were represented. Sigma profiles for the missing compounds representing the organo-functional groups of silane coupling agents (tir-amino, di-amino, 3-methacrylo, and dihydroimiazole) and polymer repeat units (PVB and PET) were determined via simulation. The surface charge distributions of the representative groups were determined by DFT calculations conducted using the Gaussian 09 computational software package [9]. The structures input into the DFT calculation were constructed in the GaussView program, with all structures preoptimized using the clean tool. The B3LYP/G6-311(d,p) basis set was used, which was the same basis set

used to generate the database. After the DFT calculation was complete, a single point energy calculation was conducted to produce a COSMO file by including the keyword scrf=cosmors. The COSMO file contains the necessary information to generate the sigma profile in conjunction with external software supplied on the Virginia Tech website [8]. It is important to note that since PVB contains approximately 12% unreacted hydroxyl groups, the sigma profile for PVB is represented here as a mixture of the sigma profiles for both the 2-propyl-1,3-dioxane-4,6-diyl)methylene groups and the vinyl groups present in the polymer.

2.3.3 *COSMO-SAC Theory and Calculations*

COSMO-SAC calculations were conducted using the software [8] provided on the Virginia Tech website. Figure 2.1 represents a brief overview of the necessary steps required to conduct a COSMO-SAC calculation. First, the surface charge polarization of the molecules in an infinite dielectric medium is computed using DFT calculations. Next, all of the possible surface interactions are integrated to yield the desired thermodynamic information. For computational simplicity, the surface of the molecule is broken into segments of finite area and the sum of all possible pairwise interactions between the segments is considered. Each segment is described by the charge distribution σ (Coulombs/Å^2), and its area. Sigma profiles, which are unique to each molecule, are described by a plot of $p(\sigma)$ versus σ, where $p(\sigma)$ represents the total amount of surface area containing a given surface charge and has units of Å^4/Coulomb. In Figure 2.1 the charge densities of ideally solvated water (top left) and ethanol (top right) molecules are shown, along with their corresponding sigma profiles (water: middle left; ethanol: middle right). The increase in neutral charge density area is immediately obvious when comparing ethanol to water.

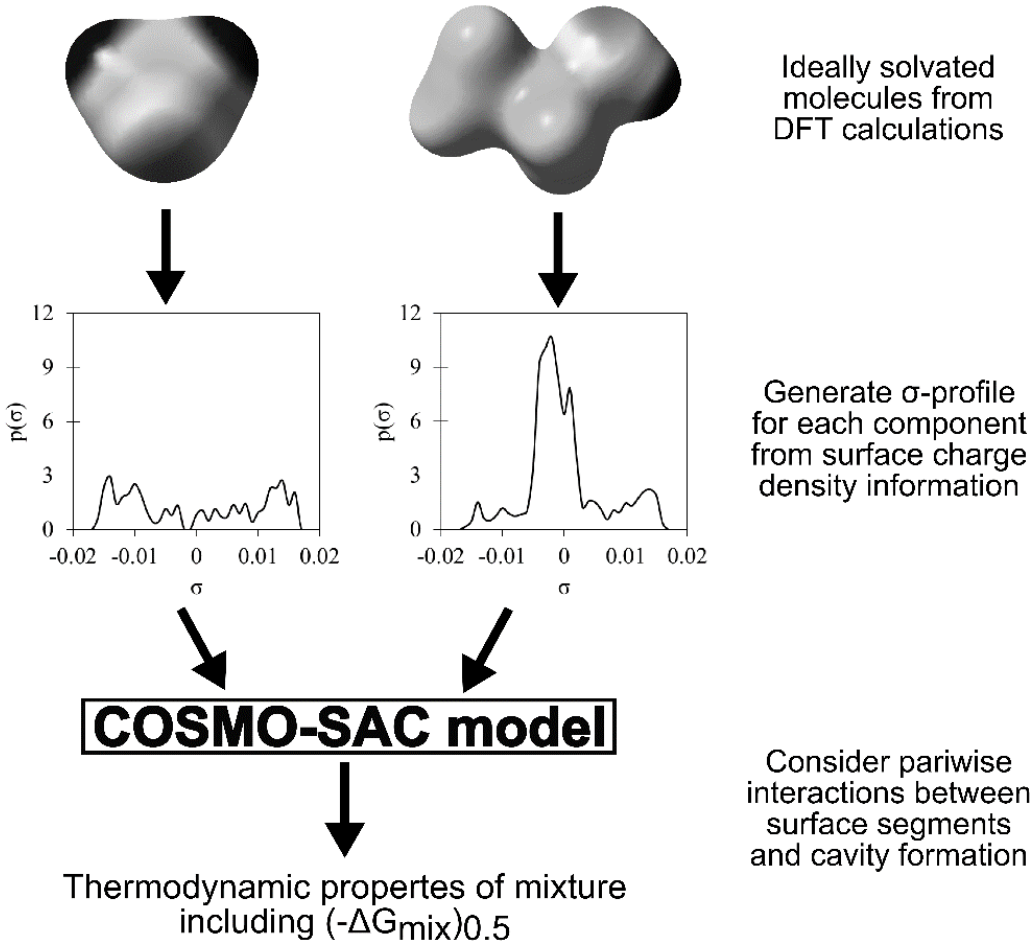

Figure 2.1- Overview of the COSMO-SAC procedure. The surface charge distribution of ideally solvated molecules is used to generate sigma profiles. The COSMO-SAC model then uses the sigma profiles to calculate solution thermodynamic properties, including the $(-\Delta G_{mix})_{0.5}$.

From the information contained in the sigma profiles alone, it is possible to calculate activity coefficients, and subsequently the Gibbs free energy of mixing. In the COSMO-SAC model used here, the activity coefficient of the i^{th} component in solution S is given by the following equation:

$$\ln \gamma_i = \ln \gamma_i^{COMB} + n_i \sum_{\sigma_m} p_i(\sigma_m)[\ln \Gamma_S(\sigma_m) - \ln \Gamma_i(\sigma_m)]. \qquad (2.1)$$

The first term γ_i^{COMB} is the Staverman-Guggenheim combinatorial term, which accounts for nonidealities associated with the size and structure of a molecule, [10,11] and is given by:

$$\ln \gamma_i^{COMB} = \ln \frac{\phi_i}{x_i} + \frac{z}{2} q_i \ln \frac{\theta_i}{\phi_i} + l_i - \frac{\phi_i}{x_i} \sum_{j=1}^{n} x_j \, l_j, \qquad (2.2)$$

where ϕ_i is the normalized volume fraction, $\theta_i$is the normalized surface area fraction, x_i is the mole fraction of component i in the mixture, z is the coordination number and is typically assigned a value of 10, $l_i = (z/2)(r_i - q_i) - (r_i - 1)$, $r_i = V_i/r$ is the normalized volume parameter, and $q_i = A_i/q$ is the normalized surface-area parameter. A_i and V_i are the cavity surface area and cavity volume, respectively, both of which are determined from the COSMO calculation. q and r are both normalization constants. The Staverman-Guggenheim term is also used in UNIFAC and many other

The second term in equation (2.1) represents the residual contribution to the activity coefficient and accounts for energetic effects. n_i is the total number of segments of component i, $p_i(\sigma_m)$ is the probability of finding a surface segment of charge density σ_m for component i, $\Gamma_S(\sigma_m)$ and $\Gamma_i(\sigma_m)$ are defined as the segment activity coefficients for a segment of surface charge density σ_m in solution, and in pure component i, respectively.

The probability of finding a segment with a given surface charge density in pure component i is given by $p_i(\sigma_m) = A_i(\sigma_m)/A_i$, while the probability of finding such a segment in the solution is given by the $p_S(\sigma_m) = \sum_i x_i A_i(\sigma_m) \,/\, \sum_i x_i A_i$. The segment activity coefficients are determined from the following equations:

$$\ln \Gamma_i(\sigma_m) = -\ln \left[\sum_{\sigma_n} p_i(\sigma_n) \Gamma_i(\sigma_n) \exp\left(-\frac{\Delta W(\sigma_m, \sigma_n)}{RT} \right) \right], \qquad (2.3)$$

$$\ln \Gamma_S(\sigma_m) = -\ln \left[\sum_{\sigma_n} p_S(\sigma_n) \Gamma_S(\sigma_n) \exp\left(-\frac{\Delta W(\sigma_m, \sigma_n)}{RT} \right) \right], \qquad (2.4)$$

where $\Delta W(\sigma_m, \sigma_n)$ is the exchange energy between two surface segments that accounts for electrostatic and hydrogen bonding interactions, R is the universal gas constant, and T is the system temperature. Dispersion forces are assumed to be constant in this model, and as a result the dispersive energetic terms cancel:

$$\Delta W(\sigma_m, \sigma_n) = \frac{\alpha'}{2}(\sigma_m + \sigma_n)^2 + c_{hb} \max[0, \sigma_{acc} - \sigma_{hb}] \min[0, \sigma_{don} + \sigma_{hb}], \tag{2.5}$$

where α' and c_{hb} are constants in this model, σ_{acc} and σ_{don} are the larger and smaller of the two surface segments σ_m and σ_n; and σ_{hb} is a constant that determines the cutoff value for determining hydrogen bonding interactions. Max and min are functions that represent the larger or smaller of their arguments, respectively. Other forms of the hydrogen bonding term exist in other variants of the COSMO-based models, and further refinement of these terms is an active area of research [12,13]. Once the activity coefficient is calculated from Equation (2.1), the Gibbs free energy of mixing is readily calculated by Equation (2.6). Figure 2.2 shows the Gibbs free energy of mixing for octadecane mixed with repeat unit of PVB.

$$\Delta G_{mix} = RTx_i \ln \sum(x_i \gamma_i). \tag{2.6}$$

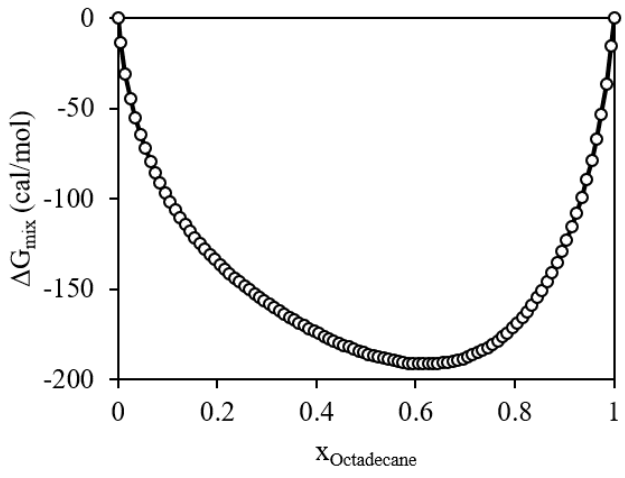

Figure 2.2 – Gibbs free energy of mixing between Octadecane and the repeat unit of PVB, calculated using COSMO-SAC

In this work, all the constants in the above equations were used as supplied in the Virginia Tech software, and the system temperature was specified at 50° C. A full derivation of the COSMO-SAC model as used in this work can be found in the original work of Lin and Sandler [7].

It should be noted that strictly speaking COSMO-SAC was developed to predict solution based thermodynamic properties of ordinary sized molecules, but many authors have found it to be useful to describe and predict properties of polymeric solutions [14,15]. The greatest challenge of describing polymer solutions is that they possess many possible conformations, and each conformation may have a unique sigma profile. In reality a weighted average of a distribution of sigma profiles may be required to account for the large configurational space large molecules can populate. This issue, along with the reality that polymers almost certainly have multiple points of contact makes modeling true polymeric solutions extremely difficult. Nevertheless, since we ae considering only the interactions present in the immediate vicinity of the interface these configurational issues associated with long chain polymers may not be as relevant for our system of interest.

2.4 Results and Discussion

Previous works had used UNIFAC to predict the relative practical adhesion between silane functionalized glass beads and four different thermoplastic polymer matrices [2–4]. The adhesion was measured using the single particle composite technique, which is useful for eliminating the effects of mechanical interlock in the dataset. Using the compiled database of adhesion values, COSMO-SAC was used to compute the $(-\Delta G_{mix})_{0.5}$ and compare the correlations obtained with those computed using UNIFAC. Figure 2.3 shows the relative practical adhesion versus the

computed $(-\Delta G_{mix})_{0.5}$, using both UNIFAC and COSMO-SAC, for PET, PEMA and PMMA. The flexural yield strength, specific adhesion energy and adhesion energy plotted are all relative indicators of adhesion. For the PET matrix, both UNIFAC and COSMO-SAC preform equally well with R^2 values > 0.96. For the PEMA and PMMA matrices, however, UNIFAC tends to outperform the results obtained by COSMO-SAC, although the correlation coefficients obtained using COSMO-SAC are still quite strong (R^2 = 0.760 for PEMA and R^2 = 0.862 for PMMA).

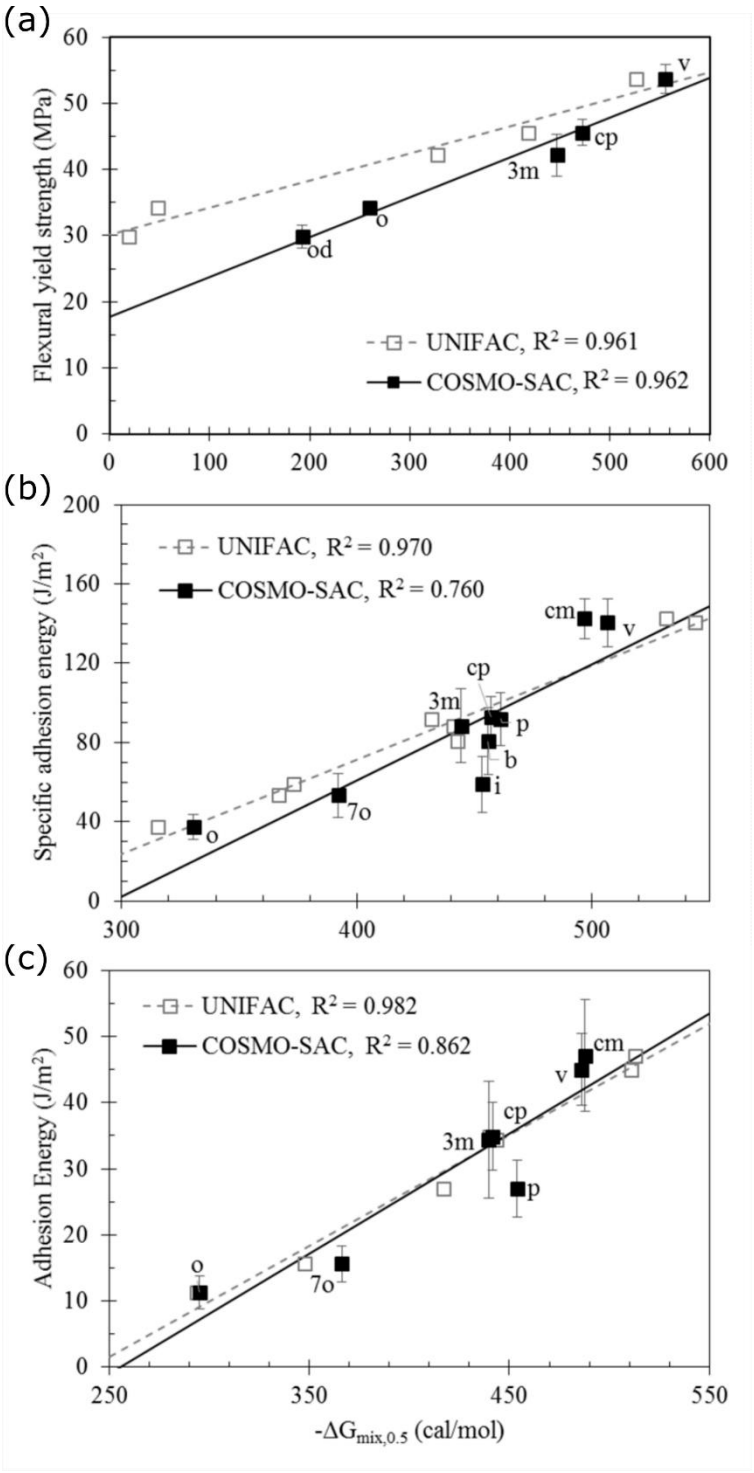

Figure 2.3 - Relationship between the practical adhesion and $(-\Delta G_{mix})_{0.5}$ for systems investigated using (a) PET, (b) PEMA, and (c) PMMA as the matrix. Open squares and the dashed line represent the data obtained using UNIFAC, while closed squares with the solid line represent the results obtained from COSMO-SAC. Abbreviations are defined in Table 2.2. Error bars correspond to the mean 95% confidence interval.

The results obtained for the silane functionalized beads embedded in the PVB matrix, as seen in Figure 2.4(a) showed a significantly worse correlation is observed for both UNIFAC and COSMO-SAC. The poor correlation highlights some of the limitations with the methods. Previous work showed that the UNIFAC was unable to successfully predict the relative adhesion for the bulkiest silane coupling agent functional groups (triamino, phenylamino, and 3-methacrylo) groups with PVB as the polymer matrix [2]. The poor correlation between them may be a result of many factors. Strictly speaking, UNIFAC and COSMO-SAC are both solution-based activity coefficient models, and are not intended for use with solid polymeric systems. Neither model accounts for the possibilities of multiple points of contact, as is likely the case for solid-polymer systems. Additionally, steric effects are absent from both models, and significant developments would need to be made to both models to accurately account for them. Many adaptations of COSMO-based methods are being developed with hopes of capturing the thermodynamics of macromolecule solutions, but they are significantly more complicated and are still in their infancy. Predicting the relative adhesion with systems that are suspected to involve such steric effects may not be feasible using either UNIFAC or COSMO-SAC alone.

Removal of the sterically hindered silanes from the PVB data-set, as shown in Figure 2.4(b), improves the correlations between the relative adhesion and $(-\Delta G_{mix})_{0.5}$ for both COSMO-SAC (R^2 = 0.528), and UNIFAC (R^2 = 0.952). The still poor correlation highlights another limitation of the COSMOSAC method, which is the inability to accurately predict thermodynamic properties of amine-containing compounds. Significant efforts are being made to improve the description of amines and other compounds that can participate in multiple hydrogen bonds. Figure 2.4(c) shows that the COSMO-SAC correlation is much improved when the bulky and amine containing silanes are removed from the PVB data-set (R^2 = 0.872).

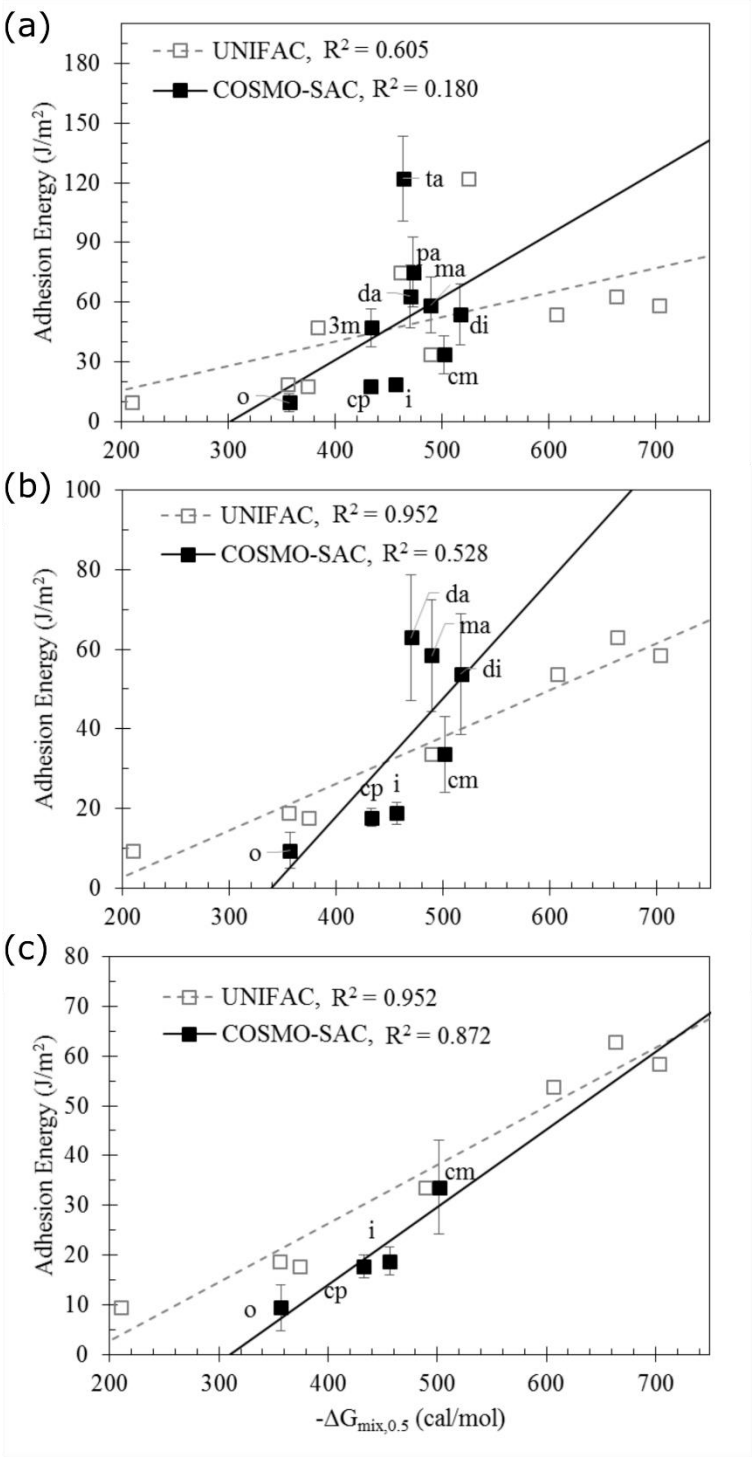

Figure 2.4 – Relationship between the practical adhesion and $(-\Delta G_{mix})_{0.5}$ for systems investigated using PVB as the matrix. (a) all silanes investigated, (b) bulky silanes omitted, and (c) bulky and amine containing silanes omitted. Open squares and the dashed line represent the data obtained using UNIFAC, while closed squares with the solid line represent the results obtained from COSMO-SAC. Abbreviations are defined in Table 2.2. Error bars correspond to the mean 95% confidence interval.

2.5 CONCLUSIONS

Here we have shown that the COSMO-SAC model is a suitable for determining $(-\Delta G_{mix})_{0.5}$ and predicting the relative practical adhesion in filled polymeric composites, with some limitations. Similar to the results obtained by UNIFAC, COSMO-SAC is unable to predict the relative adhesion if significant steric effects exist between the polymer matrix and the silane functional group. Additionally, COSMO-SAC yields less accurate results for compounds containing amines, and in general provides less accurate predictions than UNIFAC. However, due to the general applicability of the method, COSMO-SAC provides a valuable means to predict the relative practical adhesion in composite materials when UNIFAC may be inapplicable. Future refinements of the COSMO-based models will likely be able to correct for some of the inaccuracies associated with amines, but the proper accounting of steric effects is a much more difficult task and will require significant development to the model. Accounting for the large configurational space accessible to long chain polymers may require some monte-carlo sampling of polymer configurations and generation of sigma profiles for each configuration, which would increase the cost of the calculations significantly. Similarly, accounting for the steric hinderances and multiple points of contact remains an outstanding problem.

2.6 REFERENCES

1. Brockmann W, Geiß PL, Klingen J, Schröder B. Adhesion. In: Adhesive Bonding: Materials, Applications and Technology [Internet]. Wiley-VCH Verlag GmbH & Co. KGaA; 2008. p. 11–28. Available from: http://onlinelibrary.wiley.com/doi/10.1002/9783527623921.ch3/summary

2. Miller AC, Knowlton MT, Berg JC. The use of UNIFAC for the estimation of adhesion enhancement between polymers and mineral surfaces treated with silane coupling agents. Journal of adhesion science and technology. 2000;14(12):1471–1484.

3. Miller AC, Berg JC. The prediction of adhesion between polymer matrices and silane-treated glass surfaces in filled composites. Journal of Adhesion Science and Technology. 2002 Jan 1;16(5):495–507.

4. Miller AC, Berg JC. Predicting adhesion between a crystalline polymer and silane-treated glass surfaces in filled composites. Journal of Adhesion Science & Technology. 2002 Dec 2;16(14):1949–56.

5. Fredenslund A, Jones RL, Prausnitz JM. Group-contribution estimation of activity coefficients in nonideal liquid mixtures. AIChE J. 1975 Nov 1;21(6):1086–99.

6. Klamt A. Conductor-like Screening Model for Real Solvents: A New Approach to the Quantitative Calculation of Solvation Phenomena. The Journal of Physical Chemistry. 1995 Feb;99(7):2224–35.

7. Lin ST, Sandler SI. A Priori Phase Equilibrium Prediction from a Segment Contribution Solvation Model. Industrial & Engineering Chemistry Research. 2002 Mar;41(5):899–913.

8. Mullins E, Oldland R, Liu Y a., Wang S, Sandler SI, Chen C-C, Zwolak M, Seavey KC. Sigma-Profile Database for Using COSMO-Based Thermodynamic Methods. Industrial & Engineering Chemistry Research. 2006 Jun;45(12):4389–4415.

9. Frisch MJ, Trucks GW, Schlegel HB, Scuseria GE, Robb MA, Cheeseman JR, Scalmani G, Barone V, Mennucci B, Petersson GA, Nakatsuji H, Caricato M, Li X, Hratchian HP, Izmaylov AF, Bloino J, Zheng G, Sonnenberg JL, Hada M, Ehara M, Toyota K, Fukuda R, Hasegawa J, Ishida M, Nakajima T, Honda Y, Kitao O, Nakai H, Vreven T, Montgomery JA, Peralta JE, Ogliaro F, Bearpark M, Heyd JJ, Brothers E, Kudin KN, Staroverov VN, Kobayashi R, Normand J, Raghavachari K, Rendell A, Burant JC, Iyengar SS, Tomasi J, Cossi M, Rega N, Millam JM, Klene M, Knox JE, Cross JB, Bakken V, Adamo C, Jaramillo J, Gomperts R, Stratmann RE, Yazyev O, Austin AJ, Cammi R, Pomelli C, Ochterski JW, Martin RL, Morokuma K, Zakrzewski VG, Voth GA, Salvador P, Dannenberg JJ, Dapprich S, Daniels AD, Farkas, Foresman JB, Ortiz J V, Cioslowski J, Fox DJ. Gaussian 09, Revision B.01. Gaussian 09, Revision B.01, Gaussian, Inc., Wallingford CT. 2009.

10. Guggenheim EA. Mixtures; the theory of the equilibrium properties of some simple classes of mixtures, solutions and alloys. Oxford: Clarendon Press; 1952. (International series of monographs on physics).

11. Staverman AJ. The entropy of high polymer solutions. Generalization of formulae. Recl Trav Chim Pays-Bas. 1950 Jan 1;69(2):163–74.

12. Tshepelevitsh S, Oss M, Pung A, Leito I. Evaluating the COSMO-RS Method for Modeling Hydrogen Bonding in Solution. ChemPhysChem. 2013 Jun 24;14(9):1909–19.

13. Chen W-L, Lin S-T. Explicit consideration of spatial hydrogen bonding direction for activity coefficient prediction based on implicit solvation calculations. Phys Chem Chem Phys. 2017 Aug 9;19(31):20367–76.

14. Kuo Y-C, Hsu C-C, Lin S-T. Prediction of Phase Behaviors of Polymer–Solvent Mixtures from the COSMO-SAC Activity Coefficient Model. Industrial & Engineering Chemistry Research. 2013 Sep 18;52(37):13505–15.

15. Yang L, Xu X, Peng C, Liu H, Hu Y. Prediction of vapor-liquid equilibrium for polymer solutions based on the COSMO-SAC model. AIChE Journal. 2010 Oct;56(10):2687–98.

Chapter 3. IN SITU OBSERVATION OF A SELF-ASSEMBLED FIBER-MATRIX INTERPHASE

c.f. K. Caldwell, and J.C. Berg, *Journal of Composite Materials* **51**, 3877-3885 (2017).

3.1 ABSTRACT

The preferential accumulation of nanoparticles at carbon fiber surfaces, induced by the addition of a thermoplastic "migrating agent" to an epoxy resin, was monitored via *in-situ* fluorescence microscopy. (3-glydidyloxypropyl)trimethoxysilane functionalized fluorescent silica nanoparticles (GFCSP) were synthesized by a modified Stöber method to track the spatiotemporal abundance of nanoparticles. Single carbon fibers were embedded in an uncured epoxy mixture consisting of tetraglycidyl-4,4-diaminodiphenylmethane (TGDDM) and 4,4'-diamnodiphenyl sulfone (DDS), as well as thermoplastic migrating agent, poly(ether sulfone) (PES), and GFCSP. A heated microscope stage was used to monitor the fluorescence in the local vicinity of the fiber as the epoxy begins to cross-link and solidify upon heating. Our results show that the synthesized GFCSP accumulate at fiber surfaces only in the presence of PES, as verified using scanning electron micrographs of Mode I fiber fracture surfaces.

3.2 INTRODUCTION

Fiber reinforced polymeric composites (FRPC), are materials composed of high strength and modulus fibers encapsulated in a polymer matrix, which may be a thermoset, a thermoplastic or mixture thereof. The interphase, that is a thin region, of the order of 100 nm, between the fiber surface and the bulk matrix, plays a critical role in determining the bulk mechanical properties of the composite [1]. Many methods exist to improve the fiber-matrix adhesion, including fiber

oxidation [2], fiber surface functionalization [3], adsorbing adhesion promoters to the fiber surface [4], and the inclusion of nanomaterials in the fiber-matrix interphase itself [5].

Recently, the use of so called “migrating agents” has been used to selectively accumulate nanoparticles near fiber surfaces during the cure of epoxy based thermosets when directly mixed into a resin containing functionalized nanoparticles [6–8]. The system initially consists of a well-mixed resin containing the nanoparticles, the uncured epoxy and hardener, and the migrating agent, which is typically a thermoplastic polymer. As the epoxy is heated and begins to crosslink, nanoparticles begin accumulating at the interphase in the presence of migrating agent. This type of system is extremely desirable because it does not require any additional fiber functionalization, and can be readily introduced to any existing process stream by incorporating the migrating agent in the resin formulation.

The mechanism by which migrating agents concentrate material to the interphase has not been well studied, however, polymer mediated depletion forces [9,10] qualitatively explain the self-assembly of particles in the interphase. Depletion forces arise when a smaller object, such as a dissolved polymer, is excluded from the region of volume between two larger objects, known as the depletion volume, as they closely approach one another. The resulting concentration difference in the bulk polymer and the depletion volume gives rise to an osmotic pressure that further seeks to bring the objects together. The strength of the interaction is proportional to the polymeric depletant concentration, the relative size of the larger objects compared to the depletant, and the geometry of the approaching bodies. From purely geometric considerations, the depletion volume approximately twice as great for a sphere approaching a plate compared to that of two similarly sized spheres at the same separation distance. Nanoparticle-fiber interactions, which can be approximated by the sphere-plate geometry, should therefore be nearly twice as strong as particle-

particle interactions. In aqueous media control of the depletion strength can lead to preferential nanoparticle deposition at flat surfaces, without causing particle aggregation in the bulk phase [11].

Many techniques for quantifying the spatial distribution of nanoparticles in FRPC exist, such as scanning electron microscopy (SEM), transmission electron microscopy (TEM), and atomic force microscopy (AFM). These techniques, however, typically only probe the final structure of the system. In situ methodologies, however, can provide more information on the kinetics and thermodynamics of the system and capture the onset of any morphological changes. In this section inverted fluorescence microscopy was used in combination with a heated microscope stage, to track the silane functionalized fluorescent core-shell nanoparticles in an epoxy based resin in the presence of a migrating agent. By tracking the accumulation of fluorescence near the fiber surface as a function of time and temperature during the cure, the onset of migration was readily determined. The inclusion of migrating agent into the resin formulation also caused aggregation of primary particles in the bulk phase, while samples prepared without migrating agent showed no signs of aggregation in the bulk phase, indicating particle-particle interactions were also promoted by the migrating agent.

3.3 Materials and Methods

3.3.1 *Nanoparticle Synthesis and Functionalization*

Fluorescent nanoparticles were synthesized using a modified Stöber method [12,13], followed by subsequent surface functionalization, as shown schematically in Figure 3.1. First the fluorescent precursor was synthesized by dissolving Fluorescein isothiocyanate isomer l (FITC) in pure ethanol at a concentration of 50 mM, and then adding (3-aminopropyl) triethoxysilane (APS) to a concentration of 200 mM. The precursor was allowed to react for at least 6 hours, stirring at room temperature. The fluorescent nanoparticle (FNP) cores were prepared by mixing the fluorescent

precursor with an ethanolic ammonium hydroxide solution containing 0.17 M tetraethyl orthosilicate (TEOS). The water content in the mixture was 2.0 M, and the ammonium concentration was 0.85 M. The precursor solution was added to yield a concentration of 2 mg FITC for every mL of TEOS added. The resulting solution was allowed to react for at least 6 hours, stirring and covered. To protect the fluorescent core [14], and preserve the desired surface chemistry of the silica particles an additional shell of silica was added to the nanoparticles using a seeded growth technique. Additional TEOS and water were added in a stoichiometric ratio of 1:2, to grow the particles another 5-10 nm in diameter. The amount of additional TEOS added was calculated by assuming any additional TEOS added would condense on the surface of existing particles in solution. The reaction was allowed to proceed for 6 hours, covered and stirred.

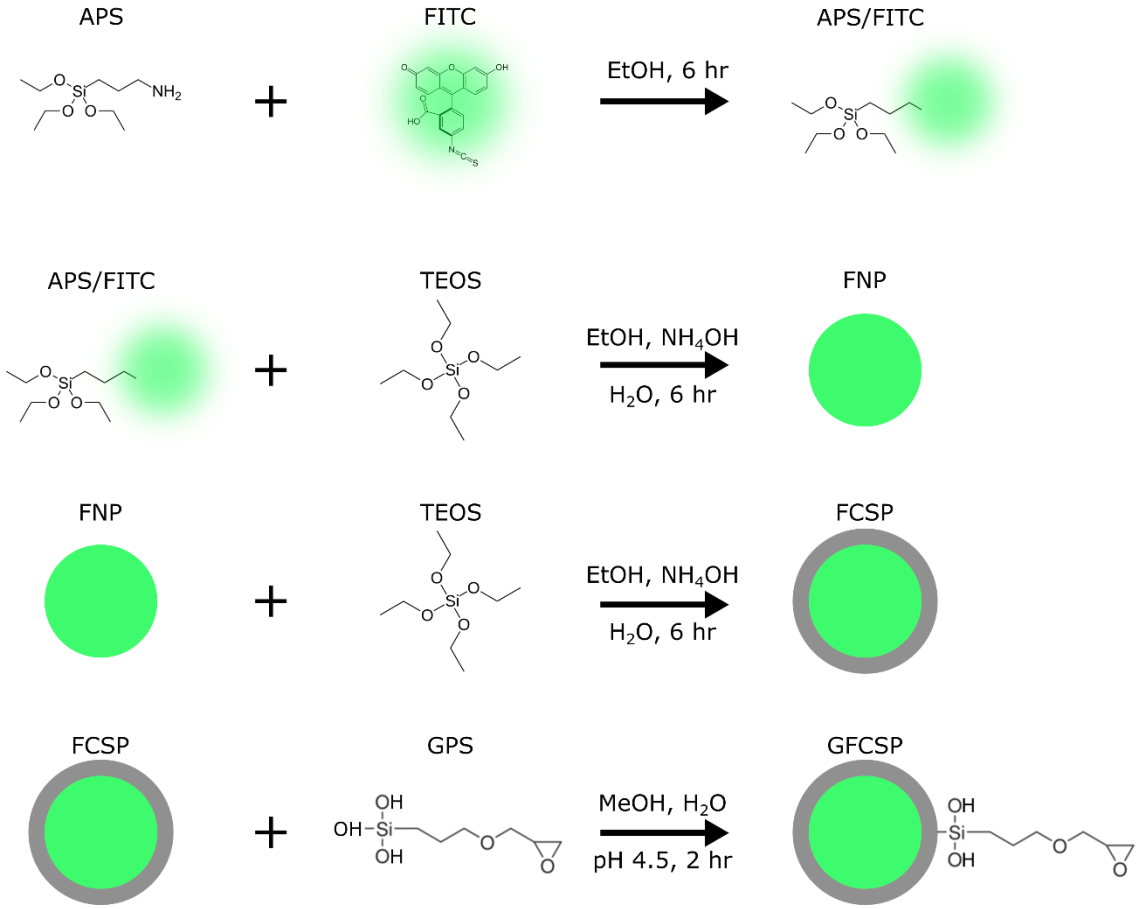

Figure 3.1 - Overview of modified Stöber process and subsequent silanization procedure used to prepare GFCSP.

Next the fluorescent particles were rinsed twice via centrifugation and subsequent resuspension in methanol. The particles were then added to a solution consisting of 95 vol % methanol and 5 vol % water, to a particle concentration of 5 % by weight. Meanwhile a silanizing solution was prepared by adjusting the pH of a 95 vol % methanol and 5 vol % water solution to 4.5 with acetic acid, and then adding 2 vol % of the silane coupling agent (3-glycidyloxypropyl) trimethoxysilane (GPS). The silanizing solution was allowed to hydrolyze for 15 minutes before the particles were introduced such that the final solution contained approximately 2 wt % particles. The silanizing reaction proceeded for 2 hours, and then particles were rinsed dispersed in pure methanol. These silane functionalized particles are designated as GFCSP. The size distributions, as measured by dynamic light scattering, for FNP, FCSP, and GFCPS are shown in Figure 3.2.

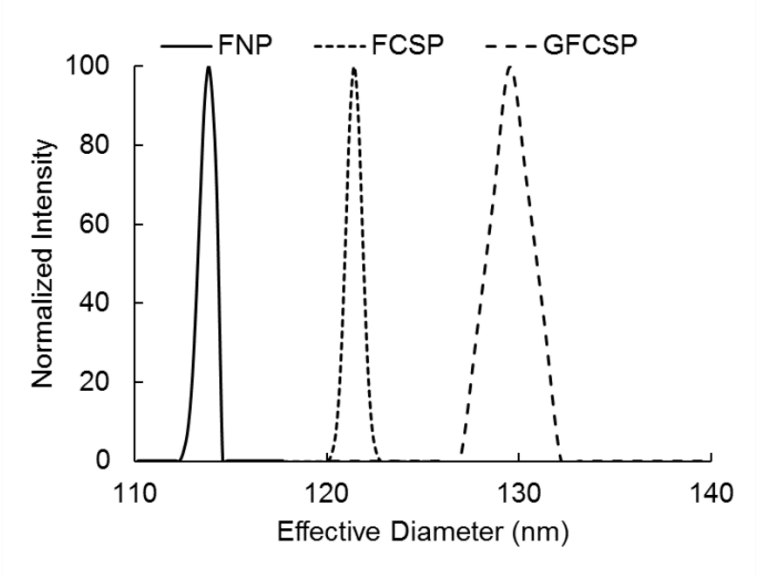

Figure 3.2 - Size distributions of synthesized FNP, FCSP and GFCSP as measured by dynamic light scattering.

3.3.2 *Sample Preparation and Observation*

The epoxy used was composed of tetraglydicyl-4,4'-diaminodiphenylmethane (TGDDM) and 4,4'-diaminodiphenyl sulfone (4,4'-DDS), and the migrating agent was a poly(ether sulfone) (PES). GFCSPs dispersed in methanol were added to TGDDM heated to 55°C in a round bottom

vacuum flask, approximately 1 mL at a time to the stirring solution before vacuum was applied to remove excess methanol. Once the particles were added, the temperature was raised to 65°C and vacuum was applied for another 2 hours to remove any excess methanol. Formulations containing PES were prepared by adding PES to the TGDDM particle mixture and then heating to 160°C for 2 hours, and mixing by hand intermittently. Finally, the DDS was added to the mixture in a mass ratio of 54:100 to TGDDM to achieve stoichiometric reaction conditions.

Samples for observation by SEM were prepared by embedding sized carbon fibers (Toray Composite Materials America, Inc.) in the formulated resin mixture and heating at a rate of 2°C-min^{-1} to 180°C, and then holding the temperature at 180°C for 2 hours. Mode I fracture surfaces, sputtered with a Gold-Palladium mixture approximately 10 nm thick, were then examined with a FEI-Sirion-XL30 scanning electron microscope with an accelerating voltage between 2-5 keV, and a working distance of 5 mm.

Samples prepared for fluorescence microscopy were prepared by knife coating a thin film of resin on a 25 mm circular cover slip at 80 °C. Fibers were spread as sparsely as possible and laid carefully over the film, before a second cover slip was placed on top of the fibers. The resin mixture was heated to 80 °C for 10 minutes to let the resin wet the fibers and cover slips. The resin was cured in a heated microscope oven (Simplex Scientific) by heating the mixture at 2 °C-min^{-1} to 180 °C and then hold the temperature constant for 2 hours. During the course of the cure fluorescent images were taken with an Olympus Ix70, inverted fluorescence microscope. The experimental setup is shown in Figure 3.3.

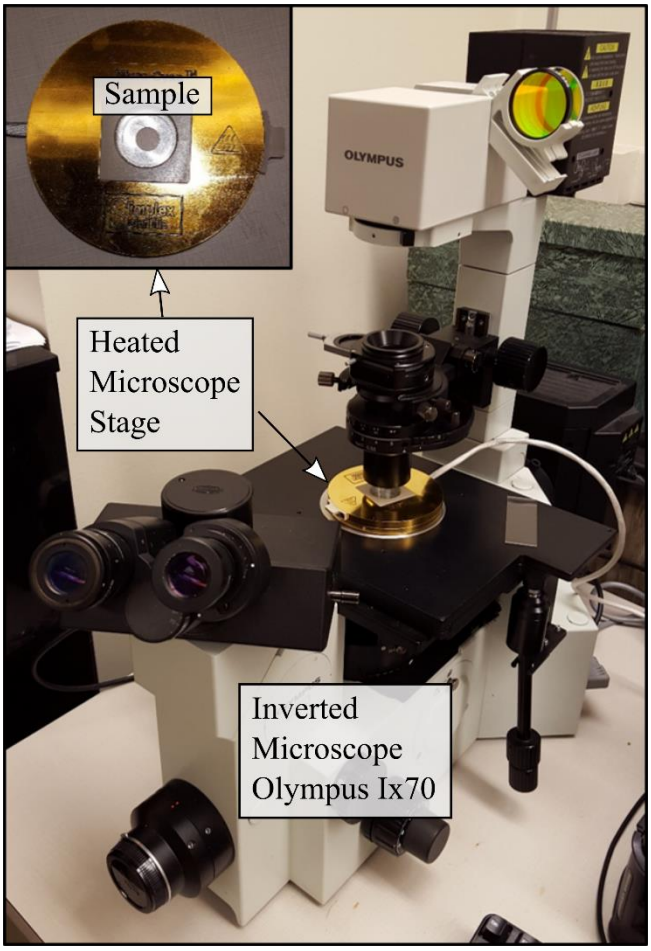

Figure 3.3 – Experimental setup for acquiring fluorescent images. The inset image is a closeup of the heated microscope stage.

3.3.3 *Analysis of Fluorescent Images*

First the images were rotated such that the fibers were oriented vertically. The fluorescence intensities were then normalized by scaling the maximum and minimum pixel intensities to 1 and 0, respectively. Average pixel intensities were then calculated in the direction of the fiber length. The figure of merit for the analysis is the peak line average intensity near a fiber surface normalized to the background fluorescence.

3.4 Results and Discussion

Mode I fracture surfaces of sized carbon fiber tows were examined using SEM to verify whether or not particles were preferentially located at the fiber-matrix interphase in fully cured samples. Figure 3.4 demonstrates that the presence of migrating agent is able to successfully direct nanoparticles to the interphase. When no migrating agent is present, a formulation containing 1.4 wt% GFCSP shows no nanoparticles at the fiber surface. Inclusion of 7.1 wt% PES in a formulation containing 1.3 wt% GFCSP, however, shows complete coverage of the fiber surface with nanoparticles. Inset images show the bulk resin for each formulation. In the absence of migrating agent GFCSPs remain well dispersed as primary particles. In contrast, the formulation containing 7.1 wt% PES shows significant aggregation of GFCSPs in the bulk phase, indicating that particle-particle interactions are also favored by the inclusion of PES.

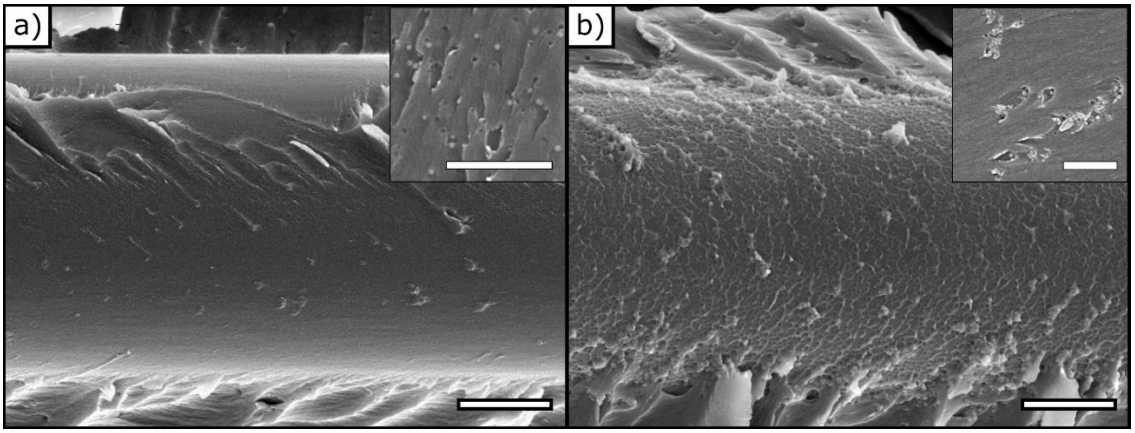

Figure 3.4 - SEM micrographs of a sized carbon fiber mode I fracture surface. (a) Carbon fiber embedded in an epoxy containing 1.4 wt% GFCSP with 0 wt% PES. (b) Carbon fiber embedded in an epoxy formulated with 1.3 wt% FNP and 7.1 wt% PES. Scale bars are 2 μm. Inset images show the particle dispersion state in the bulk resin, inset scale bars are 1 μm.

Fluoresce microscopy shows similar results for the same system, as seen in Figure 3.5. The resin formulated with 1.4 wt% GFCSP and 0% PES shows a relatively uniform background fluorescence with some small aggregates present. The primary particles are approximately 100

nm, and too small to see individually in these micrographs. In addition, the fluoresce intensity in the vicinity of the fiber is not appreciably greater than the background fluorescence. In the case of the system formulated with 1.3 wt% GFCSP and 7.1 wt% PES the fluorescence intensity near the fibers is much greater than the background fluorescence, and the aggregate structure in the bulk phase has changed significantly.

These results are consistent with depletion forces induced by the dissolved PES migrating agent. It is well known that dissolved polymers in solution can induce attractive forces between two larger bodies as they approach one another [9,10]. When the bodies are close enough they begin to exclude the polymer from the region of volume between the objects, known as the overlap volume. The exclusion of the polymer leads to an osmotic pressure difference that seeks to drive the particles further together. The magnitude of the depletion force is directly proportional to the size of the overlap volume, which depends solely on the geometry of the two approaching entities. The overlap volume between two equally sized spheres is approximately half of the overlap volume between a sphere and a flat plate. Assuming depletion interaction is the cause of the nanoparticle migration, particle-fiber interactions should be more favorable than particle-particle interactions due to the increased overlap volume between a particle and a fiber, which closely resembles the sphere-plate geometry.

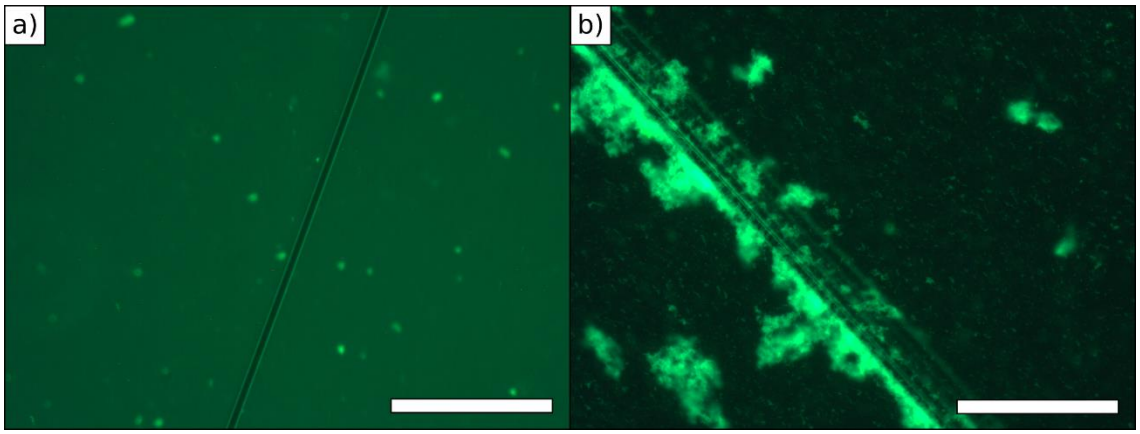

Figure 3.5 - Fluorescence micrographs of a sized carbon fiber taken after the epoxy mixture was allowed to fully react. Carbon fibers embedded in an epoxy containing (a) 1.4 wt% GFCSP with 0 wt% PES, and (b) 1.3 wt% GFCSP with 7.1 wt% PES. Scale bars represent 100 µm.

Using the heated microscope stage, the fluorescence intensity was monitored at several points during the crosslinking reaction. Figure 3.6 (a-c) shows the fluorescence intensity of a sized carbon fiber embedded in a resin containing 1.3 wt% GFCSP and 7 wt% PES at increasing times during the reaction. The samples were first held isothermally at 80 °C for 10 minutes before they were heated to 180 °C at a heating rate of 2 °C-min-1. The samples were then held isothermally for 20 minutes at 180 °C. Initially the fluorescence near the edge of the fibers was the same as the background, but as the reaction proceeds the fluorescence begins to intensify in the vicinity of the fiber surface, as seen by the emergent peak in the plotted intensity profiles.

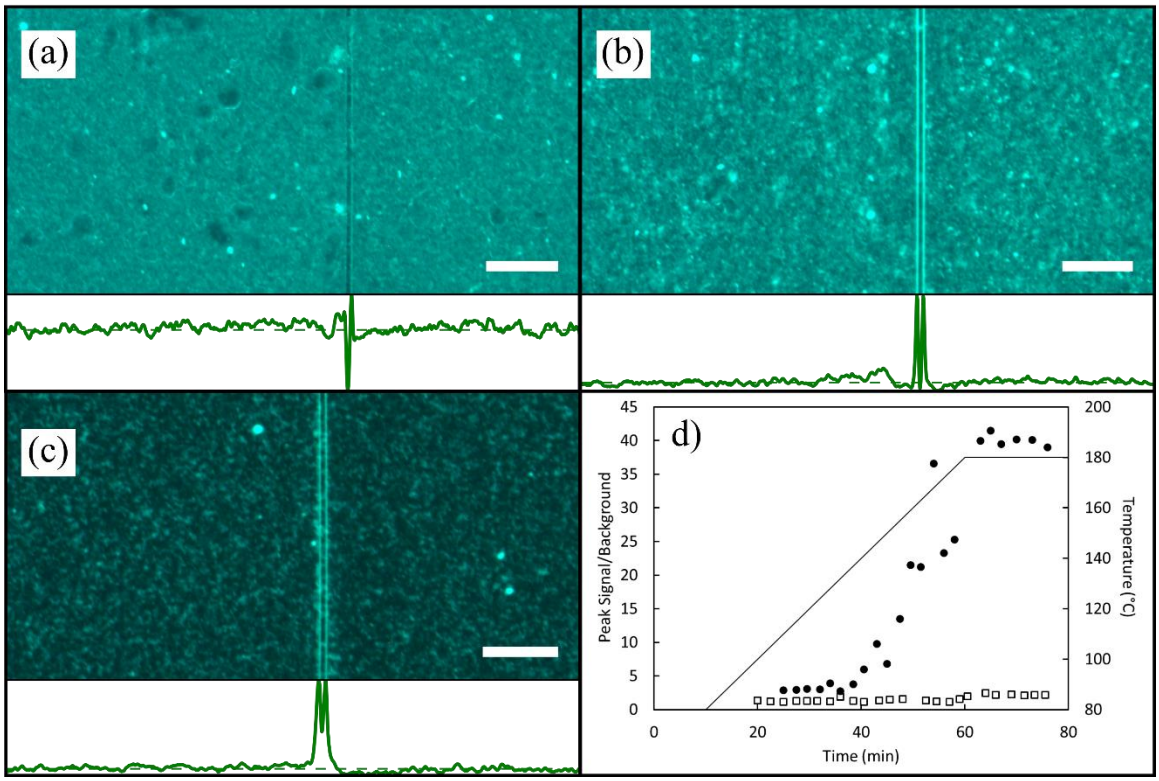

Figure 3.6 - (a-c) Fluorescence micrographs of a sized carbon fiber embedded in a resin containing 1.3 wt% GFCSP and 7 wt% PES taken at various times during the cure. (a) 35 min, (b) 45 min, (c) 75 min; scale bars are 50 µm. (d) The peak fluorescence intensity normalized by the background intensity of the sized carbon fibers embedded in (filled circles) a resin containing 1.3 wt% GFCSP and 7 wt% PES and (open squares) in a resin containing 1.4 wt% GFCSP and 0 wt% PES. The temperature profile is shown in the solid line (right axis).

Figure 3.6 (d) plots the maximum peak intensity divided by the average background intensity at various times along the reaction, as well as the temperature profile during the course of the experiments. Starting at approximately 140 °C, the fluorescence intensity near the fibers embedded in the matrix containing PES begins to increase, indicative of nanoparticles accumulating at the fiber surface. This temperature is remarkably close to the onset temperature of the exothermic crosslinking reaction, as measured by differential scanning calorimetry (see Figure 3.7; and appendix for calculation details), indicating that the particles may be weakly bound to the surface before they matrix begins crosslinking the particles in place. By 180 °C the maximum fluorescence

is achieved and as the reaction proceeds the particles are locked into place as the cross-linking density increases. Without the PES included in the formulation, the fluorescence intensity near the fiber never increases significantly over the background fluorescence, indicating no significant migration has occurred.

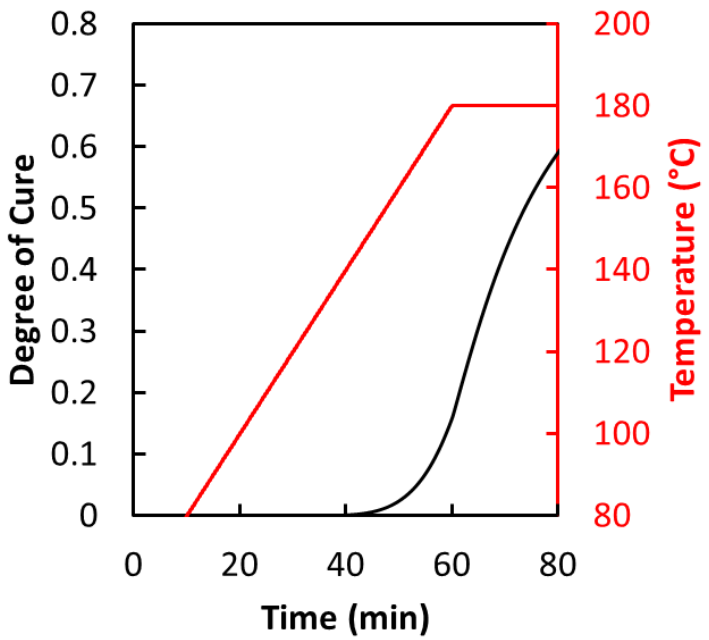

Figure 3.7 – (Black line) Degree of cure vs. time for TGDDM cured with DDS containing 1.3 wt% GFCSP and 7 wt% PES, heated at a rate of 2 °C-min^{-1} to 180 °C and then held isothermally for 20 minutes (Red line).

3.5 CONCLUSIONS

In situ fluorescence microscopy is a useful method for monitoring the relative distribution of nanoparticles in a thermosetting epoxy matrix. Using a heated microscope stage and an inverted fluorescence microscope the particle distribution may be monitored during the course of a thermally activated cure. Our results show that by including a migrating agent, such as PES, into the epoxy formulation nanoparticles preferentially accumulate at carbon fiber surfaces during the crosslinking of the epoxy matrix. The results obtained by fluorescence microscopy are consistent with results obtained from SEM micrographs. One advantage of this technique is that the onset of

migration, in a liquid or semi-solid state, can be easily determined. The onset temperature was determined to be 140 °C for a TGDDM/DDS epoxy resin containing GFCSP, with PES as the migrating agent.

While the mechanism for particle migration in these systems remains understudied, depletion interaction correctly explains the nanoparticle migration to fiber surfaces. In situ fluorescence microscopy remains a useful and flexible tool for probing the efficacy of different migrating agents in a variety of complex systems, and these methods could easily be applied to study nanoparticle distributions and morphologies in phase separating systems, or other temperature responsive systems. Processing zones and may also be readily identified as the onset of the migration agent can easily be identified using this technique.

3.6 REFERENCES

1. Herrera-Franco PJ, Drzal LT. Comparison of methods for the measurement of fibre/matrix adhesion in composites. Composites. 1992;23(1):2–27.

2. Ferreira L, Evangelista MB, Martins MCL, Granja PL, Esteves JL, Barbosa MA. Improving the adhesion of poly(ethylene terephthalate) fibers to poly(hydroxyethyl methacrylate) hydrogels by ozone treatment: Surface characterization and pull-out tests. Polymer. 2005 Nov 14;46(23):9840–50.

3. Plueddemann, E. P. Silane Coupling Agents. 2nd ed. New York: Springer US; 1991. 253 p.

4. Madhukar MS, Drzal LT. Fiber-Matrix Adhesion and Its Effect on Composite Mechanical Properties: IV. Mode I and Mode II Fracture Toughness of Graphite/Epoxy Composites. Journal of Composite Materials. 1992 Jul 1;26(7):936–68.

5. Leonard GC, Hosseinpour D, Berg JC. Modulus-Graded Interphase Modifiers in E-Glass Fiber/Thermoplastic Composites. Journal of Adhesion Science & Technology. 2009 Nov;23(16):2031–46.

6. Nguyen FN, Yoshioka K, Haro AP. Reinforced interphase and bonded structures thereof. WO2012116261 A1, 2012.

7. Nguyen FN, Nakayama Y, Kobayashi D, Kamae T, Kenichi Y. Carbon fiber's surface and its effects on an interphase formation for ultimate adhesion-related performances. In:

Proceedings of the Society for the Advancement of Materials and Process Engineering. Baltimore, MD; 2012.

8. Nguyen FN, Haro AP, Kobayashi D, Nakayama Y, Ichikawa T, Endo M, Yoshioka K, Aston E, Khoo J. Carbon fiber's surface chemistry and self-assembled interphase formation in fiber reinforced polymer composites. In: Proceedings of the International conference on composite materials. Montreal, Canada; 2013.

9. Asakura S, Oosawa F. On Interaction between Two Bodies Immersed in a Solution of Macromolecules. The Journal of Chemical Physics. 1954 Jul 1;22(7):1255–6.

10. Ye X, Narayanan T, Tong P, Huang JS, Lin MY, Carvalho BL, Fetters LJ. Depletion interactions in colloid-polymer mixtures. Physical Review E. 1996;54(6):6500.

11. Yarlagadda SC. Dynamics of hard and soft colloids in confined geometries and on structured surfaces [PhD thesis]. [Atlanta, USA]: Georgia Tech; 2015.

12. Bogush GH, Tracy MA, Zukoski Iv CF. Preparation of monodisperse silica particles: control of size and mass fraction. Journal of Non-Crystalline Solids. 1988;104(1):95–106.

13. Van Blaaderen A, Vrij A. Synthesis and characterization of colloidal dispersions of fluorescent, monodisperse silica spheres. Langmuir. 1992 Dec;8(12):2921–31.

14. Santra S, Liesenfeld B, Bertolino C, Dutta D, Cao Z, Tan W, Moudgil BM, Mericle RA. Fluorescence lifetime measurements to determine the core–shell nanostructure of FITC-doped silica nanoparticles: An optical approach to evaluate nanoparticle photostability. Journal of Luminescence. 2006 Mar;117(1):75–82.

Chapter 4. SELF ASSEMBLED NANOPARTICLE-RICH INTERPHASES USING MIGRATING AGENTS

K.B. Caldwell, and J.C. Berg, (Submitted to *Journal of Adhesion Science and Technology*)

4.1 SUMMARY

Thermoplastic additives, known as migrating agents, can be added to nanoparticle loaded thermosetting resins to form self-assembled nanoparticle structures. Most notably, in fiber reinforced thermosetting composites, self-assembled nanoparticle rich fiber-matrix interphases can be formed. While the self-assembly mechanism remains unclear, depletion interaction correctly describes the types of self-assembled structures formed. Formulations containing modest concentrations of migrating agent form self-assembled fiber-matrix interphases without causing aggregation in the bulk. Slight overdoses of migrating agent can lead to the formation of nanoparticle aggregates in the bulk phase, which can ultimately reduce the mechanical properties of the composite. Even larger overdoses of migrating agent cause the formation of large and open nanoparticle aggregates, indicative of rapid aggregation. Depletion theory predicts that larger molecular weight migrating agents should induce greater attractive forces, thus reducing the concentrations required to form these self-assembled structures. In this study, the migrating agent molecular weight dependence on the self-assembly and aggregation phenomenon are investigated. As predicted by depletion theory, larger molecular weights led to the formation of self-assembled interphases and aggregates at lower concentrations.

4.2 INTRODUCTION

The mechanical properties of polymeric composites can be improved by the inclusion of nanoparticles in the polymer matrix [1–3]. The dispersion state of the particles in these

nanocomposites is critical to realize the full potential of these materials. Large aggregates may act as local stress concentration sites, resulting in reduced mechanical properties. Nanoparticles have also been used to tailor the interphase properties in fiber reinforced polymeric composites [4–6]. These particle-reinforced interphases have been used to improve bulk mechanical properties and can often impart multifunctionality to the final composite, i.e., thermal resistance, magnetism, electrical conductivity [7,8]. Common interphase modifiers include nanoparticles, carbon nanotubes, clay particles and silane coupling agents.

Many methods for preparing engineered fiber-matrix interphases have been developed in recent years. Seeded growth techniques have been used to grow carbon nanotubes, and metal oxide nanowhiskers from a variety of fiber surfaces. Deposition of preformed particles has been achieved by chemical reaction, electrostatic deposition, and dip coating, for example [5]. Many of these processing steps require high temperature, or harsh reaction conditions that may significantly damage the fiber properties. Growing single-walled carbon nanotubes using chemical vapor deposition, for example, requires temperatures around 1000 °C [9].

In recent years, self-assembled nanoparticle-rich interphases have also been prepared in polymeric media. Nanoparticles dispersed in thermoplastic polymer films have been demonstrated to accumulate near cracks due to entropic driving forces of the polymer chains [10,11]. In thermosetting fiber reinforced composites, the addition of thermoplastic “migrating agents” has been shown to form self-assembled nanoparticle reinforced fiber-matrix interphases [12–14]. Inclusion of excess migrating agent, however, can lead to the formation of nanoparticle aggregates in the bulk phase [5].

There are several mechanisms that may result in the self-assembly of nanoparticles at surfaces in the presence of a polymeric solution, including electrostatic attraction [4], phase separation

[15,16], and depletion forces [17,18]. Electrostatic forces, while relevant in polar media, are unlikely to be significant in thermosetting polymeric solutions due to the low dielectric constants of most polymers. Phase separation may result in self-assembled interphases if both the fiber and particle surfaces are preferentially wet by the same phase. Depletion forces, while relatively unstudied in polymeric media, correctly describe the types of self-assembled structures formed in fiber reinforced thermosetting composites.

Depletion forces arise from the geometric exclusion of smaller entities, known as depletants, between two larger objects as they approach one another. The resulting concentration difference between the larger objects and the bulk solution gives rise to an osmotic pressure that acts inwards on both objects. The strength of the depletion force is strongly dependent upon the geometry and surface roughness of the approaching objects. For example, the depletion force between two smooth spheres is approximately half the force between a smooth sphere and a flat plate [19]. In fiber reinforced polymeric composites with dispersed nanoparticles, the fiber-particle geometry should closely resemble that of the sphere-plate geometry resulting in greater attractive forces.

Fiber reinforced thermosetting resin systems containing nanoparticles and insufficient amounts of migrating agent form no self-assembled structures. Increasing the migrating agent concentration slightly causes the formation of a self-assembled nanoparticle rich interphase at fiber surfaces, without causing aggregation in the bulk. Further increases in the migrating agent concentration, and thereby depletion strength, result in the formation of aggregates in the bulk phase as well as deposition at the interface. The size of the aggregates formed increases with increasing migrating agent concentration. The progressive onset of these self-assembled structures with increasing depletion strength is well documented in aqueous media. Only edge and corner deposition is observed at the lowest depletion strengths, at intermediate depletion strengths surface

deposition is also observed, and at the highest depletion strengths aggregates in the bulk begin to form [20].

Aside from geometric constraints, the magnitude of the depletion force is related to the size of the depletant and the concentration. For polymeric depletants, the interaction between the polymer and the solvent may also play an important role. Assuming that the polymer is miscible in the solvent, the strength of the depletion forces should increase with increasing molecular weight. In this study we investigate the effect of migrating agent molecular weight on the formation of the self-assembled structures in an epoxy based resin reinforced with carbon fibers. We seek to determine the onset concentrations required to form the various self-assembled structures as the migrating agent molecular weight increases.

4.3 EXPERIMENTAL

4.3.1 *Materials*

Sized carbon fibers were provided by Toray Composite Materials America, Inc ('Toray CMA') for use in this study. Four distinct commercially available poly(ether sulfone) (PES) polymers were provided by Sumika and Solvay, all of the PES variants were hydroxyl terminated on one end of the polymer chain. Table 4.1 lists the supplier, the trade names of each variant, the weight average molecular weight as determined by size exclusion chromatography using poly(styrene) standards, and the hydrodynamic diameter of the polymers as measured by dynamic light scattering in N-N-Dimethylformamide. The epoxy used in this study was Araldite MY-721, which consists of tetraglycidyl 4,4'-diaminodiphenylmethane (TGDDM). The curing agent was 4,4'-diaminodiphenysulfone (DDS). Epoxy functionalized 100 nm silica nanoparticles, dispersed in TGDDM were supplied by Admatechs.

Table 4.1 - Poly(ether sulfone) molecular weights and supplier information

Supplier	Trade Name	M_W [kDa]	D_P [nm]
Sumika	5003p	57.4	11.3 ± 0.3
Solvay	Veradel 3000RP	53.9	10.6 ± 0.2
Solvay	Virantage VW-10200	53.4	10.4 ± 0.1
Solvay	Veradel 3600RP	35.1	7.5 ± 0.2

4.3.2 *Resin Formulation*

The base resin consisted of TGDDM cured with DDS. All of the formulations were prepared to include a total of 2 wt% 100 nm epoxy functionalized silica nanoparticles, and varying concentrations of one of the four PES variant. The PES concentrations ranged from 0.25 wt% to 10 wt%.

First the particles were weighed out and diluted with additional TGDDM to achieve the desired particle loading. The particles were then dispersed in the TGDDM by applying a shear force using a FlackTek Speedmixer DAC 150.1 FVZ-K (Landrum, SC) at a setting of 3000 rpm for 1 minute. Next the poly(ether sulfone) (PES) migrating agent was added to the dispersed nanoparticle mixture, and heated to a temperature of 160 °C. The resulting mixture was stirred by hand every 30 minutes over a two-hour period to fully incorporate the PES into the resin. Then the mixture was allowed to cool down to 80 °C before the curing agent, DDS, was finally added. The final mixture was mixed in the FlackTek at a setting of 2000 rpm for a total of 10 minutes.

4.3.3 *Sample Preparation*

Carbon fibers were placed in a silicon mold and then embedded in the resins prepared above. The samples were thermally cured by ramping the temperature to 180 °C, at a rate of 2 °C·min^{-1}, and then holding the temperature constant at 180 °C for two hours. The samples were then removed

from their molds and cut, using a tile saw, to prepare 90° cross-sections. Samples were then sanded and polished for observation under a scanning electron microscope (SEM).

4.3.4 *Scanning Electron Microscopy*

Backscattered SEM images were used to generate contrast between the silica particles and the polymeric matrix and carbon fibers. A FEI-Sirion-XL30 scanning electron microscope was operated in backscattering mode with accelerating voltages ranging from 3.5 to 5 keV, and the spot sizes between 3 and 5. The samples were coated with a thin layer of conductive carbon to prevent charging artifacts.

4.3.5 *Post-Processing SEM images*

ImageJ [21] was used to post-process the images in a systematic manner. To improve the contrast in the images the ‘enhance contrast’ feature was used by selecting the ‘normalize histogram’ option.

4.4 DEPLETION THEORY

The use of macromolecules as depletants to form self-assembled structures in aqueous media has been well studied and documented [19,20]. The first mathematical model of depletion forces was proposed by Asakura and Oosawa [22], in which they describe the nature of attractive forces between two larger objects immersed in a solution containing smaller macromolecules. As the larger objects approach one another, eventually the smaller entities, commonly referred to as depletants, are physically excluded from the space between the larger entities, resulting in a region of volume containing pure solvent. The concentration difference between this region, commonly referred to as the depletion volume, and the bulk solution results in an osmotic pressure difference

that acts inwards on both objects. The Gibbs free energy associated with depletion interaction is given simply by Equation (4.1)

$$\Delta G_{dep} = -\Pi_b V \tag{4.1}$$

where Π_b is the osmotic pressure of the bulk solution, and V is the depletion volume, which depends on the geometry of the two larger entities approaching one another, and the size of the depletant. Figure 4.1 shows a schematic of depletion interaction for two spheres approaching one another, and a sphere approaching a plate across a macromolecule solution.

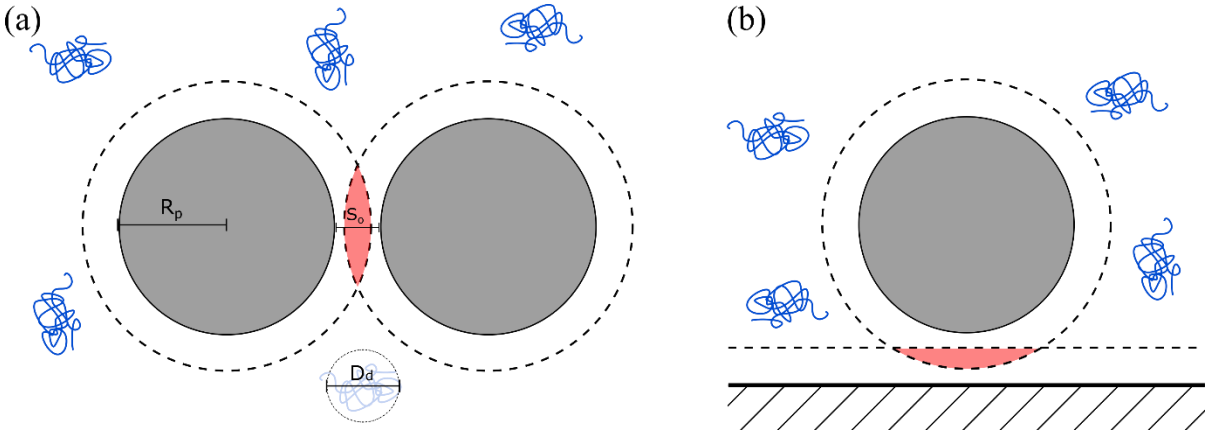

Figure 4.1 - Representation of depletion interaction for (a) two smooth spheres and (b) a smooth sphere approaching a flat plate. The dashed regions show the excluded volume, and the shaded region represents the overlap volume.

The osmotic pressure of a polymer solution is approximated well by Equation (4.2), where c_b is the polymer mass concentration in the bulk phase, R is the gas constant, T is the absolute temperature, MW is the mass average molecular weight of the polymer, and B_2 is the second osmotic virial coefficient of the polymer dispersed in the solvent phase. B_2 describes the non-ideal interactions of the polymer in a given solvent, and is typically positive if a polymer is soluble in a given solvent.

$$\Pi_b = c_b RT\left(\frac{1}{MW} + c_b B_2\right) \tag{4.2}$$

The depletion volume depends on the geometry of the larger objects, as well as their surface roughness [23]. The depletion volume for two smooth equally sized spheres, and a smooth sphere approaching a flat plate is given by Equations (4.3) and (4.4), respectively.

$$V_{ss} = \frac{\pi}{6}(D_d - S_o)^2\left(3R_p + D_d + \frac{S_o}{2}\right), \qquad for\ S_o < D_d \tag{4.3}$$

$$V_{sp} = \frac{\pi}{3}R_p(D_d - S_o)^2\left(3R_p + \frac{D_d}{2} + S_o\right), \qquad for\ S_o < D_d \tag{4.4}$$

S_o represents the distance of closest approach between the two objects, R_p is the particle radius, and D_d is the diameter of the depletant. In the limiting case where the particles are much larger than the depletants, as will be assumed herein, the equations for the overlap volume simplify to Equations (4.5) and (4.6) for two smooth spheres, and a smooth sphere approaching a flat plate. Since the depletion strength is directly proportional to the depletion volume, the attractive forces between a sphere approaching a flat plate should be approximately twice as large as two similarly sized spheres approaching one another.

$$V_{ss} = \frac{\pi}{2}R_p(D_d - S_o)^2 \tag{4.5}$$

$$V_{sp} = \pi R_p(D_d - S_o)^2 \tag{4.6}$$

The maximum depletion force between two objects occurs when the entities are in direct contact with one another, i.e., $S_o = 0$. Making the further assumption that the polymer depletant size scales with the square root of the molecular weight, which is true for ideal polymers in solution, the maximal depletion force expected can be approximated by Equation (4.7),

$$\left|\frac{\Delta G_{max}}{RT}\right| = \pi R_p F(c_b + c_b^2 B_2 MW) \tag{4.7}$$

where F is a constant that accounts for the proportionality of the depletant size with molecular weight and the geometry of the approaching objects. If the depletion force is not significantly

greater than the thermal energy of the system, represented by the quantity RT, the attractions may not be sufficient to keep the objects in contact with one another. One study suggested that the depletion forces must be approximately five times the thermal energy in order to form self-assembled structures [20]. Equation (4.7) reveals that larger molecular weight depletants should exhibit proportionately larger depletion forces for a given concentration and similar osmotic coefficients. Therefore, the amount of depletant required to form self-assembled interphases at surfaces, and aggregates in the bulk should be lower for larger molecular weight polymers of the same type.

4.5 RESULTS

The onset concentrations of PES required to form each self-assembled structure type were all determined from backscattered SEM images. The samples were polished 90° cross sections of fiber reinforced composites containing 2 wt% 100 nm silica particles and varying amounts of PES. For each PES type the onset concentration to form a self-assembled interphase around the fiber surface was the lowest. As the PES concentration is increased the formation of small aggregates in the bulk phase is observed as the aggregation onset concentration. Further increasing the PES concentration lead to the onset of rapid aggregates (> 1 μm in size). Figure 4.2 shows example micrographs for the Sumika 5003p migrating agent at various concentrations.

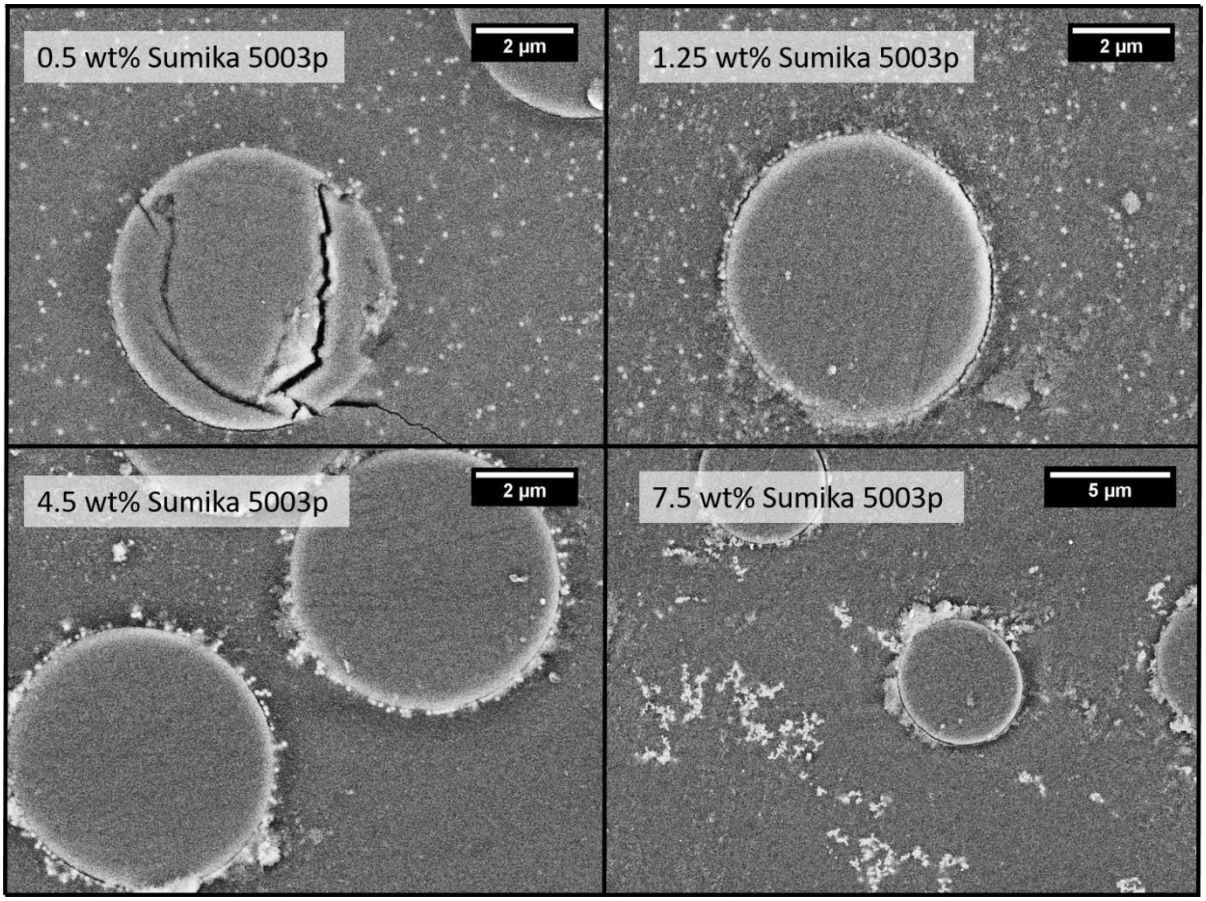

Figure 4.2 - Backscattered SEM images of 90° cross sections of samples prepared with various concentrations of Sumika 5003p PES. The resin consists of TGDDM cured with DDS, and the nanoparticle loading is 2 wt% for all samples. The bright regions are the silica particles.

The sample containing only 0.5 wt% Sumika 5003p shows that the particles remain well dispersed in the bulk phase, and no self-assembled interphase has been formed. As the concentration, and thereby depletion strength, is increased to 1.25 wt%, the formation of a self-assembled nanoparticle-rich interphase at the fiber surfaces is observed, while the nanoparticles remain well dispersed in the bulk phase. This is the ideal case that is most likely to result in the best mechanical improvements. When the concentration is increased further to 4.5 wt% Sumika 5003p, the nanoparticles are no longer well dispersed in the bulk phase and there are small aggregates deposited at the surface of the fiber. These aggregates may act as stress concentrators

and reduce the mechanical properties of the ultimate composite. Finally, samples prepared with 7.5 wt% Sumika 5003p showed extensive rapid aggregation in the bulk phase, characterized by the larger (> 1 μm) and more open structure of the aggregates. Additionally, the nanoparticle distribution within the interphase region is non-homogeneous.

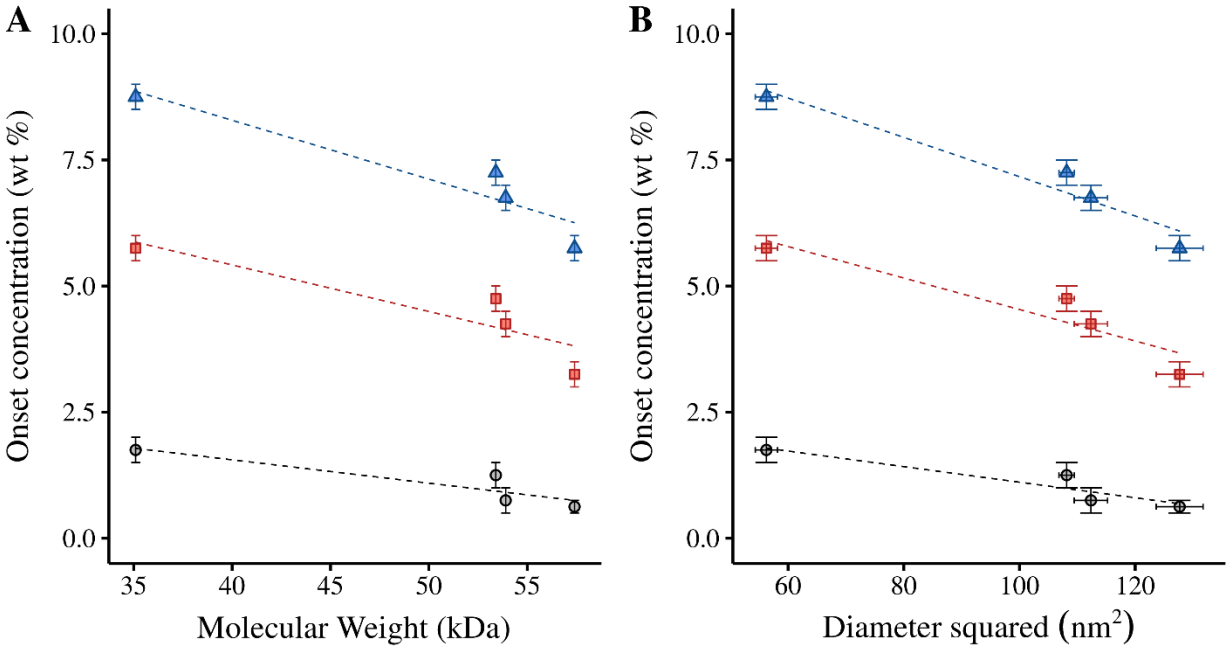

Figure 4.3 - Onset concentrations vs. PES migrating agent (A) molecular weight, and (B) diameter squared. (black circles) onset concentration of self-assembled nanoparticle rich interphases; (red squares) onset concentration for aggregation of nanoparticles in the bulk resin; (blue triangles) onset concentration to induce rapid aggregation in the bulk resin.

The onset concentrations for each migrating agent variant were determined and are plotted in Figure 4.3. The results show that for increasing molecular weight (or equivalently increasing diameter squared), lower concentrations of PES are required to induce the self-assembly of nanoparticle-rich interphases, aggregates in the bulk, and rapid aggregation. These results are in agreement with what is predicted from depletion theory, in that larger molecular weight polymer depletants produce greater depletion forces at a given concentration. By tuning the concentration and the molecular weight of the polymeric depletant the self-assembly process can be tuned to

form reinforced interphases without disrupting the dispersion state of the particles in the bulk phase.

4.6 CONCLUSIONS

As the molecular weight of the PES migrating agent increases, the concentration required to form various self-assembled structures decreased, consistent with depletion theory. Below a minimum concentration of PES, no self-assembled structures are formed. Intermediate concentrations of PES result in the formation of a self-assembled nanoparticle interphase. Larger concentrations of PES lead to the formation of aggregates in the bulk phase of increasing severity with increasing PES content. The strength of the depletion force can be tuned by altering the molecular weight and concentration of the migrating agent. Although not investigated directly here, the particle size and surface roughness of the fiber may play an additional role in the formation of the self-assembled interphase. Nevertheless, careful selection of the concentration and molecular weight of the depletant can be used to selectively form a self-assembled nanoparticle rich fiber-matrix interphase in fiber reinforced polymeric composites.

4.7 REFERENCES

1. Tsai J-L, Hsiao H, Cheng Y-L. Investigating Mechanical Behaviors of Silica Nanoparticle Reinforced Composites. Journal of Composite Materials. 2010 Feb 1;44(4):505–24.
2. Sprenger S. Improving mechanical properties of fiber-reinforced composites based on epoxy resins containing industrial surface-modified silica nanoparticles: review and outlook. Journal of Composite Materials. 2015 Jan 1;49(1):53–63.
3. Johnsen BB, Kinloch AJ, Mohammed RD, Taylor AC, Sprenger S. Toughening mechanisms of nanoparticle-modified epoxy polymers. Polymer. 2007 Jan 12;48(2):530–41.
4. Rutz BH, Berg JC. Electrostatic deposition of silica nanoparticles between E-glass fibers and an epoxy resin. J Appl Polym Sci. 2015 Feb 20;132(8):1–9.

5. Caldwell KB, Berg JC. Nanoparticles as Interphase Modifiers in Fiber Reinforced Polymeric Composites: A Critical Review. Rev Adhes Adhes. 2017 Mar;5(1):1–54.

6. Qin W, Vautard F, Askeland P, Yu J, Drzal LT. Incorporation of silicon dioxide nanoparticles at the carbon fiber-epoxy matrix interphase and its effect on composite mechanical properties. Polym Compos. 2015 Jul 1;1–9.

7. Gao S, Zhuang R-C, Zhang J, Liu J-W, Mäder E. Glass Fibers with Carbon Nanotube Networks as Multifunctional Sensors. Adv Funct Mater. 2010 Jun 23;20(12):1885–93.

8. H. Malakooti M, A. Patterson B, Hwang H-S, A. Sodano H. ZnO nanowire interfaces for high strength multifunctional composites with embedded energy harvesting. Energy & Environmental Science. 2016;9(2):634–43.

9. Kong J, Cassell AM, Dai H. Chemical vapor deposition of methane for single-walled carbon nanotubes. Chemical Physics Letters. 1998 Aug 14;292(4):567–74.

10. Gupta S, Zhang Q, Emrick T, Balazs AC, Russell TP. Entropy-driven segregation of nanoparticles to cracks in multilayered composite polymer structures. Nat Mater. 2006 Mar;5(3):229–33.

11. Balazs AC, Emrick T, Russell TP. Nanoparticle Polymer Composites: Where Two Small Worlds Meet. Science. 2006 Nov 17;314(5802):1107–10.

12. Nguyen FN, Nakayama Y, Kobayashi D, Kamae T, Kenichi Y. Carbon fiber's surface and its effects on an interphase formation for ultimate adhesion-related performances. In: Proceedings of the Society for the Advancement of Materials and Process Engineering. Baltimore, MD; 2012.

13. Nguyen FN, Haro AP, Yoshioka K. Effects of a Nanomaterial-Toughened Interphase in Carbon Fiber Reinforced Polymer Composite. In: Proceedings of the Society for the Advancement of Materials and Process Engineering. Wichita, KS; 2013.

14. Caldwell K, Berg JC. Direct observation of nanoparticle migration in epoxy based fiber reinforced composites using fluorescence microscopy. Journal of Composite Materials. 2017 Dec 17;51(28):3877-3885.

15. Mackay ME, Tuteja A, Duxbury PM, Hawker CJ, Horn BV, Guan Z, Chen G, Krishnan RS. General Strategies for Nanoparticle Dispersion. Science. 2006 Mar 24;311(5768):1740–3.

16. Williams RJJ, Hoppe CE, Zucchi IA, Romeo HE, dell'Erba IE, Gómez ML, Puig J, Leonardi AB. Self-assembly of nanoparticles employing polymerization-induced phase separation. Journal of Colloid and Interface Science. 2014 Oct 1;431:223–32.

17. Ye X, Narayanan T, Tong P, Huang JS, Lin MY, Carvalho BL, Fetters LJ. Depletion interactions in colloid-polymer mixtures. Physical Review E. 1996;54(6):6500.

18. Banerjee D, Yang J, Schweizer KS. Entropic depletion in colloidal suspensions and polymer liquids: role of nanoparticle surface topography. Soft Matter. 2015;11(47):9086–98.

19. Lekkerkerker HNW, Tuinier R. Colloids and the depletion interaction. Dordrecht ; New York: Springer; 2011. 233 p. (Lecture notes in physics).

20. Yarlagadda SC. Dynamics of hard and soft colloids in confined geometries and on structured surfaces [PhD thesis]. [Atlanta, USA]: Georgia Tech; 2015.

21. Schneider CA, Rasband WS, Eliceiri KW. NIH Image to ImageJ: 25 years of image analysis. Nat Meth. 2012 Jul;9(7):671–5.

22. Asakura S, Oosawa F. On Interaction between Two Bodies Immersed in a Solution of Macromolecules. The Journal of Chemical Physics. 1954 Jul 1;22(7):1255–6.

23. Kraft DJ, Ni R, Smallenburg F, Hermes M, Yoon K, Weitz DA, van Blaaderen A, Groenewold J, Dijkstra M, Kegel WK. Surface roughness directed self-assembly of patchy particles into colloidal micelles. Proceedings of the National Academy of Sciences. 2012;109(27):10787–10792.

Chapter 5. EFFECTS OF A SELF-ASSEMBLED FIBER-MATRIX INTERPHASE ON ADHESION

5.1 ABSTRACT

The self-assembly of nanoparticle rich interphases can be achieved in thermosetting polymers by the incorporation of migrating agents into the resin mixture. The extent to which the self-assembled interphase improves the mechanical properties of the composite has yet to be examined. The interfacial shear strength, which is a measure of adhesion between the fiber and the matrix, is one such property that might improve upon the formation of a nanoparticle reinforced interphase. Here a study is conducted to try to isolate the effects of the interphase on the composite strength, accounting for the presence of nanoparticles and migrating agent in the bulk resin. The results, however, were inconclusive. Adding nanoparticles alone was enough to improve the interphase strength to the same level as the systems containing both nanoparticles and migrating agent.

5.2 INTRODUCTION

Previous work has shown that that the mechanical properties of carbon fiber reinforced polymeric composites can be improved through the incorporation of nanoparticles into the fiber-matrix interphase [1,2]. The greatest improvements in the resulting composites were found in the fracture toughness, where an approximate 300% improvement was observed. Similar improvements have also been observed in composites containing dispersed nanoparticles [3,4]. The inclusion of thermoplastics into epoxy resins can also improve certain mechanical properties. It is difficult to isolate the reasons for the mechanical improvements observed in fiber reinforced composites containing self-assembled interphases. Careful isolation of the role of each component is needed

to probe the effects of the interphase itself. Desized fibers are useful to use since fiber sizings often contain adhesion promoters and processing aids that may complicate the analysis [5].

In this study, nanoparticles were incorporated into the interphase though the use of a so called "migrating agent", poly(ether sulfone) (PES). Studies were conducted to determine whether or not the presence of a self-assembled interphase, formed via the inclusion of PES, improved the interfacial shear strength (IFSS) of the composite utilizing the single fiber fragmentation technique (SFFT). Several controls were prepared in order to account for the improvements resulting from the inclusion of nanoparticles and the PES when added individually. The results show that the IFSS of a desized carbon fiber was increased by including PES alone, and even more-so by including nanoparticles alone. When both PES and nanoparticles were added together to form the interphase, however, the IFSS results were not statistically different from the control containing nanoparticles alone. In addition, the presence of the interphase did not statistically improve the IFSS for a sized carbon fiber.

5.3 Measuring Fiber-Matrix Adhesion

5.3.1 *Delamination Techniques*

Many experimental techniques to measure the fiber-matrix adhesion relate the interfacial strength to the force required to delaminate a bonded region of fiber [6]. Three such techniques are the fiber indentation technique [7], the fiber pullout technique [8,9], and the microdroplet test [10,11], all of which are shown in Figure 5.1.

In the indentation technique, shown in Figure 5.1-A fibers are loaded compressively with a probe until they delaminate from the matrix. Samples are prepared by taking a thin slice of a composite with the fibers in the transverse direction and then polishing the surface. The load required to delaminate the specimen depends on the loading probe geometry and the specimen

geometry. In order to determine the interfacial shear strength, a finite element analysis is required to account for the geometry and probe parameters. In addition, the local volume fraction of fibers may affect the results, leading to some scatter in the collected data. Nevertheless, commercial instruments exist for measuring the interfacial strength using the fiber indentation technique.

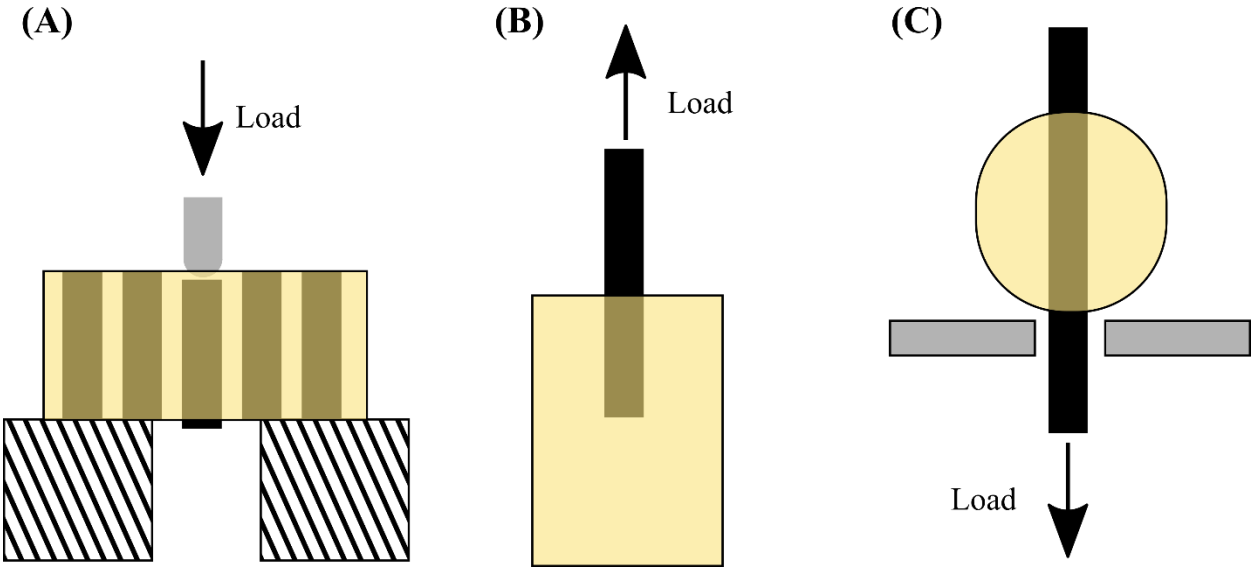

Figure 5.1 – Delamination based experimental methods for determining fiber-matrix adhesion. (A) The indentation technique, in which fibers are loaded compressively until delamination occurs. (B) Fiber pullout, in which partially embedded fibers are load in tension until delamination occurs. (C) The microdroplet technique, in which a bead of resin is deboned from a fiber as it is pulled through a fixed gap.

The fiber pullout method (Figure 5.1-B) presents a more direct method of measuring the interfacial shear strength. From a simple force balance, the stress necessary to delaminate the fiber from the matrix should be directly proportional to the embedded area. The interfacial shear strength is given by Equation (5.1);

$$IFSS = \frac{D_f \sigma_f}{4l} \tag{5.1}$$

wherein D_f is the fiber diameter, σ_f is the applied stress at failure, and l is the embedded fiber length. The maximum embedded length is limited by the ultimate tensile strength of the fibers. If the length is too great the fiber may break before delamination occurs. For example, a carbon fiber

of 7 μm, with an IFSS of 100 MPa (which is typical for the carbon fibers embedded in epoxy), and an ultimate tensile strength of 5000 MPa has a maximum embedded length less than 90 μm, making sample production difficult. In addition, the meniscus formed at the matrix-air-fiber interface can create large stress concentrations, and results in difficult determination of the true embedded length.

The microdroplet (Figure 5.1-C) test also uses Equation (5.1) to calculate the IFSS, where l is the embedded fiber length by the microdroplet. The advantage of the microdroplet test is that very short values of l can be achieved, of the order of 25 μm, allowing the measurement of small-diameter fibers with high levels of adhesion. In the technique a small droplet of resin is cured on a fiber and the fiber is placed between a rigid opening just wide enough for the fiber to fit between. The fiber is then drawn through the gap, such that the resin is stressed until it delaminates from the fiber. As with the fiber pullout technique, in the microdroplet technique the fiber-matrix-air interface may introduce stress concentrations, and the formation of a meniscus complicates the determination of the embedded length. In addition, the geometry of the opening the fiber is drawn through can affect the results. Local stress concentrations at the clamp edges can sometimes cause the sample to fail in the droplet meniscus instead of by delamination [6].

While challenges exist with all of the techniques, they are all commonly used in the study of fiber-matrix adhesion and can, at the very least, provide comparative results. That is, an improvement in the measured IFSS for each technique corresponds to an increase in the actual adhesion of the composites. While the absolute value of the IFSS may differ when measured with different techniques, each method can be used to track relative improvements in the mechanical properties of the fiber-matrix interface.

5.3.2 *Single Fiber Fragmentation*

Perhaps the most commonly used method to measure the IFSS is the single fiber fragmentation test (SFFT). The technique, developed by Kelly and Tyson, was used initially to test brittle tungsten fibers embedded in a copper matrix [12], but is applicable to any brittle fiber suspended in a ductile matrix. A single fiber is suspended in the center of a dogbone coupon and the specimen and then axially stressed. As the stress builds up in the specimen the fiber will fragment once the tensile strength, σ_c, of the fiber is reached. More and more fragments appear as additional stress is applied until the fiber is eventually saturated with breaks. Fragments shorter than this critical fragment length, l_c, do not have enough area to transfer enough stress into the fiber to cause additional breaks. Figure 5.2 shows the single fiber dogbone specimen, along with the stress profiles along the direction of the fiber for increasing applied stresses.

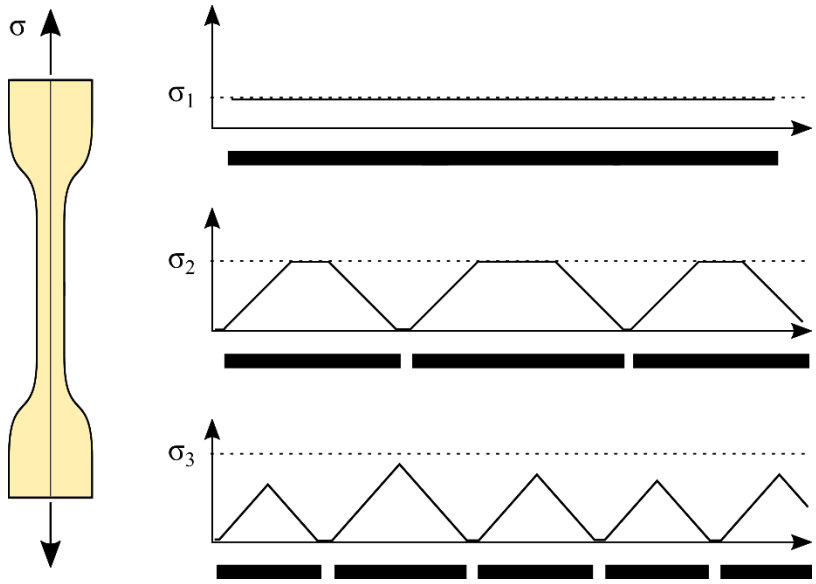

Figure 5.2 – (Left) Depiction of a single fiber dogbone composite for SFFT. (Right) Fiber fragments (shown as black bars), and the local fiber stresses plotted for increasing applied stresses ($\sigma_1 < \sigma_2 < \sigma_3$).

Determination of l_c, is typically evaluated using microscopy. This typically requires that the matrix be transparent. For transparent fibers, such as glass fibers optical microscopy can easily be

used to determine the average fragment length, l_{avg}. For opaque or black fibers, such as carbon fibers, it is more difficult to determine the location of fiber breaks, especially if the matrix does not appreciably yield during the fragmentation process. The use of cross polarized light can be helpful in counting fiber fragments in such cases [13], because it generates contrast from the strain fields near the fragment ends. Figure 5.3 shows the difference between sample observation under white light and cross polarized light, for an E-glass fiber embedded in an epoxy matrix after the specimen has been stressed to saturation.

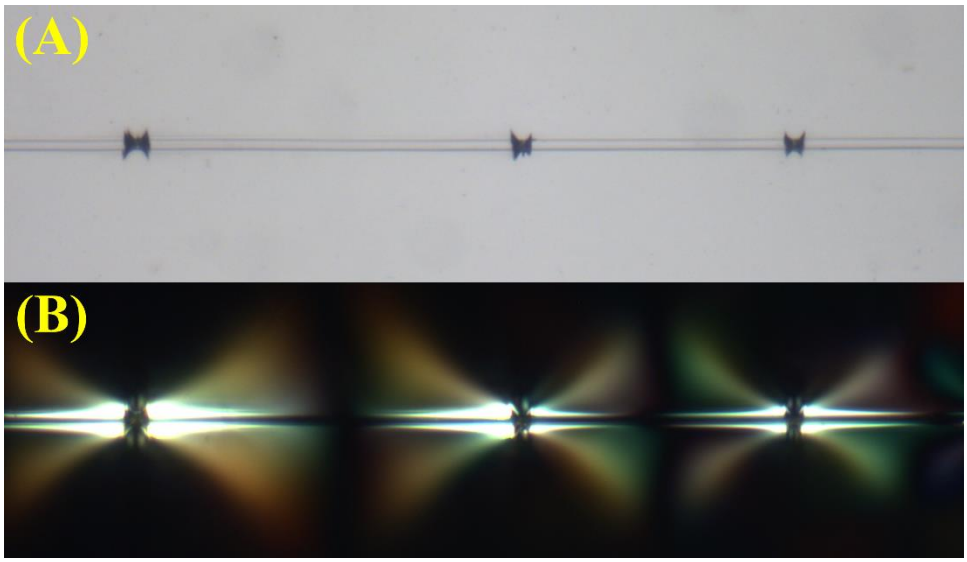

Figure 5.3 – Single fiber composite sample consisting of E-glass embedded in an epoxy matrix observed under (A) white light, and (B) cross polarized light.

In an actual experiment there is a distribution of fragment lengths, due to the stochastic fragmentation process. If a given fragment is larger than l_c it will break into two fragments. The final fragmentation event for each segment will thus produce two segments with lengths between $0.5l_c$ and l_c. If the probability of fragmenting is uniform, an equal distribution of fiber lengths should be expected, and the critical fragment length can be computed simply as: $l_c = 4/3\ l_{avg}$. In practice l_{avg} is determined by counting the number of breaks in the gauge length, and then dividing by the original gauge length and adding one.

Performing a force balance along the fragment length, assuming constant stress transfer along the entire length of the fragment, i.e. a perfectly bonded fiber with an entirely plastic response of the matrix, leads to Equation (5.2) [12].

$$IFSS = \frac{\sigma_c D_f}{2l_c} \tag{5.2}$$

where σ_c is the critical fragment strength at l_c, D_f is the fiber diameter, and l_c is the critical fragment length. Determination of σ_c requires the use of Weibull statistics, which describe the distribution of surface flaws large enough to cause failure [13,14]. Using Weibull statistics gathered from tensile data of single fibers the strength of a fiber can be determined for any fragment length. Assuming a Weibull distribution, the probability a fiber will fail for a given gauge length and applied stress is given by Equation (5.3).

$$P_F(\sigma, L) = 1 - \exp\left(-\frac{L}{L_o}\left(\frac{\sigma}{\sigma_o}\right)^m\right) \tag{5.3}$$

where L is the fiber length, L_o is gauge length the experiments were conducted at, σ_o is the characteristic strength, σ is the applied stress, and m is the Weibull modulus (sometimes called the shape parameter). The probability of failure, P_F is calculated by sorting the data according the failure stress in ascending order and using the relationship: $P_F = \frac{i-0.3}{n+0.4}$, where i represents the rank of the result and n is the total number of samples tested. The above equation can be linearized to more easily determine the characteristic strength and Weibull modulus.

$$\ln\left(\ln\left(-\frac{L_o}{L}(1 - P_F)\right)\right) = m\ln(\sigma) - m\ln(\sigma_o) \tag{5.4}$$

When the left-hand side of Equation (5.4) is plotted against the logarithm of the stresses, the slope gives the Weibull modulus, and the intercept can be used to determine the characteristic fiber

strength. For brittle fibers the quantity L_o/L is approximately equal to 1. Several dozen samples are typically required in order to have sufficient statistics for the Weibull analysis.

Finally, the critical fiber strength, at a given critical fragment length, can be calculated using Equation (5.5).

$$\sigma_c = \sigma_o \left(\frac{L_o}{l_c}\right)^{1/m} \tag{5.5}$$

It is important to note that the fiber properties significantly influence the measured value of the IFSS, and the Weibull distribution should be determined for each fiber type being investigated to compare values of the IFSS across different treatments. If a single fiber type is used and only the resin is being varied, often times the influence of the Weibull distribution is ignored and qualitative comparisons can be made with some success. In such situations investigators often use the supplied fiber strength from a datasheet as the critical fiber strength throughout the analysis [15].

5.4 MATERIALS AND METHODS

5.4.1 Carbon Fibers

The carbon fibers used in this study were as received T800S-10E fibers, supplied by Toray Composite Materials America, Inc. ('Toray CMA'). Fibers were desized by a thermal treatment in Argon. T800S-10E fibers were heated at a rate of 11.5 °C·min^{-1} to 600 °C, and then held isothermally for 10 minutes before cooling back to room temperature. Thermogravimetric analysis was conducted to find a temperature suitable to remove the sizing without resulting in degradation of the fiber itself. Approximately 7 mg of chopped T800S-10E fibesr were heated to 1000 °C at a rate of 30 °C-min^{-1} under a 20 mL-min^{-1} purge (see Figure 5.4). Below 200 °C the chemisorbed water is removed. Starting at approximately 350 °C another thermal event is observed, and is attributed to the degradation of the fiber sizing. Another thermal event starts at around 600 °C,

which is the due to the thermal degradation of the fiber itself. The temperature of 600 °C was chosen to desize the fibers, assuming that the sizing would be completely degraded without significantly damaging the bulk fiber.

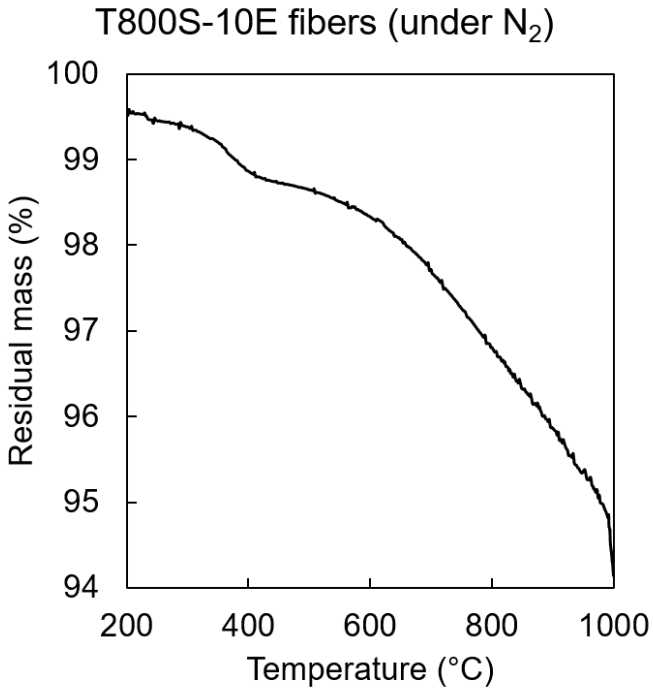

Figure 5.4 - TGA of T800S-10E fibers in a nitrogen flow rate of 20 mL·min^{-1}, heated at 30 °C·min^{-1}.

5.4.2 *Resin Formulation*

The epoxy used in this work was a 50:50 (w/w) blend of Huntsman MY721 and EPON 828. Huntsman MY721 is a commercial grade of tetraglycidyl diaminodiphenyl methane (TGDDM), while EPON 828 is primarily a bisphenol-A diglycidyl ether (BADGE) type epoxy. The PES used in this study was Sumika 5003P, and the nanoparticles used were 50 nm epoxy functionalized silica supplied in master batch form by Toray CMA. The single fiber fragmentation technique requires that the bulk resin be transparent to visualize the number of fiber breaks using optical microscopy. Larger nanoparticles scatter significantly lighter and result in opaque resin formulations, even at particle loadings as low as 0.5 wt%. Smaller nanoparticles may not

significantly improve roughness of the fiber surface and may not improve the mechanical properties [15]. For this reason, 50 nm particles were selected. For formulations containing nanoparticles, the particles were first mixed with the epoxy mixture in a FlackTek Speedmixer at 2500 rpm for 5 min before PES or the curing agent, 4,4'-Diaminodiphenyl sulfone (DDS) was added. For resins containing PES, a PES melt was conducted at 160 °C over the course of two hours after the particles had been incorporated. The samples were then cooled to 70 °C before the DDS was added. Lastly, the samples were mixed at 2500 rpm for five minutes twice, with at least five minutes in between mixes. Four primary resin formulations were made, a neat resin containing no particles or PES, a resin containing 0.5 wt% 50 nm particles, another containing 3 wt% PES, and finally a resin containing 0.5 wt% 50 nm particles and 3 wt% PES.

Scanning electron micrographs of the fiber surface were taken to confirm the existence of a nanoparticle reinforced interphase in the presence of both PES and nanoparticles. Figure 5.5 shows that in the presence of 3 wt% PES and 0.5 wt % nanoparticles, a reinforced interphase is formed, shown by the accumulation of particles at the desized fiber surface. When the same resin is prepared without the PES migrating agent, no accumulation of nanoparticles is observed at the fiber surface.

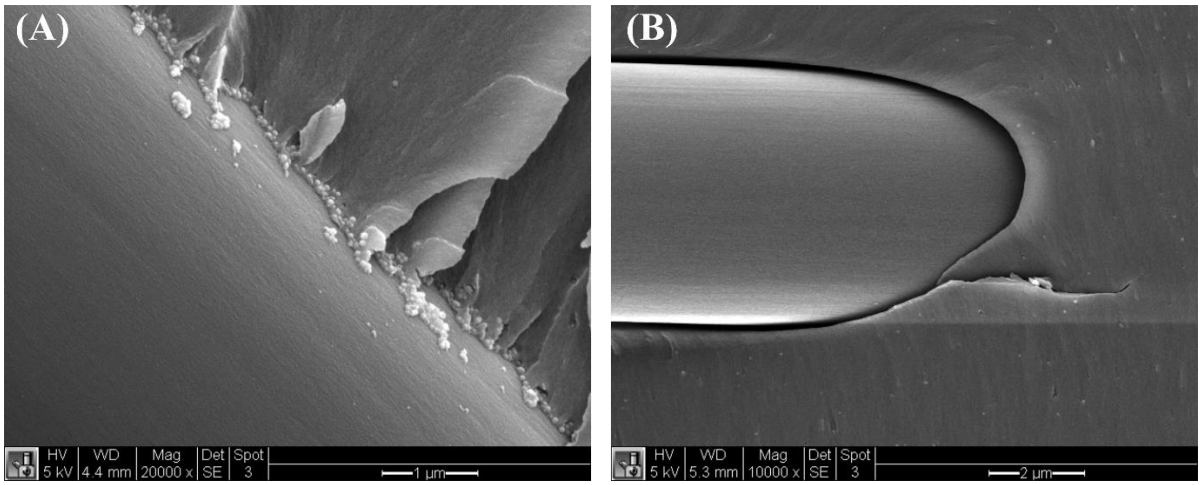

Figure 5.5 – Scanning electron micrographs of desized T800S fibers embedded in an epoxy resin consisting of TGDDM/828 cured with DDS. (A) A resin with 3 wt% PES and 0.5

wt% 50 nm epoxy functionalized particles. (B) A resin with 0 wt% PES and 0.5 wt% 50 nm epoxy functionalized particles.

5.4.3 *Single Fiber Tensile Testing*

The single fiber testing was conducted using a Satec T-1000 mechanical load frame (Satec Systems, Grove City, PA). Single fibers were placed in sturdy frames as shown in Figure 5.6-A. The gauge length was 50 mm, and the width of the sample was 40 mm, with a 10 mm boarder of the sturdy cardstock frame. The fiber is first affixed to the frame using tape near the outer edge of the frame. The fibers are then more securely fixed to the frame using a sturdy glue, such as 5-min epoxy. The glue should be placed as close to the inner edge as possible to keep the gauge length as consistent as possible. Once the glue has hardened, the samples are placed in a mechanical load frame as shown in Figure 5.6-B. Once the sample is secure in the load frame, the fiber holder is cut on both edges to leave the fiber freestanding between the clamps, and the tensile test begins. The samples were strained at a rate of .02 (mm/mm)-min^{-1} while the position and force were sampled at a frequency of 2 Hz.

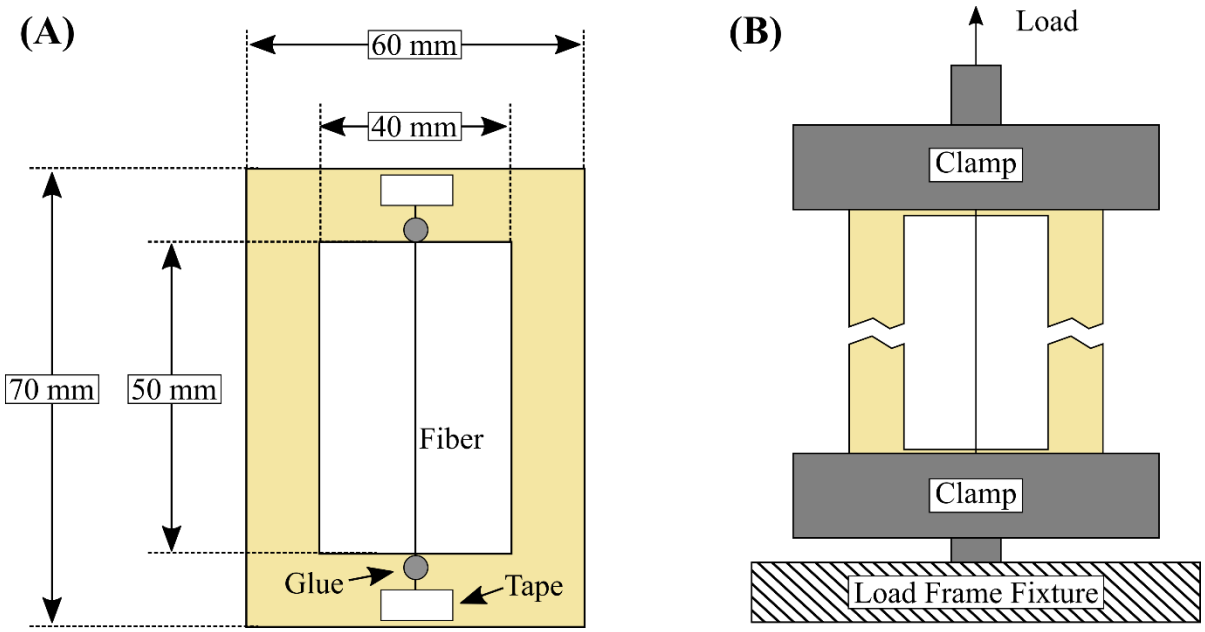

Figure 5.6 – (A) Single fibers prepared in a sturdy frame for ease of manipulation. Tape and glue are used to fix the position of the fiber. (B) Single fiber loaded in a mechanical load frame. The frame is cut on both sides once securely inserted into the load frame.

5.4.4 *Single Fiber Fragmentation*

Dogbone specimen, 2 mm thick, by 4 mm wide with a 25.4 mm gauge length were cast in a silicone mold with a single carbon fiber embedded in the middle of the mold. The fibers were pre-strained with 3.0 g of force, and then affixed with high temp tape and 5-minute epoxy. The pre-strain helps to align the fibers and to counter some of the compressive thermal stresses that arise from the thermal conductivity mismatch between the fibers and the surrounding matrix. After the samples were removed from the mold, they were sanded smooth (using 600 grit sand paper) and placed in miniature tensile load frame that was mounted on an Olympus IX70 optical microscope, as shown in Figure 5.7. The samples were strained at 0.005 (mm/mm)-min^{-1}. Fiber breaks started appearing around 4% strain and were generally saturated by 10% strain. Samples that fractured before 11 % strain were discarded and not included in the statistics for the interfacial shear strength measurements. Figure 5.8 shows some example fragmentation data in which the number of fiber

breaks in a 25.4 mm gauge length is plotted against the applied strain for a T800S-10E fiber embedded in an epoxy.

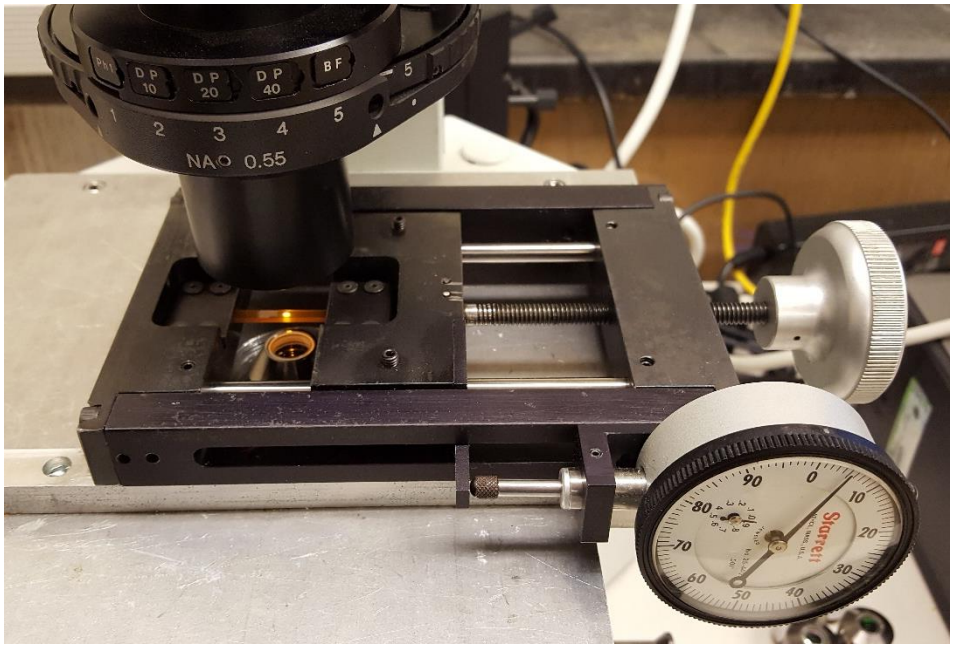

Figure 5.7 – Miniature tensile load frame mounted on an Olympus IX70 inverted microscope.

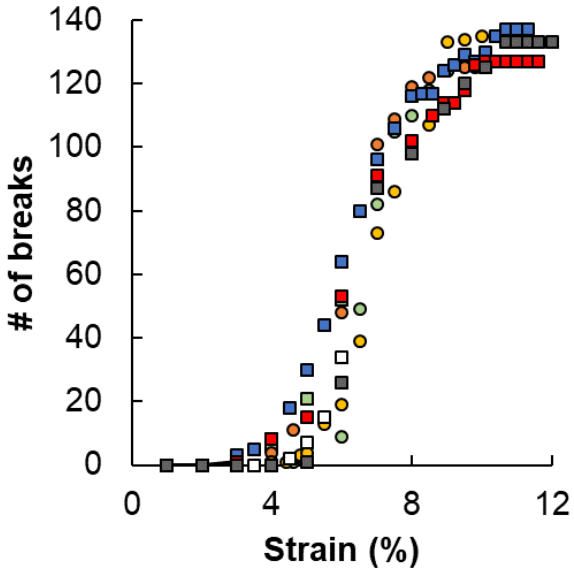

Figure 5.8 – Number of fiber breaks as a function of applied strain for sized T800S-10E fibers embedded in a matrix consisting of 50:50 wt/wt TGDDM-828 cured with DDS.

5.5 RESULTS

5.5.1 *Mechanical Testing of Fibers*

A mechanical load frame was used to strain single carbon fibers. More than 50 samples, with an initial fiber length of 50 mm were tested. A strain rate of 0.02 (mm/mm)-min^{-1} was used. The results are represented in Figure 5.9, as a violin plot with an inlaid box and whisker plots. The individual data points are also shown. The results were not statistically significant ($p = 0.09$), although the desized fibers showed decreases in the strength distribution. The Weibull plots shown in Figure 5.10 shows that desized fibers had a slightly broader failure distribution ($m_{desized} = 4.39$ vs. $m_{sized} = 4.66$), and had a slightly lower characteristic tensile strength ($\sigma_{o,desized} = 5.16$ GPa, $\sigma_{o,sized} = 4.85$ GPa). The desized fibers retained approximately 95% of the mechanical properties of the sized fibers, indicating that significant fiber degradation was avoided.

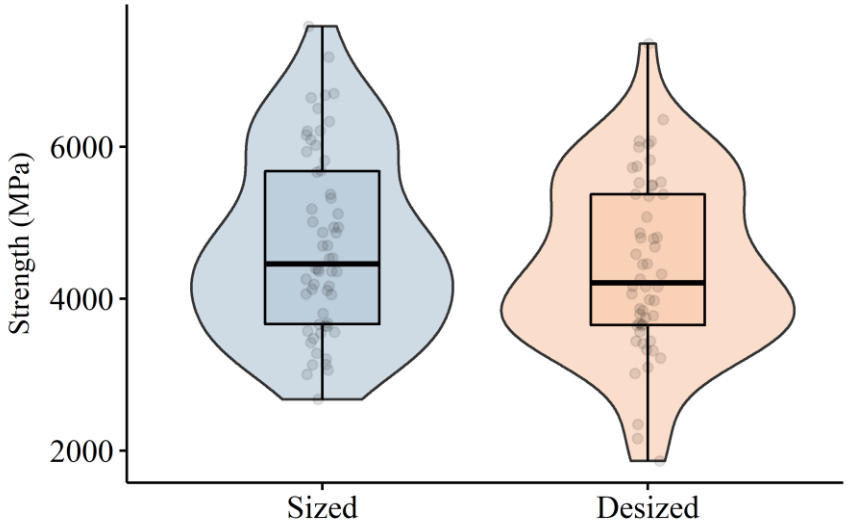

Figure 5.9 – Violin plots with inlaid box and whisker plots for sized and desized T800S-10E fiber strengths. Individual data points are also shown.

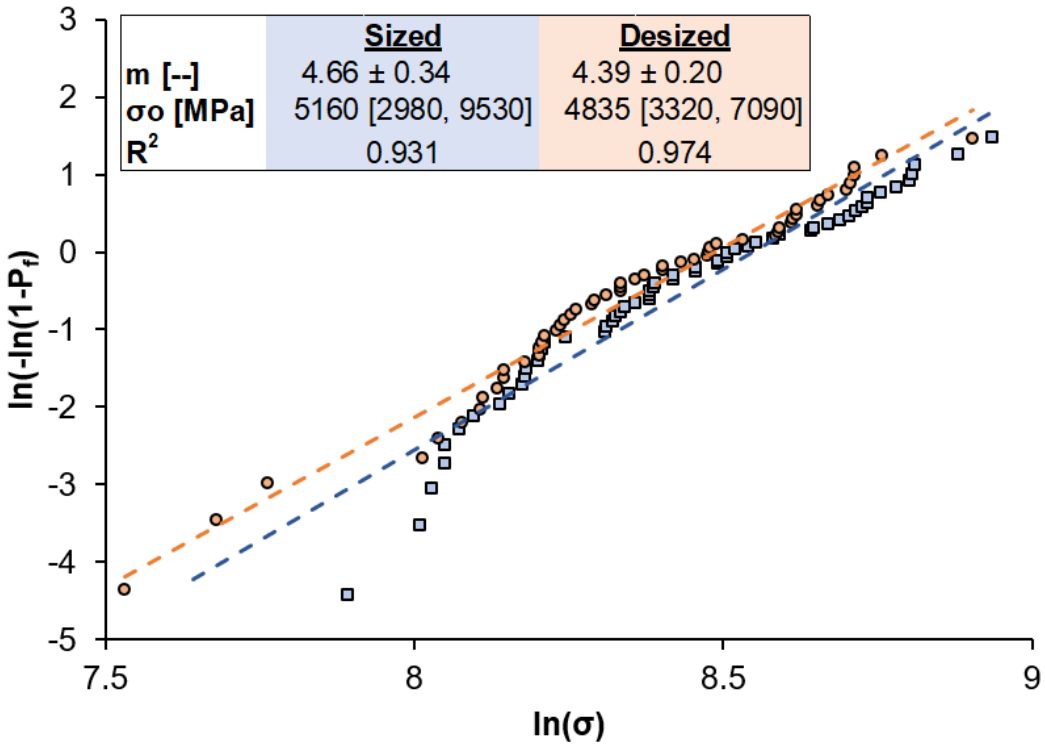

Figure 5.10 - Weibull plots for Sized T800S-10E fibers (blue triangles), and Desized T80S-10E fibers (orange squares)

5.5.2 *Interfacial Sheer Strength*

The results in Figure 5.11 show the measured IFSS for a variety of sized and desized T800S-10E fibers in several different resin formulations. The inclusion of 0.5 wt% 50 nm epoxy functionalized nanoparticles and 3 wt% PES has been previously shown to form a self-assembled nanoparticle rich interphase at carbon fiber surfaces in a variety of epoxy based thermosets. The results show that for the sized fibers there is no statistically significant difference between the fibers embedded in the neat resin and the fibers with a nanoparticle rich interphase.

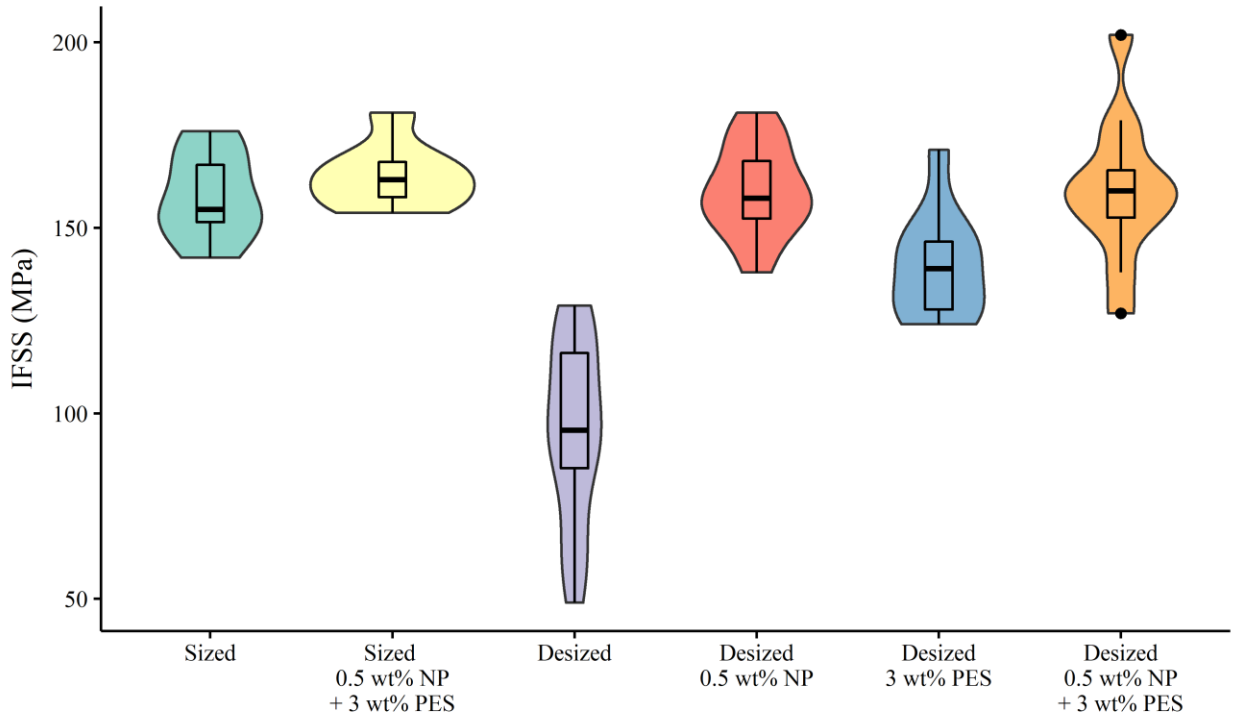

Figure 5.11 – Summarized IFSS results for all systems investigated displayed as violin plots with inlaid boxplots. The neat resin was composed of a 50:50 w/w mixture of TGDDM and BADGE epoxies, cured with 4,4'-DDS. The PES used was Sumika 5003P, and the nanoparticles were epoxy functionalized 50 nm Silica particles.

Desizing the carbon fibers decreased the IFSS from approximately 150 MPa to 95 MPa, over a 40% reduction, for a neat resin. Desized fibers in a resin containing 3 wt% PES alone increased the IFSS from 95 MPa to 140 MPa, a 47% increase. Including only 0.5 wt% 50 nm particles increased the IFSS of the desized fibers to 160 MPa, which is the statistically insignificant from the sized fiber results (with and without the interphase). Including both particles and PES in the resin formulation also increased the IFSS of the desized fiber to approximately 160 MPa, which is statistically indistinguishable from the sized fiber results and the desized fibers for the formulation containing only nanoparticles.

The results that the presence of the interphase in the sized fiber did not significantly improve the IFSS compared to the neat resin suggests that there may be an upper limit on the IFSS

achievable in these systems. Some researchers have hypothesized that the shear strength of the matrix itself may be the limiting factor for some systems [16]. The differences in the desized carbon fiber are slightly more illuminating. Resins containing PES alone and nanoparticles alone both increased the IFSS compared to the neat resin for the desized fibers. The inclusion of nanoparticles alone was enough to increase the IFSS to the apparent ceiling around 160 MPa, making it difficult to discern if the presence of a nanoparticle rich interphase had any additional improvements in the IFSS. From these results, it is impossible to tell if the presence of a nanoparticle rich interphase has any additional benefits towards increasing the adhesion between carbon fibers and that couldn't be explained entirely by the inclusion of PES and nanoparticles into the matrix.

5.6 SUMMARY

The effects of a self-assembled nanoparticle-rich interphase on the IFSS of a carbon fiber embedded in an epoxy matrix were investigated. The results were somewhat inconclusive, because there was an apparent maximum interfacial strength achieved. Desizing the fiber resulted in significant decreases in the IFSS, as expected, but the inclusion of nanoparticles alone was enough to improve the IFSS to the measured maximum. Adding migrating agent alone increased the IFSS, but not as significantly as the samples that contained nanoparticles or the samples that contained nanoparticles and migrating agent. It is possible that the shear strength of the matrix was the limiting factor in these experiments. Future experiments may need to be conducted with a tougher matrix or a system with a lower level of initial adhesion.

5.7 REFERENCES

1. Nguyen FN, Haro AP, Yoshioka K. Effects of a Nanomaterial-Toughened Interphase in Carbon Fiber Reinforced Polymer Composite. In: Proceedings of the Society for the Advancement of Materials and Process Engineering. Wichita, KS; 2013.

2. Nguyen FN, Haro AP, Tun S, Yoshioka K. Hard nanomaterial-toughened carbon fiber reinforced polymer composite. In: Proceedings of the Society for the Advancement of Materials and Process Engineering. Wichita, KS; 2013.

3. Johnsen BB, Kinloch AJ, Mohammed RD, Taylor AC, Sprenger S. Toughening mechanisms of nanoparticle-modified epoxy polymers. Polymer. 2007 Jan 12;48(2):530–41.

4. Sprenger S. Improving mechanical properties of fiber-reinforced composites based on epoxy resins containing industrial surface-modified silica nanoparticles: review and outlook. Journal of Composite Materials. 2015 Jan 1;49(1):53–63.

5. Dey M, Deitzel JM, Gillespie Jr. JW, Schweiger S. Influence of sizing formulations on glass/epoxy interphase properties. Composites Part A: Applied Science and Manufacturing. 2014 Aug;63:59–67.

6. Herrera-Franco PJ, Drzal LT. Comparison of methods for the measurement of fibre/matrix adhesion in composites. Composites. 1992;23(1):2–27.

7. Mandell JF, Chen JH, McGarry FH. A Microdebonding Test for In-Situ Fiber-Matrix Bond Strength and Moisture Effects, [Internet]. MASSACHUSETTS INST OF TECH CAMBRIDGE DEPT OF MATERIALS SCIENCE AND ENGINEERIN G, MASSACHUSETTS INST OF TECH CAMBRIDGE DEPT OF MATERIALS SCIENCE AND ENGINEERIN G; 1980 Feb [cited 2017 Nov 14]. Report No.: MIT/RR-R80-1. Available from: http://www.dtic.mil/docs/citations/ADA303021

8. Broutman LJ. Measurement of the Fiber-Polymer Matrix Interfacial Strength. In: Committee D-30, editor. Interfaces in Composites [Internet]. West Conshohocken, PA: ASTM International; 1969. p. 27–41. Available from: https://doi.org/10.1520/STP44698S

9. Deng S, Ye L, Mai Y-W. Measurement of interfacial shear strength of carbon fibre/epoxy composites using a single fibre pull-out test. Advanced Composite Materials. 1998 Jan 1;7(2):169–82.

10. Sockalingam S, Nilakantan G. Fiber-Matrix Interface Characterization through the Microbond Test. International Journal of Aeronautical and Space Sciences. 2012;13(3):282–95.

11. Wu HF, Claypool CM. An analytical approach of the microbond test method used in characterizing the fibre-matrix interface. J Mater Sci Lett. 1991 Jan 1;10(5):260–2.

12. Kelly A, Tyson WR. Tensile properties of fibre-reinforced metals: Copper/tungsten and copper/molybdenum. Journal of the Mechanics and Physics of Solids. 1965 Dec;13(6):329–50.

13. Feih S. Testing procedure for the single fiber fragmentation test [Internet]. Roskilde: Risø National Laboratory; 2004 [cited 2013 Nov 26]. Available from: http://iis03.risoe.dk/netahtml/risoe/publ_uk.htm

14. Mäder E, Liu J, Hiller J, Lu W, Li Q, Zhandarov S, Chou T-W. Coating of carbon nanotube fibers: variation of tensile properties, failure behavior, and adhesion strength. Front Mater. 2015;53.

15. Rutz BH, Berg JC. Electrostatic deposition of silica nanoparticles between E-glass fibers and an epoxy resin. J Appl Polym Sci. 2015 Feb 20;132(8):1–9.

16. Drzal LT. The effect of polymeric matrix mechanical properties on the fiber-matrix interfacial shear strength. Materials Science and Engineering: A. 1990;126(1):289–293.

Chapter 6. CONCLUSIONS AND RECOMMENDATIONS

6.1 PREDICTING ADHESION IN THERMOSETS AND CRYSTALLINE THERMOPLASTICS

6.1.1 *Effect of Matrix Cross-link Density on Adhesion*

The use of UNIFAC and COSMO-SAC to predict the adhesion of silane functionalized glass beads in thermoplastic matrices could be extended to thermosetting polymers. A series of silane functionalized glass beads can be imbedded in a thermosetting matrix, by partially curing the matrix in molds that are half-filled with resin, and then placing single beads in the molds before filling them with additional uncured matrix and then completely curing the resin. The single particle composites could then be tested to evaluate their relative adhesion with the matrix, by determining the stress required to delaminate the particles at the poles. The delamination event can be monitored optically using a stereo microscope, while the stress can be monitored simultaneously using a mechanical load frame. By noting the time of the delamination event, the stress required to delaminate the particle can be readily determined from the stress data. The instrument configuration is shown in Figure 6.1.

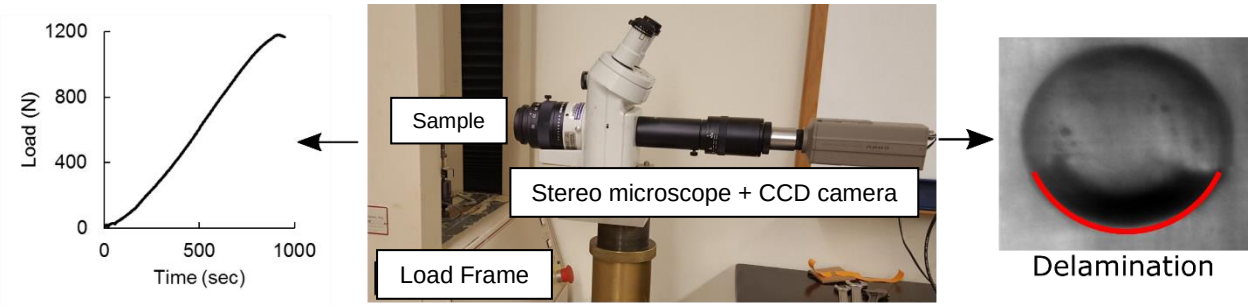

Figure 6.1 - Single particle adhesion test configuration. A polymeric composite is placed in the load frame and stressed in tension, the stress vs. time cure is recorded on a computer. Simultaneously the sample is imaged using a stereo microscope attached to a CCD camera. The specimen is video recorded using another computer. The stress at the time of delamination is used to determine the adhesion between the particle and the matrix.

The cross-link density of the matrix may play an important role in determining the adhesion between the particle and the matrix. In addition, as the cross-link density increases the brittleness of the matrix will increase and may change the failure mechanism at the poles, which is of interest in itself. It's likely that at low cross-linking density, activity coefficient models, such as UNIFAC or COSMO-SAC, will be able to predict the adhesion quite well, but it's unclear whether they will continue to accurately predict the adhesion as the cross-linking density increases. In addition, the particles may be made reactive towards the matrix, and the effects of thermodynamic compatibility vs covalently anchoring particles can be explored.

Here it is proposed to change the cross-linking density of an epoxy based matrix by using different Jeffamine diamine curing agents, which have the structure as shown in Figure 6.2, where x is the number of repeat units. The molecular weights range from 230 to 4000, which can provide a wide range of cross-link densities. A clear epoxy, such as a bisphenol A diglycidyl ether, would help to visualize the delamination process. A series of silane coupling agents could be used to functionalize the particle surfaces, as in chapter 2, some of which can be made reactive towards the epoxy matrix.

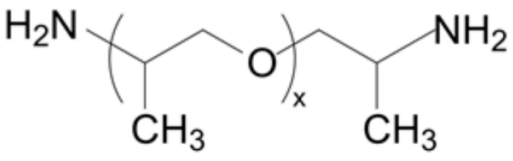

Jeffamine	MW [Da]	x
D-230	230	2.9
D-400	430	6.1
D-2000	2000	33
D-4000	4000	67

Figure 6.2 - (Left) Chemical structure of the Jeffamine diamine curing agents, along with (right) average molecular number of repeat units.

6.1.2 *Effect of Degree of Crystallinity on Adhesion*

Structural composites with formulated with thermoplastics are gaining increasing interest in recent years, partly due to the fact that they can easily be recycled. Poly(ether ether ketone) (PEEK), a semi-crystalline polymer, has gained particular interest in the aerospace community. There is

therefore a need to better understand the adhesion of solid inclusions in semi-crystalline polymers, and the single particle composite technique is well suited for investigating the effects of crystallinity has on the adhesion of solid inclusions.

In a proposed study, PEEK would be used as the polymeric matrix, and the degree of crystallinity would be controlled by changing the annealing time, and cooling rate during processing. The degree of crystallinity can be measured readily with differential scanning calorimetry (DSC). Several surface treatments predicted to have good, poor and moderate adhesion, via UNIFAC or COSMO-SAC, would be investigated to see if any universal trends are observed, and to determine if the crystallinity has any notable effect on the level of adhesion.

6.2 Self-Assembled Interphases

6.2.1 *Phase Separation*

It may be possible to form a nanoparticle reinforced interphase using a phase separation. If the nanoparticles are preferentially wet by the same phase as the reinforcing fiber surface, they may be incorporated into the interphase region. Alternatively, if the particles are partially wet by both polymer phases, i.e., the absolute value of the wetting parameter is less than one, and the fiber is completely wet by a single phase the particles may also accumulate in the interphase region at the polymer-polymer interface near the fiber surface.

Poly(styrene) (PS) and poly(propylene) (PP) mixtures are well-known to be phase separating systems, and will be used here as the polymeric matrix. Silane coupling agents, or mixtures of them, will be used to tune the relative wettability of silica particles embedded in the polymer matrix. Glass fibers can also be functionalized with silane coupling agents to alter their wetting characteristics. Tests will be performed to ensure that the surface functionalization of the fibers and the particles leads to complete or partial wetting. Once the desired surface chemistries are

achieved, the particles and the fibers will be embedded in a PS/PP blend above the lower critical solution temperature (LSCS) and mixed to ensure a homogeneous single-phase mixture. The sample will then be cooled to room temperature and allowed to undergo phase separation as the temperature cools below the LCST. Transmission electron microscopy, atomic force microscopy or scanning electron microscopy can be used to check for the formation of a self-assembled interphase for various combinations of fiber and nanoparticle surface functionalization. an interphase is formed, IFSS measurements should be performed. Certain phase separating structures, such as the "islands in the sea" morphology can improve the toughness of the matrix so the appropriate control experiments would need to be conducted to isolates the effect of the interphase on any IFSS results. If the sample becomes opaque due to the phase separation, the microdroplet or fiber pullout techniques may need to be used to measure the interphase properties, singe single fiber fragmentation requires optically transparent samples.

6.2.2 *Migrating Agents*

Additional migrating agents besides poly(ether sulfone) (PES) should be investigated to see if there is any dependence on migrating agent type and the onset of migration, aggregation, and rapid aggregation. The processing of many epoxy based composites depends on the viscosity of the uncured resin, which can be modified with thermoplastic additives. Using a variety of miscible polymers, it may be possible to alter the viscosity to the desired content and induce migration without causing aggregation. Other miscible polymers, such as poly(ethylene glycol) may be good candidates for altering the resin viscosity and inducing migration.

The particle size may also play a role in the migration event. Depletion theory predicts that the larger particles should experience greater depletion forces for smooth surfaces. Since carbon fibers have appreciable surface roughness, a smooth fiber surface should be used in future studies.

Various glass or polymeric fibers can be made smooth enough for these studies, and a range of monodisperse particle sizes could be used to probe the onset concentration of various self-assembly processes for a given migrating agents such as PES.

6.2.3 *Reaction Deposited Interphases*

Another possibility for the assembly of a nanoparticle reinforced fiber-matrix interphase is to covalently bond the particles to the fiber surface. If the nanoparticles and the fiber surface are reactive towards each other, they may be able to form an interphase during the processing of the composite. Particle and fiber surface chemistries can be adjusted using coupling agents that are reactive towards one another.

The particles and fibers can be made reactive towards each other but not with themselves by using a different coupling agent on each surface. This could be achieved, for example, by functionalizing the nanoparticle surface with an amine based coupling agent, such as 3(aminopropyl)trimethoxysilane (APS), and by treating glass fibers with an epoxy functionalized coupling agent, such as 3(glycidyloxypropyl)trimethoxysilane (GPS). If the fibers and the particles are not reactive with the bulk resin, as would be the case in a UV curable thermoset, the mixture could be heated to react the amines and the epoxide groups and form the interphase before curing the composite with UV light.

Here it is proposed to use glass fibers, functionalized with APS, and silica particles, functionalized with GPS, embedded in two types of polymeric matrices. The first matrix will be an epoxy based matrix, which is reactive towards both the particles and the fibers. The epoxy used could be a bisphenol A diglycidyl ether, and the amine curing agent will be m-phenylenediamine. The second matrix will be as non-reactive towards both the fibers and the particles as possible and could be a UV curable acrylate. In the case of the first matrix, it may be possible to form an

interphase simultaneously as the resin is hardening, since the statistical likelihood of a particle encountering and sticking to a fiber surface is greater than encountering another particle (assuming modest particle loading). While in the case of the non-reactive matrix, the particles can be given enough time to react with the fibers before the matrix is hardened.

Scanning electron microscopy could be used to determine the quality of any interphases formed, and if any interphases are formed IFSS measurements should be conducted. The results should be compared to fibers embedded in the neat matrix, and to fibers embedded in a matrix with unreactive particles to isolate the improvements associated with the presence of the interphase.

BIBLIOGRAPHY

Agnihotri, P., Basu, S., & Kar, K. K. (2011). Effect of carbon nanotube length and density on the properties of carbon nanotube-coated carbon fiber/polyester composites. *Carbon*, *49*(9), 3098–3106. https://doi.org/10.1016/j.carbon.2011.03.032

Alzina, C., Sbirrazzuoli, N., & Mija, A. (2011). Epoxy–Amine Based Nanocomposites Reinforced by Silica Nanoparticles. Relationships between Morphologic Aspects, Cure Kinetics, and Thermal Properties. *The Journal of Physical Chemistry C*, *115*(46), 22789–22795. https://doi.org/10.1021/jp2066259

An, Q., Rider, A. N., & Thostenson, E. T. (2012). Electrophoretic deposition of carbon nanotubes onto carbon-fiber fabric for production of carbon/epoxy composites with improved mechanical properties. *Carbon*, *50*(11), 4130–4143. https://doi.org/10.1016/j.carbon.2012.04.061

Araki, T., & Tanaka, H. (2006). Wetting-induced depletion interaction between particles in a phase-separating liquid mixture. *Physical Review E*, *73*(6), 061506. https://doi.org/10.1103/PhysRevE.73.061506

Arkles, B. (2006). Gelest - Silane coupling agents. Retrieved from http://ijsae.in/ijsaeems/index.php/ijsae/article/view/869

Asakura, S., & Oosawa, F. (1954). On Interaction between Two Bodies Immersed in a Solution of Macromolecules. *The Journal of Chemical Physics*, *22*(7), 1255–1256. https://doi.org/10.1063/1.1740347

Balazs, A. C., Emrick, T., & Russell, T. P. (2006). Nanoparticle Polymer Composites: Where Two Small Worlds Meet. *Science*, *314*(5802), 1107–1110. https://doi.org/10.1126/science.1130557

Banerjee, D., Yang, J., & Schweizer, K. S. (2015). Entropic depletion in colloidal suspensions and polymer liquids: role of nanoparticle surface topography. *Soft Matter*, *11*(47), 9086–9098. https://doi.org/10.1039/C5SM02072G

Bekyarova, E., Thostenson, E. T., Yu, A., Kim, H., Gao, J., Tang, J., … Haddon, R. C. (2007). Multiscale Carbon Nanotube−Carbon Fiber Reinforcement for Advanced Epoxy Composites. *Langmuir*, *23*(7), 3970–3974. https://doi.org/10.1021/la062743p

Boal, A. K., Ilhan, F., DeRouchey, J. E., Thurn-Albrecht, T., Russell, T. P., & Rotello, V. M. (2000). Self-assembly of nanoparticles into structured spherical and network aggregates. *Nature*, *404*(6779), 746–748. https://doi.org/10.1038/35008037

Bogush, G. H., Tracy, M. A., & Zukoski Iv, C. F. (1988). Preparation of monodisperse silica particles: control of size and mass fraction. *Journal of Non-Crystalline Solids*, *104*(1), 95–106.

Boroujeni, A. Y., Tehrani, M., Manteghi, M., Zhou, Z., & Al-Haik, M. (2016). Electromagnetic Shielding Effectiveness of a Hybrid Carbon Nanotube/Glass Fiber Reinforced Polymer Composite. *Journal of Engineering Materials and Technology*, *138*(4), 041001–041001. https://doi.org/10.1115/1.4033576

Brockmann, W., Geiß, P. L., Klingen, J., & Schröder, B. (2008). Adhesion. In *Adhesive Bonding: Materials, Applications and Technology* (pp. 11–28). Wiley-VCH Verlag GmbH & Co. KGaA. https://doi.org/10.1002/9783527623921.ch3

Broutman, L. J. (1969). Measurement of the Fiber-Polymer Matrix Interfacial Strength. In Committee D-30 (Ed.), *Interfaces in Composites* (pp. 27–41). West Conshohocken, PA: ASTM International. https://doi.org/10.1520/STP44698S

Caldwell, K. B., & Berg, J. C. (2017). Nanoparticles as Interphase Modifiers in Fiber Reinforced Polymeric Composites: A Critical Review. *Reviews of Adhesion and Adhesives*, *5*(1), 1–54. https://doi.org/10.7569/RAA.2017.097301

Caldwell, K., & Berg, J. C. (2017). Direct observation of nanoparticle migration in epoxy based fiber reinforced composites using fluorescence microscopy. *Journal of Composite Materials*, 51(28), 3877-3855. https://doi.org/10.1177/0021998317694704

Chen, C., Justice, R. S., Schaefer, D. W., & Baur, J. W. (2008). Highly dispersed nanosilica–epoxy resins with enhanced mechanical properties. *Polymer*, *49*(17), 3805–3815. https://doi.org/10.1016/j.polymer.2008.06.023

Chen, L., Jin, H., Xu, Z., Li, J., Guo, Q., Shan, M., … Cheng, B. (2014). Role of a gradient interface layer in interfacial enhancement of carbon fiber/epoxy hierarchical composites. *Journal of Materials Science*, *50*(1), 112–121. https://doi.org/10.1007/s10853-014-8571-y

Chen, L., Jin, H., Xu, Z., Shan, M., Tian, X., Yang, C., … Cheng, B. (2014). A design of gradient interphase reinforced by silanized graphene oxide and its effect on carbon fiber/epoxy interface. *Materials Chemistry and Physics*, *145*(1–2), 186–196. https://doi.org/10.1016/j.matchemphys.2014.02.001

Chen, W.-L., & Lin, S.-T. (2017). Explicit consideration of spatial hydrogen bonding direction for activity coefficient prediction based on implicit solvation calculations. *Physical Chemistry Chemical Physics*, *19*(31), 20367–20376. https://doi.org/10.1039/C7CP02317K

Chervanyov, A. I. (2015). Polymer-mediated interactions and their effect on the coagulation–fragmentation of nano-colloids: a self-consistent field theory approach. *Soft Matter*, *11*(6), 1038–1053. https://doi.org/10.1039/C4SM02580F

Chiu, J. J., Kim, B. J., Yi, G.-R., Bang, J., Kramer, E. J., & Pine, D. J. (2007). Distribution of Nanoparticles in Lamellar Domains of Block Copolymers. *Macromolecules*, *40*(9), 3361–3365. https://doi.org/10.1021/ma061503d

Costanzo, P. J., & Beyer, F. L. (2007). Thermally Driven Assembly of Nanoparticles in Polymer Matrices. *Macromolecules*, *40*(11), 3996–4001. https://doi.org/10.1021/ma070447t

Deka, B. K., Kong, K., Park, Y.-B., & Park, H. W. (2014). Large pulsed electron beam (LPEB)-processed woven carbon fiber/ZnO nanorod/polyester resin composites. *Composites Science and Technology*, *102*, 106–112. https://doi.org/10.1016/j.compscitech.2014.07.026

Deng, S., Ye, L., & Mai, Y.-W. (1998). Measurement of interfacial shear strength of carbon fibre/epoxy composites using a single fibre pull-out test. *Advanced Composite Materials*, *7*(2), 169–182. https://doi.org/10.1163/156855198X00129

Dey, M., Deitzel, J. M., Gillespie Jr., J. W., & Schweiger, S. (2014). Influence of sizing formulations on glass/epoxy interphase properties. *Composites Part A: Applied Science and Manufacturing*, *63*, 59–67. https://doi.org/10.1016/j.compositesa.2014.04.006

Drzal, L. T. (1990). The role of the fiber-matrix interphase on composite properties. *Vacuum*, *41*(7), 1615–1618. https://doi.org/10.1016/0042-207X(90)94034-N

Drzal, Lawrence T. (1990). The effect of polymeric matrix mechanical properties on the fiber-matrix interfacial shear strength. *Materials Science and Engineering: A*, *126*(1), 289–293.

Drzal, Lawrence T., Rich, M. J., Koenig, M. F., & Lloyd, P. F. (1983). Adhesion of Graphite Fibers to Epoxy Matrices: II. The Effect of Fiber Finish. *The Journal of Adhesion*, *16*(2), 133–152. https://doi.org/10.1080/00218468308074911

Du, S., Ren, Z., Wu, J., Xi, W., & Fu, H. (2016). Vertical α-FeOOH nanowires grown on the carbon fiber paper as a free-standing electrode for sensitive H2O2 detection. *Nano Research*, *9*(8), 2260–2269. https://doi.org/10.1007/s12274-016-1113-y

Ehlert, G. J., Galan, U., & Sodano, H. A. (2013). Role of Surface Chemistry in Adhesion between ZnO Nanowires and Carbon Fibers in Hybrid Composites. *ACS Applied Materials & Interfaces*, *5*(3), 635–645. https://doi.org/10.1021/am302060v

Ehlert, G. J., & Sodano, H. A. (2009). Zinc Oxide Nanowire Interphase for Enhanced Interfacial Strength in Lightweight Polymer Fiber Composites. *ACS Applied Materials & Interfaces*, *1*(8), 1827–1833. https://doi.org/10.1021/am900376t

Elias, L., Fenouillot, F., Majeste, J. C., & Cassagnau, P. (2007). Morphology and rheology of immiscible polymer blends filled with silica nanoparticles. *Polymer*, *48*(20), 6029–6040. https://doi.org/10.1016/j.polymer.2007.07.061

Feih, S. (2004). *Testing procedure for the single fiber fragmentation test*. Roskilde: Risø National Laboratory. Retrieved from http://iis03.risoe.dk/netahtml/risoe/publ_uk.htm

Ferreira, L., Evangelista, M. B., Martins, M. C. L., Granja, P. L., Esteves, J. L., & Barbosa, M. A. (2005). Improving the adhesion of poly(ethylene terephthalate) fibers to poly(hydroxyethyl methacrylate) hydrogels by ozone treatment: Surface characterization and pull-out tests. *Polymer*, *46*(23), 9840–9850. https://doi.org/10.1016/j.polymer.2005.08.033

Fredenslund, A., Jones, R. L., & Prausnitz, J. M. (1975). Group-contribution estimation of activity coefficients in nonideal liquid mixtures. *AIChE Journal*, *21*(6), 1086–1099. https://doi.org/10.1002/aic.690210607

Frisch, M. J., Trucks, G. W., Schlegel, H. B., Scuseria, G. E., Robb, M. A., Cheeseman, J. R., … Fox, D. J. (2009). Gaussian 09, Revision B.01. *Gaussian 09, Revision B.01, Gaussian, Inc., Wallingford CT*.

Galan, U., Lin, Y., Ehlert, G. J., & Sodano, H. A. (2011). Effect of ZnO nanowire morphology on the interfacial strength of nanowire coated carbon fibers. *Composites Science and Technology*, *71*(7), 946–954. https://doi.org/10.1016/j.compscitech.2011.02.010

Gao, S., Zhuang, R.-C., Zhang, J., Liu, J.-W., & Mäder, E. (2010). Glass Fibers with Carbon Nanotube Networks as Multifunctional Sensors. *Advanced Functional Materials*, *20*(12), 1885–1893. https://doi.org/10.1002/adfm.201000283

Gao, X., Gillespie Jr., J. W., Jensen, R. E., Li, W., (Gama) Haque, B. Z., & McKnight, S. H. (2015). Effect of fiber surface texture on the mechanical properties of glass fiber reinforced epoxy composite. *Composites Part A: Applied Science and Manufacturing*, *74*, 10–17. https://doi.org/10.1016/j.compositesa.2015.03.023

Gao, X., Jensen, R. E., Li, W., Deitzel, J., McKnight, S. H., & Gillespie, J. W. (2008). Effect of Fiber Surface Texture Created from Silane Blends on the Strength and Energy Absorption of the Glass Fiber/Epoxy Interphase. *Journal of Composite Materials*, *42*(5), 513–534. https://doi.org/10.1177/0021998307086203

Gao, X., Jensen, R. E., McKnight, S. H., & Gillespie Jr., J. W. (2011). Effect of colloidal silica on the strength and energy absorption of glass fiber/epoxy interphases. *Composites Part A: Applied Science and Manufacturing*, *42*(11), 1738–1747. https://doi.org/10.1016/j.compositesa.2011.07.029

Girard-Reydet, E., Sautereau, H., Pascault, J. P., Keates, P., Navard, P., Thollet, G., & Vigier, G. (1998). Reaction-induced phase separation mechanisms in modified thermosets. *Polymer*, *39*(11), 2269–2279. https://doi.org/10.1016/S0032-3861(97)00425-4

Guggenheim, E. A. (1952). *Mixtures; the theory of the equilibrium properties of some simple classes of mixtures, solutions and alloys.* Oxford: Clarendon Press.

Guo, J., Lu, C., An, F., & He, S. (2012). Preparation and characterization of carbon nanotubes/carbon fiber hybrid material by ultrasonically assisted electrophoretic deposition. *Materials Letters*, *66*(1), 382–384. https://doi.org/10.1016/j.matlet.2011.09.022

Gupta, S., Zhang, Q., Emrick, T., Balazs, A. C., & Russell, T. P. (2006). Entropy-driven segregation of nanoparticles to cracks in multilayered composite polymer structures. *Nature Materials*, *5*(3), 229–233. https://doi.org/10.1038/nmat1582

Herrera-Franco, P. J., & Drzal, L. T. (1992). Comparison of methods for the measurement of fibre/matrix adhesion in composites. *Composites*, *23*(1), 2–27.

H. Malakooti, M., A. Patterson, B., Hwang, H.-S., & A. Sodano, H. (2016). ZnO nanowire interfaces for high strength multifunctional composites with embedded energy harvesting. *Energy & Environmental Science*, *9*(2), 634–643. https://doi.org/10.1039/C5EE03181H

Ho, H., & Drzal, L. T. (1995). Non-linear numerical study of the single-fiber fragmentation test. Part I: Test mechanics. *Composites Engineering*, *5*(10), 1231–1244. https://doi.org/10.1016/0961-9526(95)00065-U

Hoecker, F., & Karger-Kocsis, J. (1996). Surface energetics of carbon fibers and its effects on the mechanical performance of CF/EP composites. *Journal of Applied Polymer Science*, *59*(1), 139–153.

Jensen, R. E., & McKnight, S. H. (2006). Inorganic–organic fiber sizings for enhanced energy absorption in glass fiber-reinforced composites intended for structural applications. *Composites Science and Technology*, *66*(3–4), 509–521. https://doi.org/10.1016/j.compscitech.2005.06.004

Jiang, D., Liu, L., Long, J., Xing, L., Huang, Y., Wu, Z., … Guo, Z. (2014). Reinforced unsaturated polyester composites by chemically grafting amino-POSS onto carbon fibers with active double spiral structural spiralphosphodicholor. *Composites Science and Technology*, *100*, 158–165. https://doi.org/10.1016/j.compscitech.2014.05.035

Johnsen, B. B., Kinloch, A. J., Mohammed, R. D., Taylor, A. C., & Sprenger, S. (2007). Toughening mechanisms of nanoparticle-modified epoxy polymers. *Polymer*, *48*(2), 530–541. https://doi.org/10.1016/j.polymer.2006.11.038

Kelly, A., & Tyson, W. R. (1965). Tensile properties of fibre-reinforced metals: Copper/tungsten and copper/molybdenum. *Journal of the Mechanics and Physics of Solids*, *13*(6), 329–350. https://doi.org/10.1016/0022-5096(65)90035-9

Kim, C. H., Kim, B.-H., & Yang, K. S. (2012). TiO2 nanoparticles loaded on graphene/carbon composite nanofibers by electrospinning for increased photocatalysis. *Carbon*, *50*(7), 2472–2481. https://doi.org/10.1016/j.carbon.2012.01.069

Kim, J.-K., & Mai, Y.-W. (1998). *Engineered Interfaces in Fiber Reinforced Composites*. Elsevier.

Klamt, A. (1995). Conductor-like Screening Model for Real Solvents: A New Approach to the Quantitative Calculation of Solvation Phenomena. *The Journal of Physical Chemistry*, *99*(7), 2224–2235. https://doi.org/10.1021/j100007a062

Kong, J., Cassell, A. M., & Dai, H. (1998). Chemical vapor deposition of methane for single-walled carbon nanotubes. *Chemical Physics Letters*, *292*(4), 567–574. https://doi.org/10.1016/S0009-2614(98)00745-3

Kong, K., Deka, B. K., Kwak, S. K., Oh, A., Kim, H., Park, Y.-B., & Park, H. W. (2013). Processing and mechanical characterization of ZnO/polyester woven carbon–fiber composites with different ZnO concentrations. *Composites Part A: Applied Science and Manufacturing*, *55*, 152–160. https://doi.org/10.1016/j.compositesa.2013.08.013

Kraft, D. J., Ni, R., Smallenburg, F., Hermes, M., Yoon, K., Weitz, D. A., … Kegel, W. K. (2012). Surface roughness directed self-assembly of patchy particles into colloidal micelles. *Proceedings of the National Academy of Sciences*, *109*(27), 10787–10792.

Kumar, M. S., Raju, N. M. S., Sampath, P. S., & Jayakumari, L. S. (2014). Effects Of Nanomaterials On Polymer Composites - An Expatiate View. *Reviews on Advanced Materials Science*, *38*(1), 40–54.

Kuo, Y.-C., Hsu, C.-C., & Lin, S.-T. (2013). Prediction of Phase Behaviors of Polymer–Solvent Mixtures from the COSMO-SAC Activity Coefficient Model. *Industrial & Engineering Chemistry Research*, *52*(37), 13505–13515. https://doi.org/10.1021/ie402175k

Lekkerkerker, H. N. W., & Tuinier, R. (2011). *Colloids and the depletion interaction*. Dordrecht ; New York: Springer.

Leonard, G. C., Hosseinpour, D., & Berg, J. C. (2009). Modulus-Graded Interphase Modifiers in E-Glass Fiber/Thermoplastic Composites. *Journal of Adhesion Science & Technology*, *23*(16), 2031–2046. https://doi.org/10.1163/016942409X12526743387809

Lin, S. T., & Sandler, S. I. (2002). A Priori Phase Equilibrium Prediction from a Segment Contribution Solvation Model. *Industrial & Engineering Chemistry Research*, *41*(5), 899–913. https://doi.org/10.1021/ie001047w

Lin, Y., Ehlert, G., & Sodano, H. A. (2009). Increased Interface Strength in Carbon Fiber Composites through a ZnO Nanowire Interphase. *Advanced Functional Materials*, *19*(16), 2654–2660. https://doi.org/10.1002/adfm.200900011

Loyola, B. R., Zhao, Y., Loh, K. J., & Saponara, V. L. (2013). The electrical response of carbon nanotube-based thin film sensors subjected to mechanical and environmental effects. *Smart Materials and Structures*, *22*(2), 025010. https://doi.org/10.1088/0964-1726/22/2/025010

Luo, Y., Jiang, J., Zhou, W., Yang, H., Luo, J., Qi, X., … Yu, T. (2012). Self-assembly of well-ordered whisker-like manganese oxide arrays on carbon fiber paper and its application as electrode material for supercapacitors. *Journal of Materials Chemistry*, *22*(17), 8634–8640. https://doi.org/10.1039/c2jm16419a

Lv, P., Feng, Y., Zhang, P., Chen, H., Zhao, N., & Feng, W. (2011). Increasing the interfacial strength in carbon fiber/epoxy composites by controlling the orientation and length of

carbon nanotubes grown on the fibers. *Carbon*, *49*(14), 4665–4673. https://doi.org/10.1016/j.carbon.2011.06.064

Ma, M., Gupta, M., Li, Z., Zhai, L., Gleason, K. K., Cohen, R. E., … Rutledge, G. C. (2007). Decorated Electrospun Fibers Exhibiting Superhydrophobicity. *Advanced Materials*, *19*(2), 255–259. https://doi.org/10.1002/adma.200601449

Mackay, M. E., Tuteja, A., Duxbury, P. M., Hawker, C. J., Horn, B. V., Guan, Z., … Krishnan, R. S. (2006). General Strategies for Nanoparticle Dispersion. *Science*, *311*(5768), 1740–1743. https://doi.org/10.1126/science.1122225

Mäder, E., Liu, J., Hiller, J., Lu, W., Li, Q., Zhandarov, S., & Chou, T.-W. (2015). Coating of carbon nanotube fibers: variation of tensile properties, failure behavior, and adhesion strength. *Composite Materials*, 53. https://doi.org/10.3389/fmats.2015.00053

Madhukar, M. S., & Drzal, L. T. (1992). Fiber-Matrix Adhesion and Its Effect on Composite Mechanical Properties: IV. Mode I and Mode II Fracture Toughness of Graphite/Epoxy Composites. *Journal of Composite Materials*, *26*(7), 936–968. https://doi.org/10.1177/002199839202600701

Malakooti, M. H., Hwang, H.-S., & Sodano, H. A. (2015a). Morphology-Controlled ZnO Nanowire Arrays for Tailored Hybrid Composites with High Damping. *ACS Applied Materials & Interfaces*, *7*(1), 332–339. https://doi.org/10.1021/am506272c

Malakooti, M. H., Hwang, H.-S., & Sodano, H. A. (2015b). Power generation from base excitation of a Kevlar composite beam with ZnO nanowires. In *Proc. of SPIE - Behavior and Mechanics of Multifuncitional Materials and Composites* (Vol. 9432, pp. 1–6). https://doi.org/10.1117/12.2084391

Mandell, J. F., Chen, J. H., & McGarry, F. H. (1980). *A Microdebonding Test for In-Situ Fiber-Matrix Bond Strength and Moisture Effects*, (No. MIT/RR-R80-1). MASSACHUSETTS INST OF TECH CAMBRIDGE DEPT OF MATERIALS SCIENCE AND ENGINEERIN G, MASSACHUSETTS INST OF TECH CAMBRIDGE DEPT OF MATERIALS SCIENCE AND ENGINEERIN G. Retrieved from http://www.dtic.mil/docs/citations/ADA303021

Materne, T., Buyl, F., & Witucki, G. L. (2004). Organosilane Technology in Coating Applications: Review and Perspectives. Dow Corning. Retrieved from http://www.dowcorning.com/content/publishedlit/26-1402-01.pdf

Menczel, J. D., Judovits, L., Prime, R. B., Bair, H. E., Reading, M., & Swier, S. (2009). Differential Scanning Calorimetry (DSC). In J. D. Menczel & R. B. Prime (Eds.), *Thermal Analysis of Polymers* (pp. 7–239). John Wiley & Sons, Inc. https://doi.org/10.1002/9780470423837.ch2

Merlini, C., Rosa, B. S., Müller, D., Ecco, L. G., Ramôa, S. D. A. S., & Barra, G. M. O. (2012). Polypyrrole nanoparticles coated amorphous short silica fibers: Synthesis and

characterization. *Polymer Testing*, *31*(8), 971–977. https://doi.org/10.1016/j.polymertesting.2012.07.003

Miller, A. C., & Berg, J. C. (2002a). Predicting adhesion between a crystalline polymer and silane-treated glass surfaces in filled composites. *Journal of Adhesion Science & Technology*, *16*(14), 1949–1956. https://doi.org/10.1163/15685610260427700

Miller, A. C., & Berg, J. C. (2002b). The prediction of adhesion between polymer matrices and silane-treated glass surfaces in filled composites. *Journal of Adhesion Science and Technology*, *16*(5), 495–507. https://doi.org/10.1163/156856102760070330

Miller, A. C., Knowlton, M. T., & Berg, J. C. (2000). The use of UNIFAC for the estimation of adhesion enhancement between polymers and mineral surfaces treated with silane coupling agents. *Journal of Adhesion Science and Technology*, *14*(12), 1471–1484.

Mishnaevsky Jr., L. (2015). Nanostructured interfaces for enhancing mechanical properties of composites: Computational micromechanical studies. *Composites Part B: Engineering*, *68*, 75–84. https://doi.org/10.1016/j.compositesb.2014.08.029

Mravlak, M. (2008). *Depletion force*. Seminar, University of Ljubljana. Retrieved from http://mafija.fmf.uni-lj.si/seminar/files/2007_2008/depletion.pdf

Mullins, E., Oldland, R., Liu, Y. a., Wang, S., Sandler, S. I., Chen, C.-C., … Seavey, K. C. (2006). Sigma-Profile Database for Using COSMO-Based Thermodynamic Methods. *Industrial & Engineering Chemistry Research*, *45*(12), 4389–4415. https://doi.org/10.1021/ie060370h

Netravali, A. N., & Mittal, K. L. (2017). *Interface / Interphase in Polymer Nanocomposites*. Beverly, MA: Wiley-Scrivener.

Nguyen, F. N., Haro, A. P., Kobayashi, D., Nakayama, Y., Ichikawa, T., Endo, M., … Khoo, J. (2013). Carbon fiber's surface chemistry and self-assembled interphase formation in fiber reinforced polymer composites. In *Proceedings of the International conference on composite materials*. Montreal, Canada.

Nguyen, F. N., Haro, A. P., Tun, S., & Yoshioka, K. (2013). Hard nanomaterial-toughened carbon fiber reinforced polymer composite. In *Proceedings of the Society for the Advancement of Materials and Process Engineering*. Wichita, KS.

Nguyen, F. N., Haro, A. P., & Yoshioka, K. (2013). Effects of a Nanomaterial-Toughened Interphase in Carbon Fiber Reinforced Polymer Composite. In *Proceedings of the Society for the Advancement of Materials and Process Engineering*. Wichita, KS.

Nguyen, F. N., Nakayama, Y., Kobayashi, D., Kamae, T., & Kenichi, Y. (2012). Carbon fiber's surface and its effects on an interphase formation for ultimate adhesion-related performances. In *Proceedings of the Society for the Advancement of Materials and Process Engineering*. Baltimore, MD.

Nguyen, F. N., Yoshioka, K., & Haro, A. P. (2012, August). *WO2012116261 A1*.

Ock, H. G., Ahn, K. H., & Lee, S. J. (2016). Effect of electric field on polymer/clay nanocomposites depending on the affinities between the polymer and clay. *Journal of Applied Polymer Science*, *133*(25), 1–6. https://doi.org/10.1002/app.43582

Packham, D. E. (2003). Surface energy, surface topography and adhesion. *International Journal of Adhesion and Adhesives*, *23*(6), 437–448. https://doi.org/10.1016/S0143-7496(03)00068-X

Pardieu, E., Pronkin, S., Dolci, M., Dintzer, T., Pichon, B. P., Begin, D., … Boulmedais, F. (2015). Hybrid layer-by-layer composites based on a conducting polyelectrolyte and Fe3O4 nanostructures grafted onto graphene for supercapacitor application, *3*(45), 22877–22885. https://doi.org/10.1039/C5TA05132K

Park, J. K., Do, I.-H., Askeland, P., & Drzal, L. T. (2008). Electrodeposition of exfoliated graphite nanoplatelets onto carbon fibers and properties of their epoxy composites. *Composites Science and Technology*, *68*(7–8), 1734–1741. https://doi.org/10.1016/j.compscitech.2008.02.002

Peiffer, D. G. (1979). Impact strength of thick-interlayer composites. *Journal of Applied Polymer Science*, *24*(6), 1451–1455. https://doi.org/10.1002/app.1979.070240606

Peiffer, D. G., & Nielsen, L. E. (1979). Preparation and mechanical properties of thick interlayer composites. *Journal of Applied Polymer Science*, *23*(8), 2253–2264. https://doi.org/10.1002/app.1979.070230804

Plueddemann, E. P. (1991). *Silane Coupling Agents* (2nd ed.). New York: Springer US.

Podsiadlo, P., Kaushik, A. K., Arruda, E. M., Waas, A. M., Shim, B. S., Xu, J., … Kotov, N. A. (2007). Ultrastrong and Stiff Layered Polymer Nanocomposites. *Science*, *318*(5847), 80–83. https://doi.org/10.1126/science.1143176

Qin, W., Vautard, F., Askeland, P., Yu, J., & Drzal, L. (2015a). Modifying the carbon fiber–epoxy matrix interphase with silicon dioxide nanoparticles, *5*(4), 2457–2465. https://doi.org/10.1039/C4RA11878B

Qin, W., Vautard, F., Askeland, P., Yu, J., & Drzal, L. T. (2015b). Incorporation of silicon dioxide nanoparticles at the carbon fiber-epoxy matrix interphase and its effect on composite mechanical properties. *Polymer Composites*, 1–9. https://doi.org/10.1002/pc.23715

Qin, W., Vautard, F., Drzal, L. T., & Yu, J. (2015). Mechanical and electrical properties of carbon fiber composites with incorporation of graphene nanoplatelets at the fiber–matrix interphase. *Composites Part B: Engineering*, *69*, 335–341. https://doi.org/10.1016/j.compositesb.2014.10.014

Ramanathan, T., Bismarck, A., Schulz, E., & Subramanian, K. (2001). The use of a single-fibre pull-out test to investigate the influence of acidic and basic surface groups on carbon fibres on the adhesion to poly (phenylene sulfide) and matrix-morphology-dependent fracture behaviour. *Composites Science and Technology*, *61*(12), 1703–1710.

Rausch, J., Zhuang, R. C., & Mäder, E. (2009). Application of nanomaterials in sizings for glass fibre/polypropylene hybrid yarn spinning. *Materials Technology*, *24*(1), 29–35. https://doi.org/10.1179/175355509X418016

Renna, L. A., Boyle, C. J., Gehan, T. S., & Venkataraman, D. (2015). Polymer Nanoparticle Assemblies: A Versatile Route to Functional Mesostructures. *Macromolecules*, *48*(18), 6353–6368. https://doi.org/10.1021/acs.macromol.5b00375

Rutz, B. H., & Berg, J. C. (2015). Electrostatic deposition of silica nanoparticles between E-glass fibers and an epoxy resin. *Journal of Applied Polymer Science*, *132*(8), 1–9. https://doi.org/10.1002/app.41516

Sadeghian, R., Gangireddy, S., Minaie, B., & Hsiao, K.-T. (2006). Manufacturing carbon nanofibers toughened polyester/glass fiber composites using vacuum assisted resin transfer molding for enhancing the mode-I delamination resistance. *Composites Part A: Applied Science and Manufacturing*, *37*(10), 1787–1795. https://doi.org/10.1016/j.compositesa.2005.09.010

Santra, S., Liesenfeld, B., Bertolino, C., Dutta, D., Cao, Z., Tan, W., … Mericle, R. A. (2006). Fluorescence lifetime measurements to determine the core–shell nanostructure of FITC-doped silica nanoparticles: An optical approach to evaluate nanoparticle photostability. *Journal of Luminescence*, *117*(1), 75–82. https://doi.org/10.1016/j.jlumin.2005.04.008

Schaefer, J. D., Rodriguez, A. J., Guzman, M. E., Lim, C.-S., & Minaie, B. (2011). Effects of electrophoretically deposited carbon nanofibers on the interface of single carbon fibers embedded in epoxy matrix. *Carbon*, *49*(8), 2750–2759. https://doi.org/10.1016/j.carbon.2011.02.070

Schneider, C. A., Rasband, W. S., & Eliceiri, K. W. (2012). NIH Image to ImageJ: 25 years of image analysis. *Nature Methods*, *9*(7), 671–675. https://doi.org/10.1038/nmeth.2089

Shah, T. K., Gardner, S. H., Alberding, M. R., & Malecki, H. C. (2010, August 5). *US20100192851 A1*. Retrieved from http://www.google.com/patents/US20100192851

Shah, T. K., Gardner, S. H., Alberding, M. R., & Malecki, H. C. (2012, July 26). *US20120189846 A1*. Retrieved from http://www.google.ch/patents/US20120189846

Sharma, M., Gao, S., Mäder, E., Sharma, H., Wei, L. Y., & Bijwe, J. (2014). Carbon fiber surfaces and composite interphases. *Composites Science and Technology*, *102*, 35–50. https://doi.org/10.1016/j.compscitech.2014.07.005

Sharma, S. P., & Lakkad, S. C. (2010). Compressive strength of carbon nanotubes grown on carbon fiber reinforced epoxy matrix multi-scale hybrid composites. *Surface and Coatings Technology*, *205*(2), 350–355. https://doi.org/10.1016/j.surfcoat.2010.06.055

Shirtcliffe, N. J., McHale, G., Newton, M. I., Chabrol, G., & Perry, C. C. (2004). Dual-Scale Roughness Produces Unusually Water-Repellent Surfaces. *Advanced Materials*, *16*(21), 1929–1932. https://doi.org/10.1002/adma.200400315

Sockalingam, S., & Nilakantan, G. (2012). Fiber-Matrix Interface Characterization through the Microbond Test. *International Journal of Aeronautical and Space Sciences*, *13*(3), 282–295. https://doi.org/10.5139/IJASS.2012.13.3.282

Song, B., Meng, L. H., & Huang, Y. D. (2012). Improvement of interfacial property between PBO fibers and epoxy resin by surface grafting of polyhedral oligomeric silsesquioxanes (POSS). *Applied Surface Science*, *258*(24), 10154–10159. https://doi.org/10.1016/j.apsusc.2012.06.097

Sprenger, S. (2013). Epoxy resins modified with elastomers and surface-modified silica nanoparticles. *Polymer*, *54*(18), 4790–4797. https://doi.org/10.1016/j.polymer.2013.06.011

Sprenger, S. (2015). Improving mechanical properties of fiber-reinforced composites based on epoxy resins containing industrial surface-modified silica nanoparticles: review and outlook. *Journal of Composite Materials*, *49*(1), 53–63. https://doi.org/10.1177/0021998313514260

Staverman, A. J. (1950). The entropy of high polymer solutions. Generalization of formulae. *Recueil Des Travaux Chimiques Des Pays-Bas*, *69*(2), 163–174. https://doi.org/10.1002/recl.19500690203

Survant, L., Andrejevic, M., Picker, J., Van Den Hoek, J., Fossum, E., & Lagadic, I. (2016). Surface-initiated polymerization of styrene from one-step prepared thiol-functionalized organoclays. *Polyhedron*, *114*, 37–41. https://doi.org/10.1016/j.poly.2015.09.027

Taguet, A., Cassagnau, P., & Lopez-Cuesta, J.-M. (2014). Structuration, selective dispersion and compatibilizing effect of (nano)fillers in polymer blends. *Progress in Polymer Science*, *39*(8), 1526–1563. https://doi.org/10.1016/j.progpolymsci.2014.04.002

Thostenson, E. T., Li, W. Z., Wang, D. Z., Ren, Z. F., & Chou, T. W. (2002). Carbon nanotube/carbon fiber hybrid multiscale composites. *Journal of Applied Physics*, *91*(9), 6034–6037. https://doi.org/10.1063/1.1466880

Tsai, J.-L., Hsiao, H., & Cheng, Y.-L. (2010). Investigating Mechanical Behaviors of Silica Nanoparticle Reinforced Composites. *Journal of Composite Materials*, *44*(4), 505–524. https://doi.org/10.1177/0021998309346138

Tshepelevitsh, S., Oss, M., Pung, A., & Leito, I. (2013). Evaluating the COSMO-RS Method for Modeling Hydrogen Bonding in Solution. *ChemPhysChem*, *14*(9), 1909–1919. https://doi.org/10.1002/cphc.201300186

Van Blaaderen, A., & Vrij, A. (1992). Synthesis and characterization of colloidal dispersions of fluorescent, monodisperse silica spheres. *Langmuir*, *8*(12), 2921–2931. https://doi.org/10.1021/la00048a013

Vautard, F., Ozcan, S., & Meyer, H. (2012). Properties of thermo-chemically surface treated carbon fibers and of their epoxy and vinyl ester composites. *Composites Part A: Applied Science and Manufacturing*, *43*(7), 1120–1133. https://doi.org/10.1016/j.compositesa.2012.02.018

Wang, C., Li, J., Sun, S., Li, X., Wu, G., Wang, Y., … Huang, Y. (2016). Controlled growth of silver nanoparticles on carbon fibers for reinforcement of both tensile and interfacial strength. *RSC Advances*, *6*(17), 14016–14026. https://doi.org/10.1039/C5RA22032G

Wenzel, R. N. (1949). Surface Roughness and Contact Angle. *The Journal of Physical and Colloid Chemistry*, *53*(9), 1466–1467. https://doi.org/10.1021/j150474a015

Wiegand, N., & Mäder, E. (2016). Multifunctional Interphases: Percolation Behavior, Interphase Modification, and Electro-Mechanical Response of Carbon Nanotubes in Glass Fiber Polypropylene Composites. *Advanced Engineering Materials*, *18*(3), 376–384. https://doi.org/10.1002/adem.201500447

Williams, R. J. J., Hoppe, C. E., Zucchi, I. A., Romeo, H. E., dell'Erba, I. E., Gómez, M. L., … Leonardi, A. B. (2014). Self-assembly of nanoparticles employing polymerization-induced phase separation. *Journal of Colloid and Interface Science*, *431*, 223–232. https://doi.org/10.1016/j.jcis.2014.06.022

Wu, H. F., & Claypool, C. M. (1991). An analytical approach of the microbond test method used in characterizing the fibre-matrix interface. *Journal of Materials Science Letters*, *10*(5), 260–262. https://doi.org/10.1007/BF00735651

Yan, L.-T., & Xie, X.-M. (2013). Computational modeling and simulation of nanoparticle self-assembly in polymeric systems: Structures, properties and external field effects. *Progress in Polymer Science*, *38*(2), 369–405. https://doi.org/10.1016/j.progpolymsci.2012.05.001

Yang, L., Xu, X., Peng, C., Liu, H., & Hu, Y. (2010). Prediction of vapor-liquid equilibrium for polymer solutions based on the COSMO-SAC model. *AIChE Journal*, *56*(10), 2687–2698. https://doi.org/10.1002/aic.12178

Yang, Y., Lu, C.-X., Su, X.-L., Wu, G.-P., & Wang, X.-K. (2007). Effect of nano-SiO2 modified emulsion sizing on the interfacial adhesion of carbon fibers reinforced composites. *Materials Letters*, *61*(17), 3601–3604. https://doi.org/10.1016/j.matlet.2006.11.121

Yarlagadda, S. C. (2015). *Dynamics of hard and soft colloids in confined geometries and on structured surfaces* (PhD thesis). Georgia Tech, Atlanta, USA.

Ye, X., Narayanan, T., Tong, P., Huang, J. S., Lin, M. Y., Carvalho, B. L., & Fetters, L. J. (1996). Depletion interactions in colloid-polymer mixtures. *Physical Review E*, *54*(6), 6500.

Yuan, Y., & Lee, T. R. (2013). Contact Angle and Wetting Properties. In G. Bracco & B. Holst (Eds.), *Surface Science Techniques* (pp. 3–34). Springer Berlin Heidelberg. https://doi.org/10.1007/978-3-642-34243-1_1

Zhang, J., Liu, J., Zhuang, R., Mäder, E., Heinrich, G., & Gao, S. (2011). Single MWNT-Glass Fiber as Strain Sensor and Switch. *Advanced Materials*, *23*(30), 3392–3397. https://doi.org/10.1002/adma.201101104

Zhang, J., Zhuang, R., Liu, J., Mäder, E., Heinrich, G., & Gao, S. (2010). Functional interphases with multi-walled carbon nanotubes in glass fibre/epoxy composites. *Carbon*, *48*(8), 2273–2281. https://doi.org/10.1016/j.carbon.2010.03.001

Zhang, Q., Liu, J., Sager, R., Dai, L., & Baur, J. (2009). Hierarchical composites of carbon nanotubes on carbon fiber: Influence of growth condition on fiber tensile properties. *Composites Science and Technology*, *69*(5), 594–601. https://doi.org/10.1016/j.compscitech.2008.12.002

Zhang, X., Fan, X., Yan, C., Li, H., Zhu, Y., Li, X., & Yu, L. (2012). Interfacial Microstructure and Properties of Carbon Fiber Composites Modified with Graphene Oxide. *ACS Applied Materials & Interfaces*, *4*(3), 1543–1552. https://doi.org/10.1021/am201757v

Zhao, F., & Huang, Y. (2011). Grafting of polyhedral oligomeric silsesquioxanes on a carbon fiber surface: novel coupling agents for fiber/polymer matrix composites. *Journal of Materials Chemistry*, *21*(11), 3695–3703. https://doi.org/10.1039/C0JM03128C

Appendix A – FLUORSENCE IMAGE ANALYSIS CODE

Numpy and matplotlib are required dependencies that must be installed before attempting to run the following code. Both modules are available and free to download for any computing platform. Although this particular code was written with a windows style directory in mind. Python 2.7.10 or later should be used to run the code as well. The code is not compatible with Python 3 due to differences in syntax between the two versions of python.

When the program is run the user will be prompted for several input parameters, including the full filename (including path), the desired output filename (including path), what color channels to extract, and whether to plot in black and white or in color.

```
#!/usr/bin/env/python
# -*- coding: utf-8 -*-
"""
@title: FluorAnalysis.py
@description: Rotate and analyze fluorescent intensity along x-axis
@author: Kyle Bernd Caldwell (kcal@uw.edu)
@institution: University of Washington
@department: Chemical Engineering
@Python version: 2.7.10 (default, May 23 2015)
"""
#=============================================================================
import numpy as np
import matplotlib.pyplot as plt
import matplotlib.gridspec as gridspec

#=============================================================================
def scale_image(im, bw_conv=0):
    """
im is the cropped and rotated image such that the fiber is oriented along the
y-axis. First the image will be reduced from RGB to monochrome image. If
bw_conv=1 only the green channel will be extracted. If the value is anything
else it will convert to monochrome with the following factors [R:0.333,
G:0.333, B:0.333]. The image is then averaged along the y-axis and scaled
from 0 to 1. The function returns the scaled axis averaged bw values as a
vector along the x-direction of the rotated image.
    """
    if bw_conv=='1':
        conv_matrix = [0.0, 1.0, 0.0]
    else:
        conv_matrix = [0.333, 0.333, 0.333]
    bw = np.dot(im[...,:3], conv_matrix)
```

```
    avg_bw = np.average(bw, axis=0)
    scaled = ( avg_bw - avg_bw.min() ) /( avg_bw - avg_bw.min() ).max()
    return(bw, scaled)

#=====================================================================
def analyze(scaled, frac=0.15):
    """
scaled is the y-averaged bw intensity data from the scale_image function.
frac is the fraction of the image used on the left and right edges to average
the background intensity. The function returns the maximum intensity divided
by the background intensity, and the background intensity.
    """
    n = len(scaled)
    BackgroundValues = np.append(scaled[:n*frac], scaled[-n*frac:])
    AverageBackground = BackgroundValues.mean()

    MaxPeak = scaled.max() / AverageBackground
    return(MaxPeak, AverageBackground)

#=====================================================================
# Ask for the image name and output name
FileName = raw_input('Enter the full directory name\nWindows example
C:\\\Users\\\UserName\\\Images\\\Image1.tiff\n\t')

OutputName = raw_input('Enter the full filename\nWindowsexample
C:\\\Users\\\UserName\\\Images\\\Image1_Analyzed.tiff\n\t')

#=====================================================================
#Select plotting parameters
select_green = raw_input("""Enter 1 if you wish to only select green
channel\nDefault is to average all color channel\n\t""")

bw_plot = raw_input("""Enter 1 if you wish to plot in black and
white\nDefault is to plot in color\n\t""")

#=====================================================================
#Analyze image
im = plt.imread(FileName)
bw, scaled = scale_image(im, bw_conv=select_green)
MaximumIntensity, Background = analyze(scaled)

print('The normalized peak intensity = {0:.4g}'.format(MaximumIntensity))

#=====================================================================
#plot results
plt.close('all')
fig = plt.figure()
gs = gridspec.GridSpec(2, 1, height_ratios=[3,1])
ax1 = plt.subplot(gs[0])
ax2 = plt.subplot(gs[1],sharex=ax1)
fig.subplots_adjust(hspace=0)

if bw_plot == '1':
    ax1.imshow(bw, cmap='gray')
else:
    ax1.imshow(im)
```

```
ax2.plot(scaled, 'g', lw=2)
ax2.plot([0, len(scaled) -1], [Background, Background], 'g--', lw=1)
ax2.set_axis_bgcolor('k')

for ax in fig.get_axes():
    ax.set_xticks([])
    ax.set_yticks([])

plt.axis('tight')
plt.savefig(OutputName, dpi=400, transparent=True, bbox_inches='tight',
pad_inches=0.00)
```

APPENDIX B – DEGREE OF CURE WITH AN ISOTHERMAL DWELL FROM DSC DATA

Differential scanning calorimetry (DSC) is a thermal analysis technique that is useful in determining many properties of polymeric materials [1]. Differential scanning calorimetry works by measuring the heat adsorbed or released by a material as the temperature is changed. Phase transitions from solids to liquid, and from polymer solids to melts can readily be determined using this technique. In crystalline polymers the melting of crystalline domains to form amorphous regions can also be readily detected. Physical transitions such as the glass transition temperature, T_g, are also readily measured by the technique in both thermosetting and thermoplastic polymers. DSC can also be used to monitor chemical reactions that either give off (exothermic) or require heat (endothermic). DSC is routinely used to monitor the degree of cure, α, in thermosetting polymers, which quantifies the extent of the crosslinking reaction. DCS is also used to measure the heat capacity of materials and can be used to extract kinetic parameters of various reactions.

Typically to monitor the degree of cure in a thermosetting polymer two experiments are required. First an unreacted sample is placed in the instrument and the temperature is ramped at a fixed rate. As the temperature is increased the reaction begins and eventually, as the temperature increases further, the reaction goes to completion. If the reaction is exothermic excess heat will be generated and measured in the instrument. In order to quantify how much heat was generated a baseline is drawn from the region just before the reaction begins to a point just after the reaction has ended. Other more complicated baselines can be generated, and are slightly more accurate by a few percent. The linear baseline, due to the simplicity of implementation and acceptable accuracy is widely used industrially. Once the baseline has been determined the excess heat flow can be

integrated over the reaction time to yield the total heat released by the uncured resin during cross-linking reaction, ΔH_{uc}. Figure B.1 shows some example DSC data for an epoxy resin consisting of tetraglycidyl diaminodiphenyl methane (TGDDM) cured with 4,4'-diaminodiphenylsulfone (DDS) containing poly(ether sulfone) (PES) and 100 nm silica particles functionalized with epoxy groups (see chapter 3). The sample was heated at a constant rate of 20 rate of °C-min^{-1}.

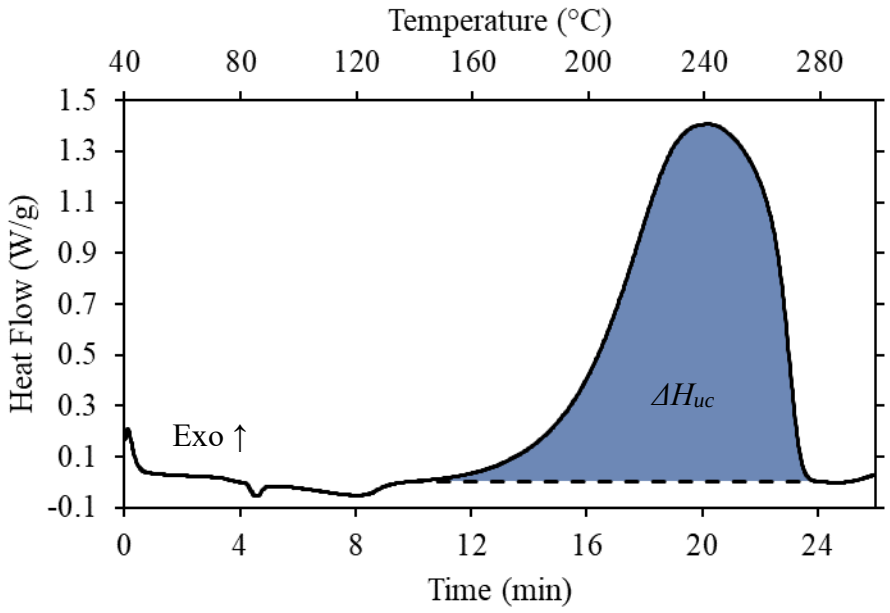

Figure B.1 – DSC curve of TGDDM cured with DDS containing PES and 100 nm epoxy functionalized nanoparticles. The heating rate was 20 °C-min^{-1}. The solid line is the heat flow curve, the dashed line is the baseline, and the blue area represents ΔH_{uc}.

To determine the degree of cure of a sample exposed to a given heat treatment another experiment is required. The resin is exposed to the thermal treatment and then placed in the DSC chamber and heated at a constant rate to determine how much residual heat is available in the sample. The residual heat measures how much more the sample could have reacted. If there is no more residual heat then the sample is 100% reacted, while any residual heat released by the sample indicates that the sample was not completely reacted after the thermal treatment. The degree of cure can be readily computed from Equation (B.1):

$$\alpha = 1 - \frac{\Delta H_{res}}{\Delta H_{uc}} \tag{B.1}$$

Where ΔH_{res} is the residual heat released during the ramp. Figure B.2 shows the residual heat of a sample that was previous exposed to a heat treatment. The dip in the heat flow data around 201 minutes corresponds to the glass transition temperature of the material. The reaction continues shortly after T_g is reached, which is commonly observed. Below the glass transition temperature, the polymer chains are not mobile enough to continue the reaction at an appreciable rate.

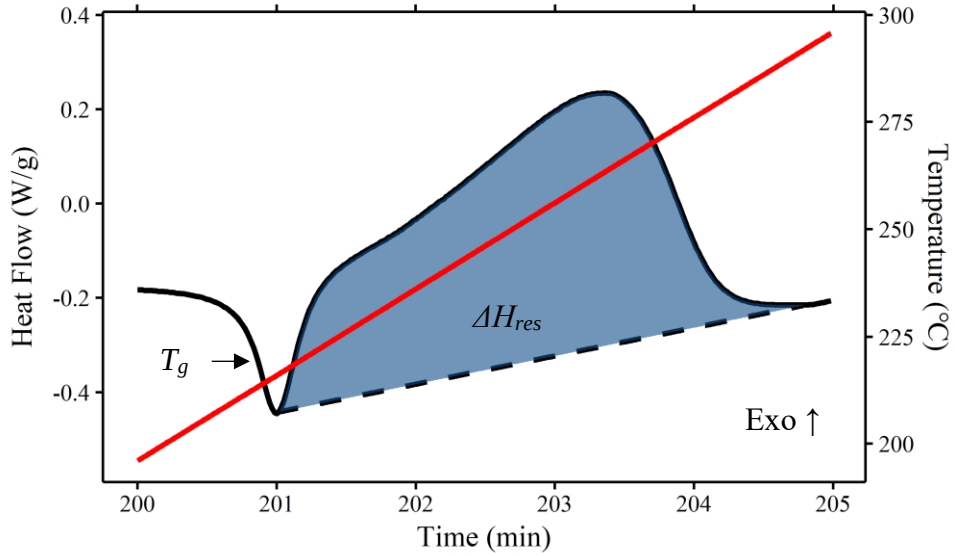

Figure B.2 – The residual heat released from a partially cured sample of TGDDM cured with DDS containing PES and 100 nm epoxy functionalized particles. The solid black line is the heat flow curve (left axis); the solid red line is the temperature (right axis) and the dashed line is the baseline. The blue area represents the residual heat, ΔH_{res}. The dip observed in the heat flow between 200 and 201 min, around 210 °C, corresponds to T_g.

Continually monitoring the degree of cure during the course of a heat treatment is considerably more difficult to achieve. Many researchers quench the reaction at intermittent stages and determine the residual heat, or T_g, at many points along the heat treatment to track the degree of cure across a given heat treatment. For near complete reactions, monitoring T_g may be a more sensitive way to monitor the degree of cure as the DSC signal becomes quite low near completion.

Regardless of whether the residual heat or glass transition is used to track the degree of cure, many experiments are required to monitor the reaction in this manner.

With some assumptions, an alternative means can be used to continually monitor the degree of cure of a thermosetting polymer exposed to a heat treatment consisting of a constant temperature ramp followed by an isothermal dwell step. The first assumption is that the total available heat released in the reaction is the sum of all of the released heat in three different steps, as described in Equation (B.2). The first segment consists of the heat released during the ramp, the second segment accounts for the heat released during the isothermal dwell, and the final segment consists of any residual heat remaining after the dwell. The heat released during the ramp, ΔH_{ramp}, can be determined by drawing a baseline that continues from the pre-reaction segment until the point of the isothermal dwell. The residual heat of reaction, ΔH_{res}, is computed in the same manner as the single point measurements. The sample is quenched as quickly as possible in the instrument to stop the reaction, and the sample is heated up at a constant rate to calculate the residual heat, as shown in Figure (B.2). The heat released during the dwell is slightly more complicated to compute. During an isothermal step in the DSC the baseline should be constant. The location of the baseline can be calculated by forcing the equality in Equation (B.2) to hold true, since all of the other parameters can be measured. ΔH_{uc} must be measured in a separate experiment, as described above and is a constant for the given resin system. The location of the dwell baseline can then be calculated in order to meet the equality $\Delta H_{dwell} = \Delta H_{uc} - \Delta H_{ramp} - \Delta H_{res}$. Some error is introduced in estimating the ramp baseline, and assuming that the baseline instantaneously settles to the isothermal position. However, these errors are small compared to the total heat released by the system and have been estimated to account for a few percent error.

$$\Delta H_{uc} = \Delta H_{ramp} + \Delta H_{dwell} + \Delta H_{res} \qquad \text{(B.2)}$$

An illustration showing the ramp and well regions and released heats is shown in Figure B.3. In this particular example the sample, consisting of TGDDM cured with DDS containing PES and 100 nm epoxy functionalized particle, is heated at a constant rate of 2 °C-min^{-1} before being held isothermally at 180 °C for 2 hours. The sample was then quenched quickly and heated at a rate of 20 °C-min^{-1} to 300 °C to obtain the residual heat, ΔH_{res}. The shaded areas represent the released heat in each segment and the dashed lines represent the baselines.

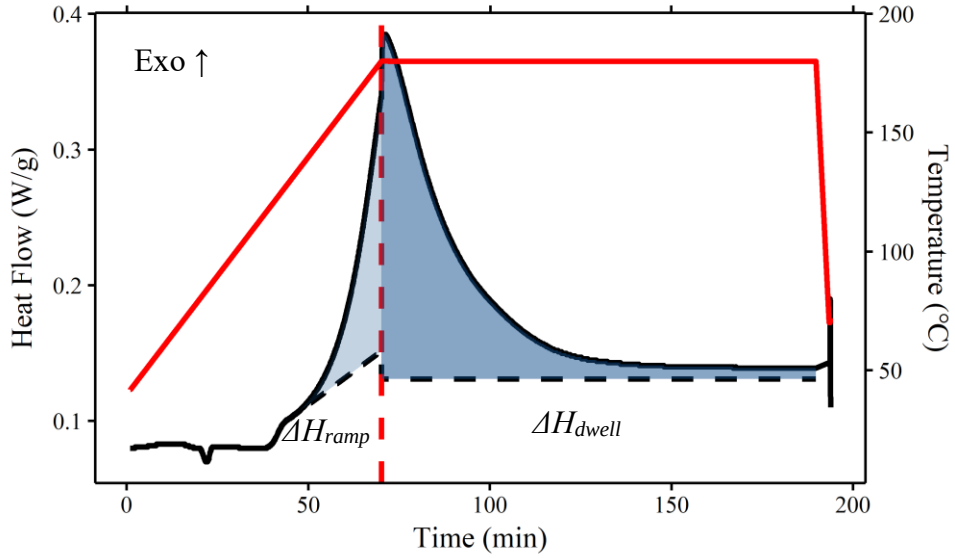

Figure B.3 – Example of a DSC trace for TGDDM cured with DDS containing PES and 100 nm epoxy functionalized silica particles heated at 2 °C-min^{-1} to 180 °C and then being held isothermally for two hours. The dashed lines represent the calculated baselines, the light blue area represents the heat released during the ramp step, and the dark blue shaded area represents the heat released during the isothermal dwell. The red line is the temperature profile (right axis).

Using the described method above, the degree of cure can be continually monitored for a thermosetting resin containing a single isothermal dwell. Two experiments are required. The first is to determine the total available heat of the cross-linking reaction. In the next experiment the sample is exposed to the desired heat treatment followed by a quench and second ramp step to determine the residual heat of reaction. Based on the heat released during the ramp step, the residual heat and total available heat, the isothermal baseline can be determined and the cumulate

heat released at any point along the reaction can be determined, *ΔH(t)*. The degree of cure at any point in the heat treatment is then determined from Equation (B.3).

$$\alpha(t) = \frac{\Delta H(t)}{\Delta H_{uc}} \tag{B.3}$$

The degree of cure and temperature profile for TGDDM cured with DDS containing some PES and 100 nm epoxy functionalized nanoparticles is shown in Figure B.4. The results show that the degree of cure is still relatively low (~0.1) by the time the isothermal dwell temperature is reached. The reaction proceeds rapidly at first and then slows down as the sample begins to cross-link and vitrify. By the end of the isothermal dwell the degree of cure is approximately 0.85. Heating the sample to 300 ℃ releases the rest of the residual heat and the degree of cure eventually reaches 1.

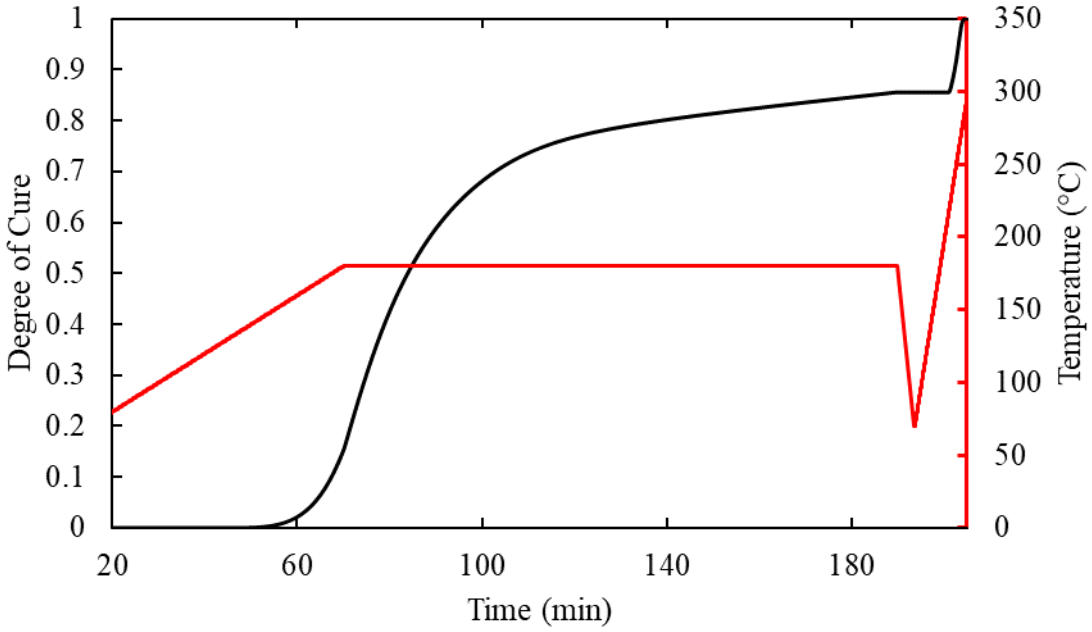

Figure B.4 – Figure showing the degree of cure (left axis, black) and temperature (right axis, red) vs. time. The sample consisted of TGDDM cured with DDS and contained PES and 100 nm epoxy functionalized particles.

PRIMARY REFERENCE

1. Menczel JD, Judovits L, Prime RB, Bair HE, Reading M, Swier S. Differential Scanning Calorimetry (DSC). In: Menczel JD, Prime RB, editors. Thermal Analysis of Polymers. John Wiley & Sons, Inc.; 2009. p. 7–239.

VITA

KYLE BERND CALDWELL

Born

September 10, 1988, in San Diego, California, USA

Education

High School Diploma: University City High School, 2006
B.S. in Chemical Engineering: University of California at Berkeley, 2010
M.S. in Chemical Engineering: University of Washington, Seattle, 2016
Ph.D. in Chemical Engineering: University of Washington, 2017

Publications

"Self-Assembly of Nanoparticle-Rich Interphases in Fiber Reinforced Polymeric Composites Using Migrating Agents" K.B. Caldwell, J.C. Berg, *Journal of Adhesion Science and Technology,* (Submitted 2017)

"Nanoparticles as Interphase Modifiers in Fiber Reinforced Polymeric Composites: A Critical Review" K.B. Caldwell, J.C. Berg, *Reviews of Adhesion and Adhesives,* 5(1), 1-54, (2017)

"Direct Observation of Nanoparticle Migration in Epoxy Bases Fiber Reinforced Composites Using Fluorescence Microscopy" K. Caldwell, J.C. Berg, *Journal of Composite Materials,* 51(28), 3877-3855, (2017)

"The Use of COSMO-SAC to Predict Relative Adhesion Between Polymer Matrices and Silane-Treated Glass Surfaces in Filled Particulate Composites" K. Caldwell, J.C. Berg, *Journal of Adhesion Science and Technology*, 28(13) 1312-1322, (2014)

"Screening Nonspecific Interactions of Peptides Without Background Interference" A.J. Keefe, K.B. Caldwell, A.K. Nowinski, A.D. White, A. Thakkar, S. Jiang, *Biomaterials,* 34(8), 1871-1877, (2013)

"Standardizing and Simplifying Analysis of Peptide Library Data" A.D. White, A.J. Keefe, A.K. Nowinski, Q. Shao, K. Caldwell, S. Jiang, *Journal of Chemical Information and Modeling*, 53(2), 493-499, (2013)

"NOx Interactions with Dispersed BaO: Adsorption Kinetics, Chemisorbed Species, and Effect of Oxidation Catalyst Sites" B.M. Weiss, K.B. Caldwell, E. Iglesia, *Journal of Physical Chemistry C*, 115(14), 6561-6570, (2011)